Jussila, Topias; Philip, Anish; Tripathi, Tripurari; Nielsch, Kornelius; Karppinen, Maarit

Atomic layer deposition of magnetic thin films : Basic processes, engineering efforts, and road forward

Published in:
Applied Physics Reviews

DOI:
10.1063/5.0172732

Published: 29/12/2023

Document Version
Publisher's PDF, also known as Version of record

Applied Physics Reviews

REVIEW ARTICLE | DECEMBER 29 2023

Atomic layer deposition of magnetic thin films: Basic processes, engineering efforts, and road forward

Topias Jussila ; Anish Philip ; Tripurari Tripathi; Kornelius Nielsch ; Maarit Karppinen

Appl. Phys. Rev. 10, 041313 (2023)
https://doi.org/10.1063/5.0172732

Applied Physics Reviews REVIEW pubs.aip.org/aip/are

Atomic layer deposition of magnetic thin films: Basic processes, engineering efforts, and road forward

Cite as: Appl. Phys. Rev. **10**, 041313 (2023); doi: 10.1063/5.0172732
Submitted: 18 August 2023 · Accepted: 17 November 2023 ·
Published Online: 29 December 2023

View Online Export Citation CrossMark

Topias Jussila,[1] Anish Philip,[1] Tripurari Tripathi,[2] Kornelius Nielsch,[3] and Maarit Karppinen[1,a)]

AFFILIATIONS

[1]Department of Chemistry and Materials Science, Aalto University, FI-00076 Aalto, Finland
[2]Low Temperature Laboratory, OtaNano, Aalto University, FI-00076 Aalto, Finland
[3]Leibniz Institute of Solid State and Materials Research, Helmholtzstr. 20, 01069 Dresden, Germany and Institute of Materials Research, University of Technology, Dresden, Germany

[a)]Author to whom correspondence should be addressed: maarit.karppinen@aalto.fi

ABSTRACT

Atomic layer deposition (ALD) is known as a key enabler of the continuous advances in device engineering for microelectronics. For instance, the state-of-the-art transistor technology depends entirely on ALD-grown high-κ materials. Another application branch where ALD could potentially play a similar important role in future is the magnetic thin film devices. Spin-based devices based on high-quality magnetic thin films are anticipated to provide high-efficiency operations with low power consumption. The strict quality demands the magnetic thin films must fulfill in the next-generation applications form the strong bases for the efforts to implement ALD in this application area. In this first comprehensive review on the topic, our aim is to provide an insightful account of the ALD processes so far developed for magnetic materials and to highlight the application-relevant magnetic properties of the thus fabricated thin films. Moreover, we discuss the various innovative engineering efforts made toward different multi-layered and nanostructured composite materials and complex architectures uniquely enabled by the sophisticated self-terminated film-growth mechanism of ALD. The review is finished with a brief outlook toward the future prospects and challenges in the field.

TABLE OF CONTENTS

I. INTRODUCTION

Magnetic materials in the form of high-quality thin films are essential for modern microelectronics and spintronics applications such as magnetic data storage, sensors, and information technology.[1–3]

Many of these strongly emerging applications require ultra-thin and conformal magnetic coatings, which can also be fabricated at relatively low temperatures and integrated with other device components for advanced architectures. Atomic layer deposition (ALD) is a uniquely suited thin-film technology to address these demands, as it has the superior capability to produce uniform and pinhole-free thin films over complex substrate structures for a wide material repertoire ranging from complex metal oxides and chalcogenides to pure metals and intermetallics.[4–10] Importantly, ALD is already the state-of-the-art technology in microelectronics and beyond,[11–14] which allows novel ALD processes to be readily integrated into the current industrial setup.

Despite this obvious increasing demand, the progress made in the magnetic ALD thin-film research segment has deserved only limited attention. There are recent comprehensive reviews focusing on the prospective role of ALD in specific application fields, such as catalysis,[15] batteries,[16–18] photovoltaics,[13,19,20] thermoelectrics,[21] fuel cells,[22,23] optoelectronics,[14] and semiconductors,[7] but no reviews dedicated to the ALD-grown magnetic materials. It is, therefore, the intention of this first comprehensive review specifically focusing on magnetic thin films to provide a full account of their fabrication process development gradually made over the years, highlight the most exciting results obtained thereof, and offer an outlook to the future research of this topic, including an insight into prospective magnetic material classes, which could highly benefit of the inherent advantages of the ALD technique. Figure 1 displays the annual numbers of published ALD reports related to magnetic thin films, and the division of these publications into the different magnetic material families: binary iron oxides, ternary/quaternary iron oxides, other metal oxides, single-metal cobalt, nickel and iron, metal alloys/intermetallics, as well as other materials including transition metal carbides, selenides, inorganic–organic thin films, and some multilayer structures. It should be noted that not all these publications include magnetic property characterization, but a considerable fraction of the papers focus on the precursor and deposition process development, essential for the production of high-quality magnetic thin films. However, for each material included one publication in minimum presents magnetic property characterization data.

The very first ALD process reported for a well-established magnetic material was the ternary process for $LaMnO_3$ films by Nilsen *et al.*[24] This low-temperature ferromagnetic (FM) perovskite and its derivatives had already been extensively investigated for years in the bulk form for their versatile magnetic and magnetoresistance properties,[25] but the challenge for the ALD growth was the optimization of the deposition parameters for a process with multiple precursors. Another example from the nearly opposite end of the timeline is the recent success in depositing *in situ* crystalline ε-Fe_2O_3 thin films from the two simple precursors, $FeCl_3$ and H_2O.[26,27] This ferrimagnetic (FiM) polymorph of trivalent iron oxide is extremely difficult to stabilize through conventional synthesis and, hence, not widely known; nevertheless, ε-Fe_2O_3 is a highly promising candidate for next-generation spintronic devices due to its giant room-temperature (RT) magnetic coercivity (up to 20 kOe), ferroelectricity, and zero-field FM resonance.[28,29]

Viable ALD processes have been developed for magnetic metals (Fe, Co, and Ni) and metal alloys/intermetallics as well. These depositions are challenging though, as they require highly reductive co-

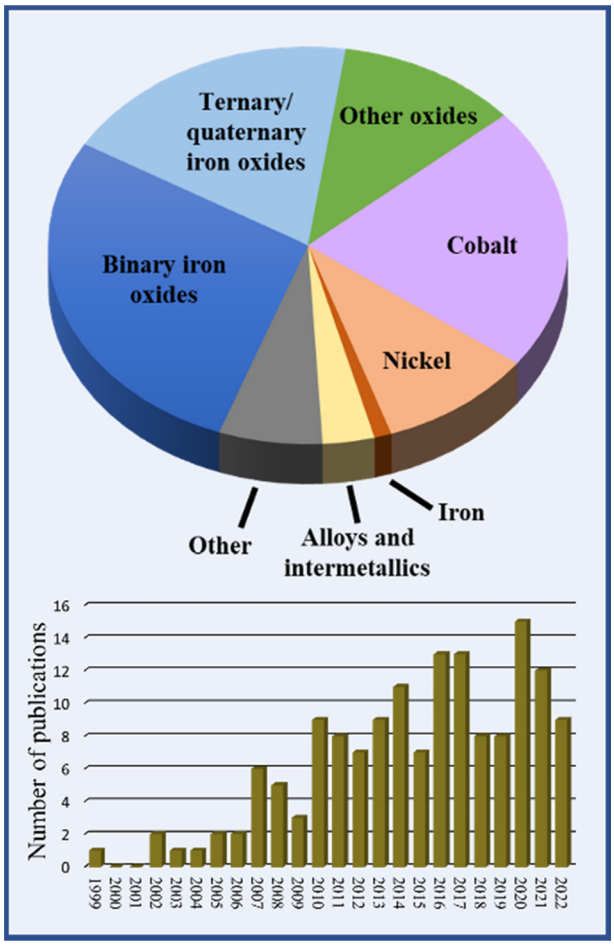

FIG. 1. Division of ALD-grown magnetic thin films into magnetic material families (top): binary iron oxides, ternary/quaternary iron oxides, other oxides, cobalt, nickel, iron, alloys/intermetallics, and others (transition metal carbides, selenides, inorganic–organic thin films, and multilayers). Annual ALD publications of magnetic thin films (bottom); note that not all of these publications on magnetic materials include magnetic-property characterization but may instead focus on the ALD process development.

reactants such as H_2 plasma and also often result in island-type film growth, which leads to discontinuous and granular films.[8] Great process and precursor development efforts have been made especially for cobalt—an important FM material—to overcome these issues.[30,31] For instance, Kerrigan *et al.*[32] deposited *in situ* crystalline and continuous cobalt thin films at appreciably low temperatures on both platinum and copper substrates. The same ALD process was later successfully applied for the deposition of ultra-thin cobalt films on the topological insulator material, Sb_2T_3.[30,33] Also excitingly, the ALD of so-called van der Waals (vdW) two-dimensional (2D) transition metal dichalcogenides is already rather well-established for certain materials such as MoS_2.[34] So far, though, the majority of the published works on the vdW 2D ALD films have focused on their electronic and electrochemical properties.[35] The potential of both vdW and non-van der Waals (non-vdW) 2D magnetic materials is briefly discussed in the outlook.

Application-wise, ALD processes of magnetic thin films have been investigated and developed, e.g., for high-density data storage applications,[36,37] magnetic tunnel junctions,[38,39] magneto-optics,[40] sensing devices,[38,40] microelectromechanical systems (MEMS),[41] magnonics,[42] and different flexible devices.[37,43,44] In light of this wide scope of potential applications, it was somewhat surprising that only one patent was found in which ALD was used as the key fabrication technique for a magnetic device; this patent from 2002 describes magnetic tunnel junctions such as $Co/Al_2O_3/Co$ fabricated either partly or solely with ALD.[45] In Sec. VII, we will discuss this issue of lacking patents in more detail, in connection to the apparent need to invest more efforts to device planning in order to forward this field further. The high-quality demands the magnetic thin films must fulfill in the next-generation applications underline the increased interest in implementing ALD as the deposition technique for these advanced thin-film materials. Moreover, ALD is known for its superior capability to produce highly conformal thin-film overlayers and coatings, which provides unique opportunities for fundamental studies related to the geometrical effects on magnetic properties.[46]

The goal of this review is to provide the current status and future prospects of ALD grown magnetic thin films and their potential applications. We start the review with introduction to the current variety of magnetic materials and their magnetic properties most relevant to thin-film applications (Sec. II) as well as the ALD technique and its extension to multilayer structures (Sec. III). Section IV then provides a comprehensive account of the ALD fabrication processes so far developed for different magnetic materials. In Secs. V and VI, respectively, we highlight some exciting material-engineering concepts challenged for ALD-grown magnetic thin films, and the magnetic property characteristics so far realized for these materials. In Sec. VII, we will provide a brief outlook to the future prospects and challenges of the field, and finally, the review is wrapped up to a short conclusion in Sec. VIII.

II. BRIEF ACCOUNT OF MAGNETIC MATERIALS AND THEIR APPLICATIONS

A. Magnetic material variety

Magnetic materials are an integral part of our society, with their annual market value of tens of billions of dollars.[3,47] Ferro- and ferrimagnetic materials cover the lion's share of the commercially used magnetic materials, some of which are collected in Fig. 2. Most of these materials are based on a few 3D transition metals (Fe, Co, and Ni) and 4f lanthanides (Nd and Sm) with unpaired electrons. Barium and strontium ferrites, the most important bulk hard ferrites, are used in a wide spectrum of applications from fridge magnets to motors. The more expensive but high-performance neodymium-based Nd–Fe–B alloys, on the other hand, are used in demanding applications such as wind turbines.[48] The so-called electrical steel (Fe–Si), also used in motors and other electrical machines, is the market leader among the bulk soft magnetic materials.[47] The Co–Fe alloy, used as a high-performing electromagnet, has a giant magnetic saturation that enables high magnetic flux densities, which is highly beneficial for applications where reduced size and weight of the device is of significance.

The major industry branch of magnetic thin films is set up by magnetoresistive devices and magnetic recording media.[49] For instance, the data of magnetic memory devices are processed with giant magnetoresistance (GMR) or tunneling magnetoresistance (TMR) reading and writing heads, while GMR/TMR sensors are extensively used in automotive industry. Moreover, the magnetoresistance-based spin valve devices and also other FM thin film structures are piercing into other commercial fields as well such as biomedical and chemical sensing applications.[50–52]

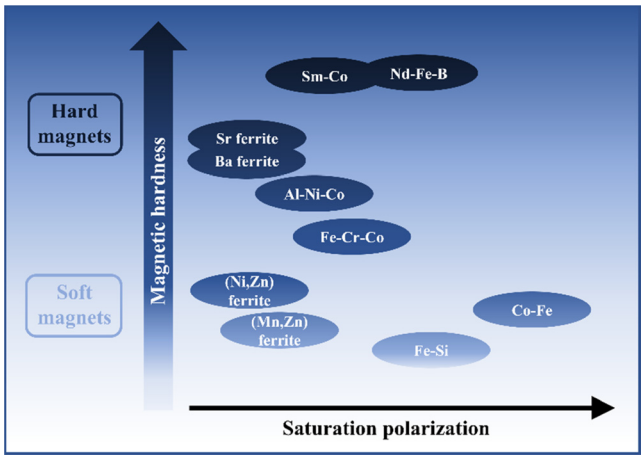

FIG. 2. Schematic summary of the commercial bulk magnetic (FM/FiM) materials sorted based on their most characteristic magnetic properties: magnetic hardness and magnetic saturation.

For the thin film materials, ferromagnetic metals and alloys have been the most common choice in a large part of the applications; Ni–Fe and Co–Fe alloys have been used for the writing and reading heads, while magnetically hard CoCrPt-oxide and Fe-Pt have been developed for the magnetic media to replace the previously used γ-Fe_2O_3 to reach higher data storage densities.[47,53] Novel material choices are increasingly pursued for the spin-based applications. For instance, Fe_3O_4 is an appealing candidate due to its ferromagnetic and half-metallic nature. Other spinels, such as $CoFe_2O_4$, are also explored for magnetic recording among other applications, due to their versatile magnetic and magneto-optical properties. The ternary oxide thin films can be deposited through ALD with excellent control over the composition and magnetic properties.[40]

In recent years, increasing interest has been devoted to multiferroic thin films as enablers of future spintronics applications.[2] Multiferroic materials have at least two of the following properties: ferromagnetism, ferroelectricity, and ferroelasticity.[54] The most interesting and widely pursued combination is ferromagnetism plus ferroelectricity with magnetoelectric (ME) coupling. This combination of properties would enable the electrical control of magnetic properties and vice versa, which is the essence of the spintronics devices with low power consumption and high operating efficiency.[2] For instance, fast electric writing and nondestructive magnetic reading would open new pathways for next-generation nonvolatile data storage devices.

Only a fraction of all known magnetic materials is in commercial use, since there are several requirements from material properties to economic aspects that must be fulfilled to break the market. One of the crucial properties is the Curie temperature (T_C) below which the unpaired spin moments of the paramagnetic (PM) phase are collectively aligned for the material to become FM, FiM, or antiferromagnetic (AFM). Most FM and FiM materials have T_C values well below

the typically desired operation temperatures, which inhibits their utilization in practical applications. For example, in consumer applications the T_C value should be well above room temperature.

Here, it should be noted that even though FM and FiM materials cover most of the application platforms of magnetics, other types of magnetism are also pivotal for various applications. For example, AFM NiO is used in spin valves (e.g., reading heads) as a pinning layer,[47] whereas PM metal chelates are used in magnetic resonance imaging.[55] At the same time, biomedical applications are in need for novel superparamagnetic systems. For instance, biocompatible iron oxides are heavily studied for magnetically controlled drug delivery, in which the drug molecules are released by external magnetic field to efficiently target the drug molecules to specific areas, such as tumors. Other biomedical applications requiring superparamagnetic materials include biosensors, and magnetic hyperthermia in cancer treatments.[55–58]

B. Hysteresis loop and coercive field

Magnetic hysteresis is the most essential property of FM and FiM materials.[59] Schematic magnetization (M) curves as a function of an applied external magnetic field (H; M-H curve) of hard (blue) and soft (light blue) FM/FiM materials are shown in Fig. 3. Upon increasing the external field, the magnetic domains gradually orient according to H, and the material reaches its saturation magnetization (M_s) when the domains get fully oriented. Then, when switching the external field to zero ($H = 0$), the magnetic domains are aligned according to the magnetic easy axis (a preferred direction of spin orientation), resulting in non-zero net magnetization (remanent magnetization; M_r) despite the absence of the external field. Typically, $M_r < M_s$ due to imperfect alignment of crystallites (magnetic domains). The zero net magnetization ($M = 0$; magnetic domains randomly orientated) is reached once sufficient external field (coercive field; H_c) is applied in the opposite direction of the initial magnetization. The magnitude of H_c depends on how well the material can retain its magnetic ordering under the opposing external field. Materials with low H_c and high H_c are classified as soft and hard magnets, respectively. Once the external field is further increased from $H = H_c$, the material will again reach the M_s of the same magnitude but in the opposite direction.

The hysteresis loop is observed only for FM and FiM materials; a PM material is magnetized according to the external field, but the magnetization is not preserved when the external field is switched off. Also, their magnetization (spin orientation) is weak in comparison to ferromagnets. Superparamagnetic materials, on the other hand, are nanoscale FMs or FiMs with strong intrinsic magnetization but zero M_r; when the particle size of a FM grain is decreased to ~10 nm, the magnetic ordering is readily overcome by thermal fluctuations as the energy required to break the magnetic ordering is in the range of k_BT.[60] Thus, the magnetization is lost in the absence of an external field. The smaller the particle size, the higher the temperature at which FM/FiM turns into superparamagnetism (blocking temperature). Accordingly, a relatively large particle size is needed to obtain strong FM/FiM. However, as-deposited films are often of low crystallinity and, hence, as-deposited hard magnets can be tough to achieve. Often, once thermal annealing is performed, the degree of crystallinity and the crystal size increase, which enhances the interaction volume and magnetocrystalline anisotropy of the magnetic domains, thus leading to stronger FM/FiM.[61]

Generally, a H_c value of 100 Oe is considered a minimum requirement for hard ferromagnets though it is still quite low compared to most permanent magnets.[3,62] For instance, the coercivity of commercial bulk hard magnets such as Nd–Fe–B, Al–Ni–Co, $CoSm_x$, and MnAl is on a scale of 1–10 kOe.[47] High coercivity is particularly important for thin-film applications due to scaling effects. To increase the data storage density of current magnetic memory devices, the individual magnetic crystallites per unit area must be increased, i.e., the

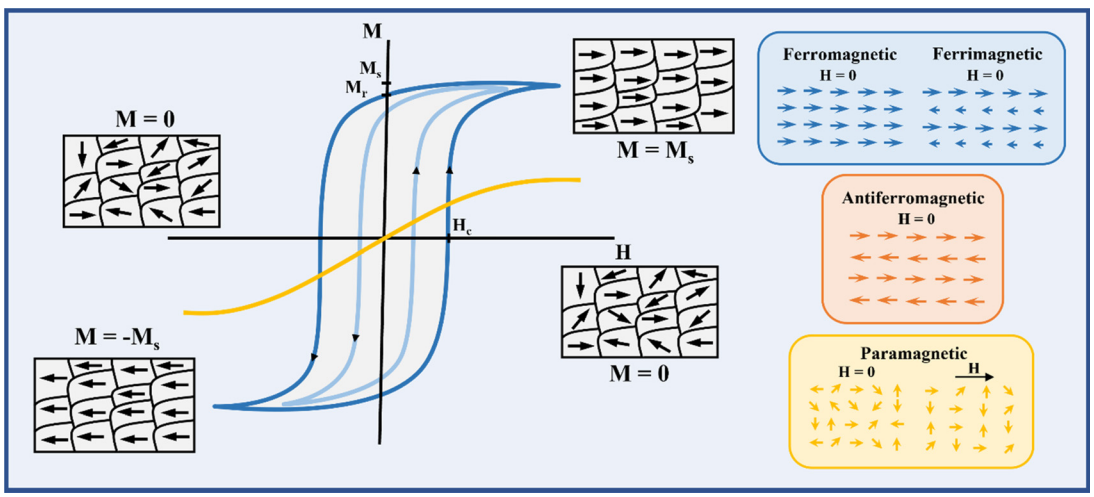

FIG. 3. Schematic representation of the M-H curves and spin alignment of FM, FiM, AFM (M-H curve excluded), and PM materials. Orientation of the magnetic domains are sketched for $M = M_s$ (domains are orientated according to the external field; net magnetization) and $M = 0$ (domain are orientated randomly in the absence of external field; zero net magnetization). The blue and light blue M-H curves correspond to hard and soft FM/FiM, respectively; hard magnets have higher coercive field (H_c) and, thus, broader hysteresis compared to the soft magnets. PM materials have zero net magnetic ordering in the absence of external field and, hence, no hysteresis. Furthermore, the ability of PM materials to magnetize according to external field is weaker compared to FM/FiM materials, resulting in lower M_s.

size of the magnetic crystallites must be decreased.[63,64] This requires thin-film materials with high magnetic coercivity since harder magnets have a higher ability to retain the FM characteristics when the size of the magnetic domains is decreased. In the case of a soft FM with weaker magnetic interactions, the magnetic ordering of small crystallites and domains is easily lost due to thermal energy (superparamagnetism), resulting in the loss of the information stored in the magnetic units.

C. Magnetic anisotropy in thin films

Magnetic anisotropy of thin films derives at least from two factors: magnetocrystalline anisotropy is an intrinsic material property that depends on the crystal structure, while shape anisotropy is an engineered property.[65] For hard FMs, the magnetocrystalline anisotropy is large meaning that the tendency for magnetization is significantly higher for the so-called crystallographic magnetic easy axis compared to other crystallographic directions (hard axes). On the contrary, the magnetocrystalline anisotropy is low for magnetically soft materials, though it can be increased through stress (strain) or non-stoichiometry.

For thin films, shape anisotropy is of major importance as the small film thickness induces a strong demagnetization field perpendicular to the film surface. As a consequence, the magnetic easy axis is readily formed along the film surface (in-plane; Fig. 4). This relatively strong effect can easily overcome the magnetocrystalline anisotropy; even though the magnetocrystalline easy axis would be perpendicular to the surface (out-of-plane), the overall magnetic easy axis is forced in-plane by the shape anisotropy. However, for applications rather the perpendicular magnetic anisotropy (PMA) is often pursued, as the out-of-plane magnetization enables the higher magnetic domain density, which in turn would allow the higher magnetic data-storage density.

Surface anisotropy, induced by anisotropic surroundings or surface atoms, is highly important especially for ultra-thin films. It can drive the film either toward in-plane or out-of-plane magnetization. Indeed, multilayer structures built up of multiple ultra-thin layers is an effective route to achieve PMA. In cobalt-based multilayers, such as Co/Pt and Co/Pd, the seed layer (e.g., Ru, Ta, Pd) directs the crystallographic easy axis toward out-of-plane, which is further intensified by the interfaces of the multilayer structure.[66,67]

Strain induced by a lattice-mismatching substrate or defects is another important parameter for magnetic thin films. For instance, for $CoFe_2O_4$ the PMA can be tailored by using a MgO substrate to create in-plane strain or by inducing oxygen deficiency to create compressive strain and strong out-of-plane coercivity.[68,69]

Similarly, 3D nanostructuring can be utilized to achieve PMA (Fig. 4). Since the magnetic easy axis is bound to be in-plane for most cases, having the film surface perpendicular to the substrate turns the easy axis in perpendicular direction with respect to the substrate. Therefore, magnetic nanotubes in combination with the ALD technique owing to its excellent conformality could provide us with an exciting platform to challenge the PMA; both magnetic metal oxide (Fe_3O_4) and metallic (Co, Ni) nanotubes with preferred out-of-plane magnetization have been demonstrated, as will be discussed in more detail in Sec. VI.[46,70] The nanotube architectures could be applied for advanced switching purpose such as high-density magnetic bit storage, especially when sophisticated multilayer core/shell structures are applied.[71]

III. INTRODUCTION TO ATOMIC LAYER DEPOSITION TECHNIQUE

The unique precursor pulsing scheme, which makes the ALD technique so attractive, was originally developed for ZnS electroluminescent displays by Suntola and co-workers in Finland around the 1970s.[72,73] Up to this date, ALD has been mainly applied in the semiconductor industry (e.g., high-κ dielectric HfO_2 in transistor technology), but there is an ever-increasing interest in other application fields such as photovoltaics and other energy harvesting/storage technologies, MEMS, and 3D nanodevice fabrication.[74–78] In this section, the basics of ALD processes and precursor chemistry are shortly introduced. All the metal precursors used for the ALD of magnetic thin films are listed in Table I. Moreover described is the concept of supercycles applied for the more elaborated multi-layer structures.

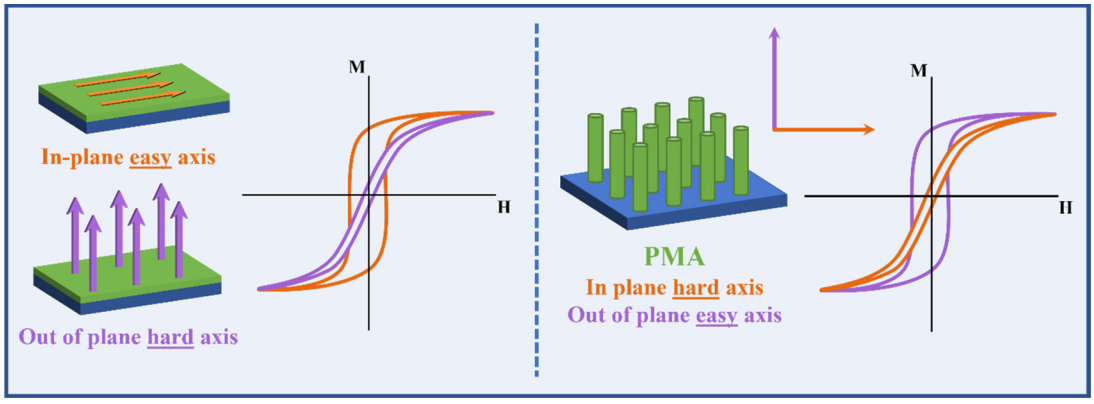

FIG. 4. Schematic representation of the magnetic anisotropy of thin films (left) and perpendicular nanotubes (right). The arrows drawn for each case depict in-plane (orange) and out-of-plane (purple) magnetization direction. The magnetic hysteresis is stronger along magnetic easy axis (and saturation is achieved with smaller external field) compared to hard axis. For thin films, the magnetic easy axis is typically in in-plane direction due to shape anisotropy, while for the nanotubes the easy axis is shifted to out-of-plane (PMA) direction with respect to the substrate due to the orientation of the nanotubes. In consequence, the strong in-plane hysteresis shifts to the out-of-plane direction.

A. Conventional ALD method

Atomic layer deposition is an advanced thin-film technique based on self-terminating gas–solid interface reactions;[79,80] the self-termination derives from the condition that the gaseous chemical precursors react only with active sites on the surface and not with each other in the gas phase. Figure 5(a) illustrates a typical ALD process of a binary material. The first precursor is introduced into the reaction chamber with the help of an inert carrier gas (N_2 or Ar). Once the surface is saturated and (ideally) one monolayer has been formed, the excess precursor and by-products formed during the gas–solid reactions are removed from the reaction chamber by inert gas purging to prevent gas-phase reactions with the upcoming precursor. Then the second precursor pulsed to the reaction chamber will react with the surface formed during the previous precursor pulsing, thus forming a new saturated surface. The excess precursor and by-products are again removed, and the next ALD cycle may start again. As a result, the film is grown layer-by-layer in a highly controlled manner.

The so-called growth-per-cycle (GPC) value depicts the thickness of each layer formed during one ALD cycle.[75] Ideally, it would equal the thickness of an ideal saturated material layer but due to effects such as steric hinderance of precursor ligands and the chemistry of the surface, GPC is often somewhat less than the ideal monolayer thickness. Typically, within a certain deposition temperature range, the chemical reactions are self-terminating, and the film surface is saturated during each deposition cycle, resulting in an essentially constant film growth rate over the deposition temperature range. Outside this temperature window, the self-terminating and saturated film growth may be corrupted for reasons such as precursor decomposition (excessive temperature) or condensation (low temperature), which cause abrupt changes in the growth rate and quality of the growing film.

However, the growth rate is not always constant within the self-terminating temperature range either due to, for instance, changes in the density of active sites (e.g., OH-groups) on the surface,[81] or orientation of the growing crystals. Hence, the most crucial criterion for the ideal ALD film growth is that the chemical reactions are self-terminating, seen as a saturation of the GPC value once a sufficient precursor pulse length is applied [Fig. 5(b)]. Sufficient purging length is also crucial for the ALD process as it ensures that ALD sub-cycles do not overlap and cause undesired gas-phase reactions. Another indication of the ideal layer-by-layer film growth is that the film thickness increases linearly with the number of ALD cycles applied. Here, some deviations can be seen during the initial ALD cycles due to the different surface chemistry and morphology of the substrate compared to the surface of the growing film. The self-terminating chemistry is the very origin for the superior properties of ALD including the excellent uniformity, pinhole-free structure even for ultra-thin films, facile thickness control through the number of ALD cycles, and excellent conformality even for extreme aspect ratios.

B. Extension of ALD to multilayer concepts

Due to the layer-by-layer type film growth mechanism, the different ALD cycles are modular in the sense that they can be combined in any arbitrary manner for the growth of various multilayer structures. The strong connection between the different layers is achieved owing to the fact that the ALD films grow via chemical surface reactions. Through the use of ALD supercycles (Fig. 6), both variously substituted binary metal oxide films (e.g., $Fe_{3-x}Co_xO_4$)[40] and ternary (e.g., $BiFeO_3$, $SrCoO_{3-\delta}$)[82,83] and even quaternary materials (e.g., $La_{1-x}Sr_xCoO_{3-\delta}$, $La_{1-x}Ca_xMnO_3$)[84,85] have been grown with ALD. The supercycles enable having arbitrary sequence of different precursor species, thus allowing full freedom for engineering of the chemical composition. Also, it is possible to create nanolaminate-type structures by combining compatible ALD processes and repeating those sequentially for the growth of the two different materials on top of each other (e.g., ε-Fe_2O_3:SiO_2).[86] Similarly, it is also possible to replace the co-reactant (e.g., H_2O) with an organic precursor (e.g., hydroquinone) in the supercycle sequence to grow inorganic:organic superlattice (SL) structures (Fig. 6). In this latter case, the organic precursor-based deposition cycle is called MLD (molecular layer deposition), as the organic layers grow in molecular steps.[87] Thus, the full cycle is referred to as ALD/MLD supercycle.

As an example of inorganic ternary thin films, multiferroic $BiFeO_3$ thin films have been fabricated through the deposition of alternating ultra-thin BiO_x and FeO_x layers from triphenyl bismuth [Bi(ph)$_3$] and O_3, and iron(III) tris(2,2,6,6-tetramethyl-3,5-heptodionate) [Fe(thd)$_3$] and O_3 precursors, respectively.[88] In this case, the crystallization of the targeted ternary phase requires a post-deposition annealing. The challenge is the tendency of the two individual metal oxide phases, Bi_2O_3 and Fe_2O_3, to crystallize if the mixing of the metals remains incomplete. However, if the ALD processes of both oxides are well-defined, the layer thicknesses of the both binary oxides, and, thus, the final composition and structure can be easily controlled with high precision, which enables a facile engineering of the functional properties of the film; it has been shown that $BiFeO_3$ thin films with both bismuth-rich and iron-rich layers exhibit better overall multiferroic properties compared to stoichiometric $BiFeO_3$ thin films (Sec. VI).[89] Moreover, post-annealing is not a prerequisite for multicomponent ALD as *in situ* crystalline ternary thin films ($Co_xFe_{3-x}O_4$) can be achieved with robust control over the stoichiometry simply through the sequence of the supercycle containing both metal species (Sec. IV B).[40]

The strategy to combine single MLD cycles with ALD cycles for the fabrication of inorganic:organic SL structures was originally developed for ZnO-based superlattices in which the embedded monomolecular organic layers were shown to efficiently suppress the thermal conductivity of the films.[90,91] Later similar efforts to insert organic layers within the inorganic ALD-grown matrix have been made also to bring mechanical flexibility or bandgap control for the films.[92–94] Moreover, both regular SLs and irregular/gradient structures have been demonstrated.[95] Most excitingly, flexible, optically controlled RT ferromagnetic ε-Fe_2O_3:azobenzene (ADA) SL thin films have been grown through the ingenious ALD/MLD technique (Secs. V A and VI).[37,43]

C. Precursors

Chemical precursors are the key to successful ALD as the deposition process is predominantly governed by the precursor chemistry. The main features concerning the precursors are self-terminating chemistry, thermal stability, and volatility.[75,81,96,97] Same precursor molecules cannot react among themselves, but the different precursors of a specific ALD process should have high reactivity toward each

TABLE I. Metal precursors employed in the ALD processes for magnetic thin films discussed in this review. The precursors are divided based on the ligand type. Sublimation temperature refers to the precursor heating temperature used in the ALD process.

	Ligand system	Ligand abbreviation	Metal	Precursor/Sublimation temp. (°C)		Reference
β-diketonates	2,2,6,-tetramethyl-3,5-heptanedionate	thd	Fe, Co, Ni, Bi, Mn, Er, Ca, Sr, La, Sm, Tb, Y, Yb, Lu	110–130	$Fe(thd)_3$	Fe[82,88,105–111]
				93–120	$Co(thd)_2$	Co[107,108,112,113]
				115	$Ni(thd)_2$	Ni[113,114]
				140–168	$Bi(thd)_3$	Bi[82,110,111,115]
				115–116	$Mn(thd)_3$	Mn[24,39,112,116–119]
				150–160	$Er(thd)_3$	Er[109,120]
				195	$Ca(thd)_2$	Ca[85]
				N/A	$Sr(thd)_2$	Lu[117]
				162–185	$La(thd)_3$	Sr[39]
				139–141	$Sm(thd)_3$	La[24,39,85,117,118]
				128–130	$Tb(thd)_3$	Sm[117]
				123	$Y(thd)_3$	Tb[117]
				123	$Yb(thd)_3$	Y[116,117,119]
				123	$Lu(thd)_3$	Yb[117]
	Acetylacetonate	acac	Fe, Ni	80	$Fe(acac)_3$	Fe[121,122]
				180–200	$Ni(acac)_2$	Ni[123–125]
				183	$Mn(acac)_3$	Mn[126]
				155	$Co(acac)_3$	Co[127]
	Bis(acetylacetonate) N,N,N′,N′-tetramethyl-ethylenediamine	$(acac)_2$tmeda	Ni	95	$Ni(acac)_2$tmeda	Ni[103]
	Bis(acetylacetonate) dipyridine	$(acac)_2(py)_2$	Ni	130	$Ni(acac)_2(py)_2$	Ni[103]
Alkoxides and iminoalkoxides	Tert-butoxide	O^tBu	Fe	100–105	$Fe[(O^tBu)_3]_2$	Fe[36,41,42,46,89,128–132]
	Pyridine tert-butoxide	$O^tBu(C_5H_5N)$	Fe, Gd	150–170	$GdFe(O^tBu)_6(C_5H_5N)_2$	Fe, Gd[133]
	Methoxide	OMe	Ti	130	$Ti(OMe)_4$	Ti[127]
	Isopropoxide	$OCH(Me)_2$	Ti	35	$Ti(OCH(Me)_2)_4$	Ti[134]
	2,3-dimethyl-2-butoxide	dmb	Bi	85	$Bi(dmb)_3$	Bi[41,89,131,132]
	1-methoxy-2-methyl-2-propoxy	mmp	Bi	135–145	$Bi(mmp)_3$	Bi[135–139]
	(N-isopropyl) ketoiminate	^{i}pki	Fe	100	$Fe(^i pki)_2$	Fe[101,140]
	1-(tert-butylimino)-2,3,3-trimethylbutan-2-olate	^{t}BuMeCOCN^{t}Bu	Fe	120	$Fe(^t BuMeCOCN^tBu)_2$	Fe[102]
	1-(tert-butylimino)-2,3-dimethylbutan-2-olate	^{i}PrMeCOCN^{t}Bu	Co, Ni	130	$Co(^i PrMeCOCN^tBu)_2$	Co[102]
				120	$Ni(^i PrMeCOCN^tBu)_2$	Ni[102]
Metallocenes	Cyclopentadienyl (metallocene)	cp	Fe, Co, Ni	80–200	$Fe(cp)_2$	Fe[38,40,46,61,71,115,120,128,129,135–169]
				78–100	$Co(cp)_2$	Co[31,40,44,70,128,158–161,167,168,170–178]
				50–90	$Ni(cp)_2$	Ni[40,42,70,128,149,151,165,167,168,179–185]
				150	$Y(cp)_3$	Y[166]
	Methylcyclopentadienyl	MeCp	Co	56	$Co(MeCp)_2$	Co[186]
	2,4-methylpentadienyl	2,4-MeCp	Fe	55	$Fe(2,4\text{-}MeCp)_2$	Fe[187]
	Tert-butyl cyclopentadienyl	(^{t}BuCp)cp	Fe	65	(^{t}BuCp)FeCp (=TBF)	Fe[188]
	Ethylcyclopentadienyl	EtCp	Co, Ru	70	$Co(EtCp_2)$	Co[104]
				N/A	$Ru(EtCp_2)$	Ru[189]

TABLE I. (*Continued.*)

	Ligand system	Ligand abbreviation	Metal	Precursor/Sublimation temp. (°C)		Reference
	Methylcyclopentadienyl trimethyl	(MeCp)Me_3	Pt	75	(MeCp)$PtMe_3$	Pt[178]
	(η^3-cyclohexenyl)(η^5-cyclopentadienyl)	(Chex)cp	Ni	50	Ni(Chex)cp	Ni[190]
	(Dimethylaminomethyl) metallocene	DMAMcp	Fe	N/A	DMAMFeCp (=DMAMFc)	Fe[144,191]
Carbonyls	Carbonyl	CO	Co	RT	$V(CO)_6$	V[192,193]
				25	$Co_2(CO)_8$	Co[193,194]
	Cyclopentadienyl dicarbonyl	$Cp(CO)_2$	Co	20–45	$CpCo(CO)_2$	Co[194,195]
	Tertbutylallyl tricarbonyl	^{t}Bu-Allyl$(CO)_3$	Co	35	^{t}Bu-Allyl$Co(CO)_3$	Co[196]
	Cyclohexadiene tricarbonyl	$C_6H_8(CO)_3$	Fe	-	$C_6H_8Fe(CO)_3$	Fe[197]
	Trimethylsilyl cyclopentadienyl dicarbonyl	TMSCp$(Co)_2$	Co	40	TMSCp$Co(Co)_2$	Co[195]
Halides	Chloride	Cl	Fe	158–175	$FeCl_3$	Fe[26,27,189,198]
				164	$BiCl_3$	Bi[199]
				162	$HfCl_4$	Hf[169,200]
				160	$ZrCl_4$	Zr[126,200]
	N,N,N′,N′-tetramethyle-thylenediamine dichloride	Cl_2(TMEDA)	Co	140–185	$CoCl_2$(TMEDA)	Co[10,201–203]
Amidinates	N,N′-di-t-butylacetamidinato	^{t}Bu-MeAMD	Fe	75–120	Fe(^{t}Bu-MeAMD)$_2$	Fe[98,204]
	N,N′-diisopropylacetamidinato	^{i}Pr-MeAMD	Co, Ni	50–65	Co(^{i}Pr-MeAMD)$_2$	Co[171,204–207]
				55	Ni(^{i}Pr-MeAMD)$_2$	Ni[204]
	1,4-di-tert-butyl-1,3-diazabutadienyl	tBu_2DAD	Co, Ni	128–130	Co(^{t}Bu$_2$DAD)$_2$	Co[30,32,33,208–211]
				140	Ni(^{t}Bu$_2$DAD)$_2$	Ni[100,212]
	N, N′ diisopropyl-propionamidinate	DIPPA	Fe	80	(DIPPA)$_2$Fe	Fe[99]
	N-tert-butyl-N′-ethylpropionamidinato	CoAMD	Co	80	CoAMD	Co[213–217]
	Cyclopentadienyl isopropyl acetamidinate	Co(cpAMD)	Co	75	Co(cpAMD)	Co[218]
	N,N′-diisopropyl-2-dimethylamidoguanidinato	DPDMG	Gd	120–135	Gd(DPDMG)$_3$	Gd[140]
	bis(trimethylsilyl)amide	Fe(btmsa)$_2$	Fe	65	Fe(btmsa)$_2$	Fe[219]
Alkyls	Phenyl	ph	Bi	200	Bi(ph)$_3$	Bi[88,163,164]
	Methyl	CH_3	Bi	···	$(CH_3)_3$Bi	Bi[197]
	Ethyl	et	Zn	RT	Zn(et)$_2$	Zn[160–162,167,168,184]
	Tributyl hydride	TBH	Sn	30	TBTH (Sn)	Sn[10,203]

other. Thermal stability is crucial as precursor decomposition is detrimental to the self-terminating chemistry and saturated film growth. Volatility again can be an issue especially for solid precursors since a sufficient vapor pressure is required to produce an adequate number of gaseous precursors to the gas phase. In addition to these three main precursor characteristics, the reactivity of the precursor is also of great importance; it largely defines the feasible co-reactants and deposition temperature range.

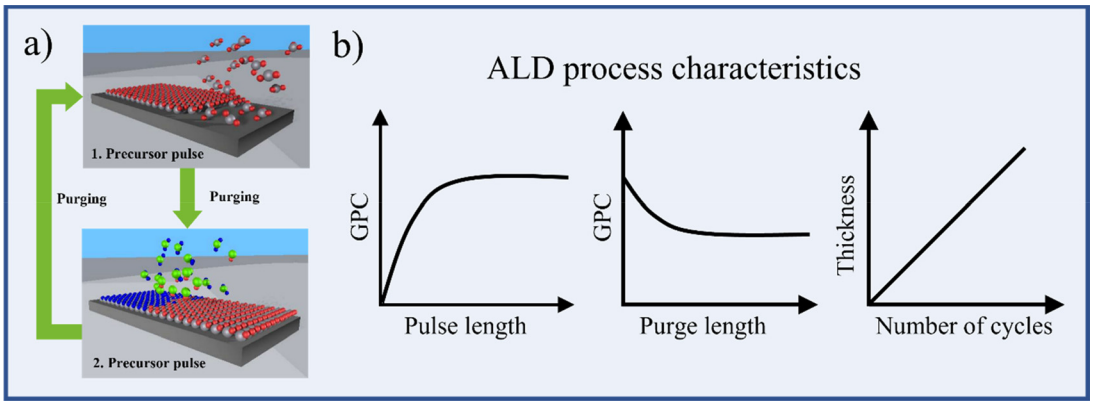

FIG. 5. (a) Schematic representation of the ALD cycle for a binary material such as a metal oxide. The chemical precursors of both components (metal and oxygen) are introduced to the reaction chamber one at the time. The precursors react on the substrate surface forming one monolayer during each cycle. The different precursors are separated by inert gas purging, which removes all the excess gas-phase precursor and by-product molecules from the reaction chamber, thus preventing the occurrence of undesirable gas-phase reactions, which would result from overlapping precursor pulsing. Adapted with permission from Knez *et al.*, Adv. Mater. **19**, 3425 (2007). Copyright 2007 WILEY-VCH Verlag GmbH & Co. KGaA, Weinheim.[78] (b) Schematic illustrations of the basic ALD process characteristics. The film growth rate (GPC value) is saturated with sufficient precursor pulse length (left); at the saturation regime, the GPC is independent of the pulse length since all the active sites on the surface are consumed, i.e., increasing the pulse length does not affect the growth rate once the saturation is achieved. On the other hand, sufficient precursor purge length is required to separate the different precursor sub-cycles (middle). Insufficient purging results in increased GPC (and poor film quality) due to gas-phase reactions. Once the purging length is sufficient, the GPC remains constant. The controlled layer-by-layer film growth enabled by the precursor saturation provides highly linear film growth with the number of ALD cycles applied (right).

The different precursor types used in the ALD processes of magnetic materials discussed in this review are sketched in Fig. 7. Metalorganic β-diketonates and metallocenes are widely used ALD precursors due to their robustness and viable self-terminating chemical reactions. On the other hand, due to their low reactivity, these precursors often need a strong oxidizer (e.g., O_3) as the second precursor. In the case of highly reactive metal halides, water can be used as the oxygen source but, in turn, corrosive by-products (e.g., HCl) are formed in the surface reactions. Metal amidinates are relevant precursor choices for both metal oxide water processes and for the deposition of metallic thin films.[32,98–100] However, the amidinates can suffer from low thermal stability due to the relatively weak metal-nitrogen bonding. Iminoalkoxides and ketoimidinates, composed of both strong metal-oxygen and weak metal-nitrogen bonds, can overcome this issue

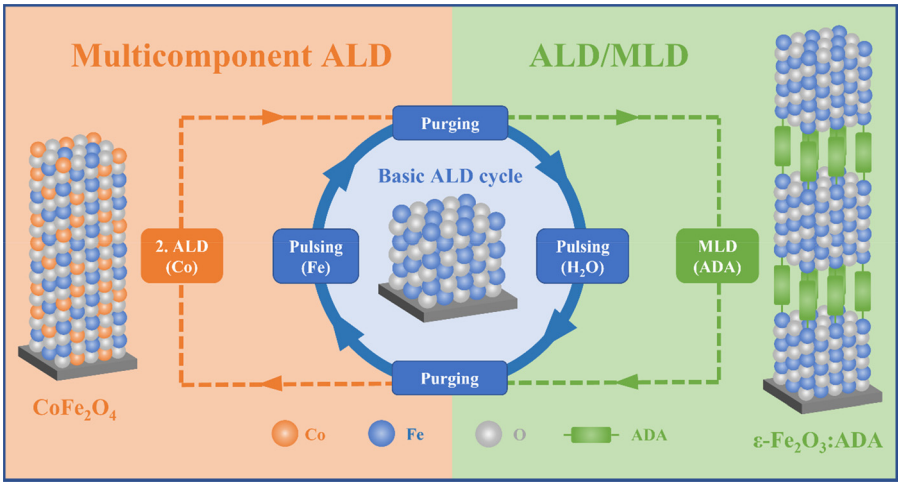

FIG. 6. Schematic illustration of multicomponent ALD for doped/ternary/quaternary inorganic thin films (left), and ALD/MLD for inorganic–organic thin films (right) through the use of supercycle sequencing. The basic ALD cycle consisting of a sequential pulsing of two precursors is shown in the middle. By utilizing the supercycle method, the basic ALD cycle can be combined with another (or several) ALD cycle(s) to bring another (or more) metal component(s) to the material, or with an MLD cycle to combine monomolecular organic layers with inorganic layers. In both cases, high-precision engineering of the different material layers and thereby the overall chemical composition of the resultant thin film is achieved. In our example here, the basic ALD process is for iron oxide thin films; the multicomponent ALD approach is for ternary $CoFe_2O_4$ spinel films and the ALD/MLD approach for ε-Fe_2O_3:ADA superlattice films.

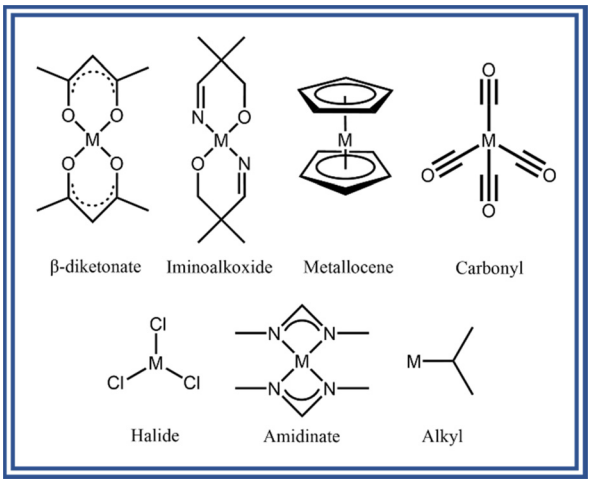

FIG. 7. Metal precursor types used in the ALD processes of magnetic thin films.

by combining the stability of metal alkoxides while preserving the high reactivity of metal amidinates and diketiminates.[101,102] Drawing the inference, each precursor type has its advantages and disadvantages, which highlights the importance of having a large variety of precursors to meet the demands of various ALD processes.

All the metal precursors employed (and their vaporization temperatures) in the ALD processes of different magnetic thin films are listed in Table I based on the ligand type. The classifications are not punctual as, for instance, β-diketonates would belong to the alkoxides but due to their well-established role as ALD precursors, using a separate precursor class for them is justified. All the typical ALD precursor types are well represented, including various metal β-diketonates, metallocenes, metal halides, and amidinates. Based on the number of references of each precursor, it can be deduced that the use of $M(thd)_x$ (M = metal) and $M(cyclopentadienyl)_2$ are the most common. There are also various heteroleptic derivatives of these well-known precursor types such as N,N,N′,N′-tetramethyl-ethylenediamine [bis(acetylacetonate)] nickel(II) and ethylcyclopentadienyl cobalt(II). The purpose of these modifications is to improve the reactivity and to increase the growth rate or decrease the viable deposition temperature range compared to the standard precursor molecule.[103,104] Some of the metal amidinates such as M(N,N′-diisopropylacetamidinato)$_2$ and M(1,4-di-tert-butyl-1,3-diazabutadienyl)$_2$ have also been used in several reports while there are only individual reports of metal carbonyl precursors. The ALD processes of some of the precursors in Table I are highlighted in the upcoming Sec. IV.

IV. ALD PROCESSES OF MAGNETIC THIN FILMS

Like for other ALD applications, the majority of the processes developed for magnetic thin films are metal oxide processes. The binary processes so far developed are almost exclusively for different iron oxides known for their versatile magnetic properties;[220,221] these are discussed in Sec. IV A. In addition to the iron oxides, especially metallic cobalt thin films (Sec. IV C) have drawn notable attention owing to their interesting magnetic properties in combination with their attractive electrical characteristics. In this section, the ALD processes developed for magnetic thin films are systematically summarized, starting from binary oxides (Table II), and ternary and quaternary oxides (Table III), then moving to the metals (Table IV), and ending up with short segments on 2D chalcogenides (Table V) and metalorganic thin films (Table VI).

A. Binary oxides

Among the binary oxides, the focus in ALD research (as far as the magnetic property characterization is included) has been on the mixed-valence magnetite Fe_3O_4. These thin films are typically fabricated using a two-step process: deposition of trivalent α-Fe_2O_3 and its post-deposition reduction to Fe_3O_4 through annealing under a reductive atmosphere.[38,46,128,142–145,147–151] The most common ALD precursors in these depositions have been ferrocene and O_3. The final film composition depends strongly on the reductive annealing conditions: insufficient reduction may leave behind iron(III) oxides as impurity phases while excessively strong reduction leads to metallic iron.[38] Interestingly, magnetite films have also been obtained *in situ* using ferrocene by controlling the oxygen source dosing.[61,152] In both approaches, though, one of the main challenges is the phase purity of Fe_3O_4, as iron(III) oxide traces tend to remain in the films.[143,144,146,152]

The versatility of different ALD processes for the trivalent hematite α-Fe_2O_3 films is notably wider compared to the magnetite case, but the final magnetic-property characterization of these films is only seldomly done (high RT coercivity recently demonstrated).[189] Instead, the α-Fe_2O_3 films are often characterized for their electrical and optical properties having the eye on other than magnetic applications.[156,157] The often-used ferrocene precursor has several advantages, such as commercial availability, thermal stability, and easy handling,[40] but it unfortunately requires the use of a strong oxidizer (O_3) or at least a high deposition temperature (350–450 °C).

From Table II, it can be seen that besides the ferrocene, there is a wide variety of iron precursor alternatives for the α-Fe_2O_3 depositions. Avila *et al.*[98] deposited amorphous iron oxide thin films well below 200 °C from iron bisamidinate [Fe(^{t}Bu-MeAMD)$_2$] and water. As shown in Fig. 8, a clear saturation of the iron precursor was obtained over a rather wide deposition temperature range. However, an excessive purging time of 30 s was required to remove all physisorbed Fe(^{t}Bu-MeAMD)$_2$ from the reactor.[98] Peeters *et al.*[101] demonstrated the suitability of a water-assisted ALD for amorphous α-Fe_2O_3 films at 105–150 °C using iron ketoiminate Fe(ipki)$_2$ precursor, motivated by its mixed oxygen and nitrogen bonding to the metal ion, which was anticipated to provide both high stability of diketonates and high reactivity of diiminates. On the other hand, Selvaraj *et al.*[219] introduced a novel iron amide precursor, Fe(btmsa)$_2$, for the *in situ* deposition of α-Fe_2O_3 films with moderate crystallinity at relatively low temperatures (150–175 °C) using H_2O_2 as the oxidizer. All these processes showed self-terminating chemistry, surface saturation, and linear film growth at low or moderate temperatures and without the need for O_3.

Arguably the most fascinating material among the iron oxides for the next-generation spintronic devices is ε-Fe_2O_3 due to its extremely strong RT magnetic coercivity and ferroelectric properties.[29] Fabrication of phase-pure ε-Fe_2O_3 has been highly challenging in bulk form due to its metastable nature; ε-Fe_2O_3 is easily transformed to the more stable α-Fe_2O_3 and γ-Fe_2O_3 polymorphs. Excitingly, the deposition of *in situ* crystalline ε-Fe_2O_3 thin films has been successful

TABLE II. ALD processes for magnetic binary oxide thin films. The criterion for a material to be included in this list is that the magnetic properties have been investigated for this material at least in one of the publications. AOO = anodic aluminum oxide, CNC = carbon nanocoil, PZN-PT = $Pb(Zn_{1/3}Nb_{2/3})O_3$-$PbTiO_3$, PMN-PT = $_{0.67}Pb(Mg_{1/3}Nb_{2/3})O_{3}$-$_{0.33}PbTiO_3$, FTO = fluorine-doped tin oxide, YSZ = yttrium stabilized zirconium oxide, PEN = polyethylene naphthalate.

	ALD process parameters						
Material	Precursors [Subl. Temp. (°C)]		Dep. Temp. (°C)	GPC (Å)	Substrate	Cryst. Cond.	References
Fe_3O_4	$Fe(cp)_2$ (80–100)	O_3	200–500	0.07–0.3	Si, Si/SiO_2, ZnO, AAO, AAO/SiO_2, AAO/ZrO_2, CNC/Al_2O_3, graphene	400–450/Ar or N_2, H_2	38,46,71,128,141–145,147–151
	$Fe(cp)_2$	O_3	300–500	0.32–0.41	Si:SnO_2	as-dep.	146
	$Fe(cp)_2$	O_2	400	⋯	Si, AAO	400/Ar, H_2	61,152
	$Fe(cp)_2$ (150)	O_2	350–450	3	Si, AAO, Si/SiO_2/Pt, Pt/PZN-PT, PMN-PT	as-dep.	61,152–155
	$[Fe(O^tBu)_3]_2$ (100)	H_2O	130–170	0.25–0.26	AAO, AAO/SiO_2, AAO/ZrO_2	400/Ar, H_2	36,46,128–130
	$Fe(2,4\text{-}C_7H_{11})_2$ (55)	H_2O_2	65–120	0.4–0.6	Si, SiO_2, FTO	as-dep.	187
	DMAMFc	O_3	325–450	0.14–0.70	Si/SiO_2	450 / N_2, H_2	144
α-Fe_2O_3	$Fe(cp)_2$ (80–100)	O_3	200–250	0.2–1.4	Si, Si/SiO_2, FTO, FTO/m-WO_3	as-dep.	156,157
	$Fe(cp)_2$ (55)	O_2	350–600	0.6–1.4	Si, AAO	as-dep.	223
	$Fe(2,4\text{-}MeCp)_2$ (55)	O_3	65–120	0.5–0.9	Si, SiO_2, FTO	as-dep.	187
	$Fe(btmsa)_2$ (65)	H_2O_2 (35)	100–225	0.35	Si	as-dep.	219
	$Fe(thd)_3$ (114)	O_3	138–380	0.11–0.12	glass, α-Al_2O_3, Si, MgO	as-dep.	105,106
	$Fe(^tBu\text{-}MeAMD)_2$	H_2O	130–200	0.55	Si	500/air	98
	TBF (65)	O_2 plasma	150–350	0.2–1.2	Si/SiO_2	as-dep.	188
	$FeCl_3$ (175)	H_2O or H_2O/O_2	200–500	0.2–1.0	Si, quartz, glass, FTO	as-dep.	189,198,224
	$Fe(acac)_3$ (80)	O_3	25–230	⋯	Si/SiO_2/Al_2O_3, YSZ	⋯	121,122
	$Fe(^ipki)_2$ (100)	H_2O	100–275	0.47	Si/SiO_2, FTO	500/air	101
	DMAMFc	O_3	230	0.25	TiO_2, F:SnO_2	as-dep.	191
	$(DIPPA)_2Fe$ (80)	Ar/H_2O plasma	23–25	1.5	Si, PEN	Amorphous	99
ε-Fe_2O_3	$FeCl_3$ (158)	H_2O or H_2O/O_2	260–300	1.0–0.65	Si, Si/SiO_2, glass	as-dep.	26,27,189
Ni_xO	$Ni(acac)_2$	•O	200	⋯	Si, Si/SiO_2, glass	as-dep.	125
	$Ni(cp)_2$ (110)	O_3	230	0.92	Si/SiO_2	as-dep.	185
	$Ni(thd)_2$ (115)	O_3	200	0.2	Si, glass, AAO	as-dep.	114
	$Ni(^tBu_2DAD)_2$ (150)	O_3	185–200	0.12	Si/SiO_2, Si/TiN	as-dep.	212

through a simple ALD process at 260–300 °C using $FeCl_3$ and H_2O precursors.[26,27] Until now, it is the only known ALD process for this metastable iron(III) oxide polymorph.

Also the antiferromagnetic NiO should be underlined here as there are only few ALD studies on AFM materials.[222] Most appealingly, Napari *et al.*[125] recently deposited *in situ* crystalline nonstoichiometric $Ni_{0.7}O$ thin films through PE-ALD using $Ni(acac)_2$ as the metal precursor and demonstrated the antiferromagnetic nature of the films with magnetization and exchange bias measurements.

B. Ternary and quaternary oxides

Spinel-type ferrites (metal substituted Fe_3O_4) and $BiFeO_3$ are the target materials in most of the ALD process developments related to the magnetic ternary and quaternary oxides. The majority of the processes in Table III are based on well-established metal precursors (metallocenes, β-diketonates), presumably due to the challenge of finding compatible metal precursors for multicomponent ALD. The magnetic ternary and quaternary metal oxide thin films have been fabricated either by direct deposition or via deposition of individual binary layers

TABLE III. ALD processes for magnetic ternary and quaternary metal oxides; the criterion for a material to be included in this list is that the magnetic properties have been investigated for this material at least in one of the publications. HOPG = highly oriented pyrolytic graphite, CNT = carbon nanotube, R = La, Sm, Tb, Y, Yb, or Lu.

	ALD process parameters					
Material	Precursors [Subl. Temp. (°C)]		Dep. Temp. (°C)	GPC (Å)	Substrate	Cryst. cond.	Reference
$Co_xFe_{3-x}O_4$	$Fe(cp)_2$ (100), $Co(cp)_2$ (100)	O_3	230	···	Si/SiO_2	700/Ar	160
	$Fe(cp)_2$ (100), $Co(cp)_2$ (90)	O_3	250	0.4–0.5	Si, AAO, $SrTiO_3$	as-dep.	40,158,159
	$Fe(thd)_3$ (115), $Co(thd)_2$ (110)	O_3	185–310	0.12–0.15	Si, glass, MgO, α-Al_2O_3	$800/O_2$	108
	$Fe(thd)_3$ (130), $Co(thd)_2$ (120)	•O	200	CoO:0.7, Fe_2O_3:0.5	Si, $SrTiO_3$	$450–750/O_2$	107
	$Co(cp)_2$ (90), $Fe(^ipki)_2$ (130)	O_3	250	···	$SrTiO_3$/ $Sr_3Al_2O_6$	as-dep.	44
$Co_yZn_zFe_xO_4$	$Fe(cp)_2$ (100), $Co(cp)_2$ (100), $Zn(Et)_2$	O_3 H_2O	230 80	···	Si/SiO_2	700/Ar	160
$Ni_xFe_{3-x}O_4$	$Fe(cp)_2$ (100), $Ni(cp)_2$ (80)	O_3	200	0.3	Si	700/Ar	40
$Zn_xFe_{3-x}O_4$	$Fe(cp)_2$ (100–148) $Zn(Et)_2$ (23)	O_2 or O_3 H_2O	230–400 80–200	···	Si/SiO_2, Si/Si_3N_4	400–800/Ar or air	161,162
$(Mn,Co)_3O_4$	Mn(thd)3 (116) Co(thd)2 (93)	O_3	140–160	0.2	Si/SiO_2	as-dep.	112
$(Co_{1-x}Ni_x)_3O_4$	$Co(thd)_2$ (90) $Ni(thd)_2$ (115)	O_3	200	0.2	Si, glass	as-dep.	113
$Y_3Fe_5O_{12}$	$Y(cp)_3$ (150) $Fe(cp)_2$ (80)	H_2O O_3	220	Y_2O_3:0.92 Fe_2O_3:0.16	$Y_3Al_5O_{12}$	$700–1000/O_2$	166
$Gd_xFe_yO_z$	$Fe(^ipki)_2$ (100–130) $Gd(DPDMG)_3$ (120–135)	O_3	250	FeO:0.4 GdO:0.6	Si, Si/SiO_2	$800/O_2$	140
	$Fe(cp)_2$ (90) $Gd(DPDMG)_3$ (120–135)	O_3	250	FeO:0.1 GdO:0.6	Si, Si/SiO_2	$800/O_2$	140
	GdFe $(O^tBu)_6(C_5H_5N)_2$ (150–170)	O_3	200	0.19	Si/SiO_2	$800/O_2$	133
(Fe, Co,Ni) ZnO	$Fe(cp)_2$ (80) $Co(cp)_2$ (80) $Ni(cp)_2$ (80) $Zn(et)_2$	O_3 H_2O	180	1.5	Si/SiO_2	as-dep.	167,168
$Ru:Fe_2O_3$	$Ru(EtCp)_2$ $FeCl_3$	H_2O/O_2	270–360	···	Si	as-dep.	189
$BiFeO_3$	$Bi(dmb)_3$ (85) $[Fe(O^tBu)_3]_2$ (105)	H_2O	140–150	···	Si/SiO_2/Pt	$500–550/N_2$	41,89,131,132
	$Bi(ph)_3$ (200), $Fe(thd)_3$ (200)	O_3	220	···	$Si/SrTiO_3$	250–500/air	88
	$Bi(ph)_3$ (200), $Fe(cp)_2$ (180–185)	O_3	250–290	0.44–0.6 0.3	Si/SiO_2, Si/SiO_2/ Ti/Pt	450–600/air or O_2 or N_2	163,164
	$Bi(mmp)_3$ (135–145), $Fe(cp)_2$ (90–91)	O_3	200–250	···	Si/SiO_2, $SrTiO_3$, Nb:$SrTiO_3$, YSZ, HOPG	27–740/vac. or air	135,136,138
	$Bi(mmp)_3$ (140), $Fe(cp)_2$ (90)	O_3	250	···	Kapton	Amorphous	137,139

TABLE III. (*Continued.*)

Material	ALD process parameters					Cryst. cond.	Reference
	Precursors [Subl. Temp. (°C)]		Dep. Temp. (°C)	GPC (Å)	Substrate		
	$Bi(thd)_3$ (150), $Fe(thd)_3$ (130)	•O	190–230	0.65 0.49	Si, $SrTiO_3$, Nb: $SrTiO_3$	450–750/O_2	110,111
	$Bi(thd)_3$ (140) $Fe(thd)_3$ (120)	H_2O	250	0.05	Nb:$SrTiO_3$	···	82
	$Bi(thd)_3$ (168) $Fe(cp)_2$ (90)	O_3	220–250	0.2	Si/SiO_2, $SrTiO_3$, CNT	650/O_2	115
	$(CH_3)_3Bi$ $C_6H_8Fe(CO)_3$	H_2O	490–520	0.87	Si/$LaNiO_3$	as-dep.	197
$ErFeO_3$	$Fe(cp)_2$ (60) $Er(thd)_3$ (160)	O_3	375	0.021 0.004	Si/SiO_2	as-dep.	120
	$Fe(thd)_3$ (110) $Er(thd)_3$ (150)	O_3	280–300	0.01	Si/SiO_2	650–700/N_2	109
$Ho_2Ti_2O_7$	$Ho(thd)_3$ (125) $Ti(OCH(Me)_2)_4$ (35)	O_3	300	0.25 0.45	Si/SiO_2	600–1000/N_2	134
Co:TiO_2	$Ti(OMe)_4$ (130) Co $(acac)_3$ (155)	O_3, H_2O	300	0.15–0.4	Si/SiO_2, glass	650/N_2 400/N_2, H_2	127
$RMnO_3$	$R(thd)_3$ (123–162) $Mn(thd)_3$ (123)	O_3, •O	225–350	0.18–0.9	Si, $LaAlO_3$, $SrTiO_3$, YSZ	600–1000/N_2 or O_2	116–119
	$La(thd)_3$ (175) $Mn(thd)_3$ (115)	O_3	200–400	0.1–0.2	Si, glass, Al	as-dep.	24
$La_{1-x}Ca_xMnO_3$	$La(thd)_3$ (185) $Mn(thd)_3$ (135) $Ca(thd)_2$ (195)	O_3	180–325	···	Si, MgO, $SrTiO_3$, $LaAlO_3$, SiO_2, Al_2O_3	850/O_2	85
$La_{1-x}Sr_xMnO_3$	$La(thd)_3$ $Mn(thd)_3$ Sr.,$(thd)_2$	O_3	283, 450	···	Si/SiO_2	Amorphous	39

followed by post-deposition annealing. The latter procedure is required especially when the deposition conditions of the different metal precursors are not compatible. For instance, Zhang *et al.*[162] fabricated $ZnFe_2O_4$ films through the deposition of double-layer Fe_3O_4/ZnO structures. The magnetite layer was deposited at 400 °C using ferrocene and O_2, while the ZnO layer was deposited at 200 °C using diethylzinc and H_2O. The $ZnFe_2O_4$ film was then obtained by annealing in air at 500 °C.

Remarkably, Chong *et al.*[40] deposited *in situ* crystalline ferrimagnetic $Ni_xFe_{3-x}O_4$ and $Co_xFe_{3-x}O_4$ films through supercycles of the corresponding metallocenes and ozone. These films had excellent RT ferrimagnetic properties without any post-deposition treatments, in contrast to most of the reports on ternary ferrites. The elemental composition could also be easily controlled through the ALD cycles as shown in Fig. 9(a): the atomic Fe:M (M = Co, Ni) ratio in the films was found to linearly increase with the increased Fe:M pulsing ratio, thus demonstrating the high controllability of the depositions.

In another report, having the flexible devices such as magnetoresistive sensors in mind, engineering-wise elegant $CoFe_2O_4$ thin films were fabricated taking advantage of water-soluble sacrificial $Sr_3Al_2O_3$ interlayers.[44] After the growth of polycrystalline $CoFe_2O_4$, the sacrificial layer was removed using a polymer support or the direct floating method. Finally, the magnetic layer could be planted on a desired substrate such as polyethylene terephthalate [PET; Fig. 9(b)] without compromising the film quality [Fig. 9(c)] or functional properties; the magnetic properties of $CoFe_2O_4$ were not affected by the exfoliation processes and, most important for future flexible magnetic applications, the magnetic properties were probed under different bending radii of the flexible substrate.[44]

Even though the perovskites are known for their versatile magnetic properties,[225] only $BiFeO_3$ among the ALD-grown perovskite films has been well investigated (Table III). The great interest in $BiFeO_3$ derives from its RT ME coupling, which is highly uncommon for single-phase materials but a prerequisite for any application which utilizes the coupling of ferromagnetic and ferroelectric properties.[110,226] The multiferroic properties of $BiFeO_3$ are enhanced at the nanoscale, and, thus, high-quality $BiFeO_3$ thin films are of high importance.[131,227]

Zhang *et al.*[82] and Akbashev *et al.*[135] initially demonstrated the fabrication of $BiFeO_3$ films via deposition of Bi_2O_3 and Fe_2O_3 binary layers at 250 °C, followed by post-deposition crystallization of the $BiFeO_3$ phase through annealing. On the other hand, Liu *et al.*[197]

TABLE IV. ALD processes for magnetic metallic thin films; the criterion for a material to be included in this list is that the magnetic properties have been investigated for this material at least in one of the publications. DMP = dimethylaminopropyl.

	ALD process parameters						
Material	Precursors [Subl. Temp. (°C)]		Dep. Temp. (°C)	GPC (Å)	Substrate	Cryst. Req.	Reference
Co	$Co(cp)_2$ (90)	O_3	240–330	0.22–0.45	Si/SiO_2,AAO/TiO_2	400–430/Ar, H_2	70,128,170
	$Co(cp)_2$ (90)	H_2O, H_2	240–330	⋯	AAO/TiO_2	as-dep.	70
	$Co(cp)_2$ (78)	NH_3 plasma	250–400	0.21–1.4	Si, Si/SiO_2, Si-H	as-dep.	31,171–174,177
	$Co(cp)_2$ (78)	N_2/H_2 plasma	150–450	0.26–0.65	Si-H, Si/SiO_2, Ru, Ta	as-dep.	175,176
	$Co(MeCp)_2$ (56)	NH_3 plasma	300	0.4–0.6	Si, Si/SiO_2	Amorphous	186
	$Co(EtCp)_2$	NH_3 plasma	125–225	0.12	Si/SiO_2	as-dep.	104
	$Co(^iPr\text{-}MeAMD)_2$ (65)	H_2	340–350	0.12–0.5	Si/SiO_2, Si-H, C, glass, WN	as-dep.	171,204,205,207
	$Co(^iPr\text{-}MeAMD)_2$ (65)	NH_3	350	0.26	Si/SiO_2, Si-H	as-dep.	207
	$Co(^tBu_2DAD)_2$ (128–130)	HCO_2H (23)	160–240	0.95–0.98	Ru, Pd, Pt, Cu	as-dep.	208–210
	$Co(^tBu_2DAD)_2$ (130)	$(CH_3)_3CNH_2$ or $(CH_3CH_2)_2NH$ or $N(CH_2CH_3)_3$	170–200	0.35–0.98	Ru, Cu, Pt, Sb_2Te_3	as-dep.	30,32,33,210
	$Co(^tBu_2DAD)_2$ (115)	H_2	200	⋯	Si/SiO_2/Ru	as-dep.	211
	Co $(^iPrMeCOCN^tBu)_2$ (130)	$BH_3(NHMe_2)$ (80)	180	0.07	Si/SiO_2/Ru	⋯	102
	CoAMD (80)	H_2	215–290	0.04–0.05	SiO_2/TaN/Cu	as-dep.	213,214
	CoAMD (80)	H_2O	180–270	0.3	Si/SiO_2, MgO	200–500/D_2 or H_2 or D or Al	215,216
	Co(CpAMD) (75)	NH_3 plasma	200–250	0.5	Si, Si/SiO_2	⋯	218
	$CoCl_2$(TMEDA) (170)	H_2O	225–300	0.06–0.38	Si/SiO_2, TiN	250/N_2, H_2	201
	$CoCl_2$(TMEDA) (140)	$Zn(DMP)_2$ (40)	155–165	0.3	Si/SiO_2, Si/SiO_2/Au, Si/SiO_2/Pt	Amorphous	202
	^{t}Bu-Allyl$Co(CO)_3$ (35)	$H_2NN(CH_3)_2$	140	0.5	Si-H	⋯	196
	$Co_2(CO)_8$ (25)	H_2 or N_2 plasma	75–110	1.2	Si	⋯	194
	$CpCo(CO)_2$ (45)	$(CH_3)_3CNH_2$ (25)	275–325	0.45	Si, Si/Pt, glass, sapphire	500/N_2	195
	$CpCo(CO)_2$ (20)	H_2 or N_2 plasma	125–175	1.1	Si	⋯	194
	$TMSCpCo(Co)_2$ (40)	$(CH_3)_3CNH_2$ (25)	275–325	0.30	Si, Si/Pt, glass, sapphire	500/N_2	195
Co_3Sn_2	$CoCl_2$(tmeda) (170–185) TBTH (30)	⋯	170–200	0.7–1.3	Si, glass	as-dep.	10,203
Co-Pt (NP)	$Co(cp)_2$ (85) $(MeCp)PtMe_3$ (75)	O_3 O_2	250 300	0.46	Si/SiO_2	700/N_2, H_2	178
$CoFe_2$	CoAMD $Fe(^tBu\text{-}MeAMD)_2$	H_2	250	0.08–0.12	PMN-PT	⋯	217
Co_xC_y	$Co(acac)_2$ (155)	C_3H_7OH	300–390	⋯	Si/SiO_2, AAO	as-dep.	232
	$Co(^iPr\text{-}MeAMD)_2$ (50)	H_2 plasma	70–160	0.66	Si, glass	as-dep.	206

TABLE IV. (*Continued.*)

Material	ALD process parameters: Precursors [Subl. Temp. (°C)]		Dep. Temp. (°C)	GPC (Å)	Substrate	Cryst. Req.	Reference
Ni	$Ni(cp)_2$ (90)	O_3	150–330	0.12–0.3	Si/SiO_2, AAO, AAO/TiO_2, CNC/Al_2O_3, graphene	400–450/Ar or N_2, H_2	70,128,149,151,179,180
	$Ni(cp)_2$ (80)	H_2O, H_2 plasma	160–175	0.13–0.33	Si/Al_2O_3, GaAs/Al_2O_3	350/N_2, H_2	181
	$Ni(cp)_2$ (90)	H_2O, H_2	270–330	⋯	AAO/TiO_2	as-dep.	70
	$Ni(cp)_2$ (50)	H_2O, •H	165	1.9	Si/SiO_2/TiN, TaN	as-dep.	182
	$Ni(cp)_2$ (80)	NH_3 plasma	260–280	0.2	Si/SiO_2	as-dep.	183
	$Ni(cp)_2$ (73)	•NH_2	250	0.63	Si-H, Si/SiO_2	as-dep.	233
	$Ni(^iPr\text{-}MeAMD)_2$ (55)	H_2	250	0.04	Si/SiO_2, C, glass, WN	as-dep.	204
	Ni(iPrMeCOCNtBu)$_2$ (120)	$BH_3(NHMe_2)$ (80)	180	0.09	Si/SiO_2/Ru	⋯	102
	$Ni(tBu_2DAD)_2$ (140)	$(CH_3)_3CNH_2$ or $(CH_3CH_2)_2NH$ or $N(CH_2CH_3)_3$	160–220	0.6	Pt, Ru, Cu	as-dep.	100
	$Ni(acac)_2$ (180–200)	CH_3OH or CH_3CH_2OH or $CH_3CH_2CH_2OH$	250–300	0.08	Si/SiO_2, AAO	as-dep.	123
	$Ni(acac)_2$tmeda (95)	N_2H_4 (40)	240–280	2.1	Si/SiO_2	as-dep.	103
	$Ni(acac)_2(py)_2$ (130)	N_2H_4 (40)	225–250	0.79	Si/SiO_2	as-dep.	103
	Ni(Chex)cp (50)	NH_3 or H_2	320–340	0.27–1.1	Si/SiO_2, graphene	as-dep.	190
NiFe	$Ni(cp)_2$ (80), $Fe(cp)_2$ (100)	O_3	200	0.26	Si/SiO_2, AAO	400/Ar, H_2	165
	$Ni(cp)_2$ (80), $Fe_2(O^tBu)_6$ (100)	H_2O, H_2 plasma	170	0.15–0.20	Si, Si/Al_2O_3, $Si/GaAs/Al_2O_3$	380/N_2, H_2	42
Fe	$Fe(^tBu\text{-}MeAMD)_2$ (75)	H_2	250	0.08	Si/SiO_2, C, glass, WN	as-dep.	204
	Fe ($^tBuMeCOCN^tBu)_2$ (120)	$BH_3(NHMe_2)$ (80)	225	0.07	Si/SiO_2/Ru	⋯	102

TABLE V. ALD processes for magnetic 2D thin films; the criterion for a material to be included in this list is that the magnetic properties have been investigated for this material at least in one of the publications.

Material	ALD process parameters: Precursors [Subl. Temp. (°C)]		Dep. Temp. (°C)	GPC (Å)	Substrate	Cryst. Req.	Reference
CoSe	$Co(acac)_2$ (175)	H_2Se	330–440	2.6	Si/SiO_2	as-dep.	124
NiSe	$Ni(acac)_2$ (170)	H_2Se	340–410	5.0	Si/SiO_2	as-dep.	124

TABLE VI. ALD/MLD processes for magnetic metal-organic materials; the criterion for a material to be included in this list is that the magnetic properties have been investigated for this material at least in one of the publications. TCNE = tetracyanoethylene.

	ALD process parameters						
Material	Precursors [Subl. Temp. (°C)]		Dep. Temp. (°C)	GPC (Å)	Substrate	Cryst. Req.	Reference
$V(TCNE)_x$	$V(CO)_6$ (RT)	TCNE (RT)	RT	9.8	Si, glass	···	192,193
$Co(TCNE)_x$	$Co_2(CO)_8$ (RT)	TCNE (RT)	RT	8.0	Si	···	193
$Co_xV_y(TCNE)_z$	$V(CO)_6$ (RT) $Co_2(CO)_8$ (RT)	TCNE (RT)	RT	···	Si	···	193

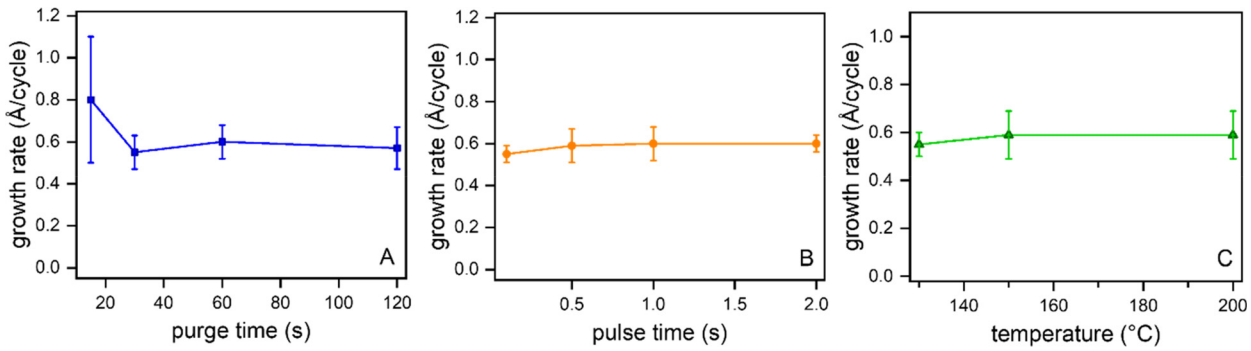

FIG. 8. Characteristics of the ALD process for iron oxide thin films from Fe(^{t}Bu-MeAMD)$_2$ and water: effects of (a) purge time, (b) pulse time, and (c) deposition temperature on the growth rate. The purging and pulsing times were investigated at 150 °C. The deposition process revealed saturation of the Fe precursor already with 0.5 s pulse time and a wide temperature window with a constant growth rate, but an extensive purging of 30 s was required to avoid overlapping sub-cycles. Adapted with permission from Avila *et al.*, ACS Appl. Mater. Interfaces **7**, 16138 (2015). Copyright 2015 American Chemical Society.[98]

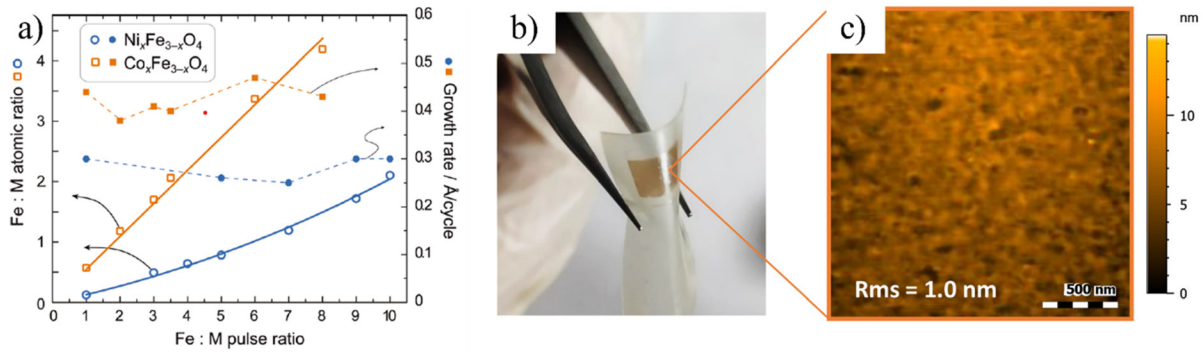

FIG. 9. (a) Dependence of the Fe:M (M = Co, Ni) atomic ratio and growth rate of $M_xFe_{3-x}O_4$ films on the Fe:M pulsing ratio. Essentially linear dependence of the pulsing ratio and atomic ratio were achieved while the growth rate remained practically constant for all pulsing ratios for both materials. Reprinted with permission from Chong *et al.*, Chem. Mater. **22**, 6506 (2010). Copyright 2010 American Chemical Society.[40] (b) and (c) Intact $CoFe_2O_4$ thin film transferred to (transparent) PET substrate through water immersion and the surface morphology of the transferred, smooth, and uniform, $CoFe_2O_4$. Reproduced with permission from Salles *et al.*, ACS Appl. Mater. Interfaces **14**, 12845 (2022). Copyright 2022 Authors, licensed under a Creative Commons Attribution (CC BY) License.[44]

fabricated *in situ* epitaxial ultrathin $BiFeO_3$ films at 500 °C. Later, the ALD research related to $BiFeO_3$ has solely focused on the two-step fabrication process, which allows moderate deposition temperatures as the crystallization occurs after the deposition. However, the post-deposition annealing must be well-controlled since it can have a major impact on the final Fe:Bi ratio due to the different evaporation tendencies of the two metal species especially at high annealing temperatures.[164] Obviously, the final metal ratio can be also controlled by the initial Fe:Bi ratio defined through the ALD process.[89] Thicknesses of the as-deposited binary layers can also play an important role in the final structure.[88] Deposition of thicker (few nm) BiO_x layers may result in Bi_2O_3 crystallites already during the deposition, whereas very thin

layers (few Å) prevent the formation of binary crystallites and improve the crystallization process of $BiFeO_3$ during the post-deposition annealing through high cation intermixing and shorter diffusion paths for Fe and Bi.[88,164]

An appropriate heterometallic precursor could bypass the need to combine several different metal precursor sources and ALD cycles. The single heterometallic precursor enables the fixed stoichiometry, thus allowing robust process control. For the ternary magnetic materials, stoichiometric and phase-pure $GdFeO_3$ films have been successfully deposited using the bimetallic $[GdFe(O^tBu)_6(C_5H_5N)_2]$ single-source precursor with the targeted 1:1 ratio for Gd and Fe.[133] On the other hand, similar well-behaving bimetallic precursors may not be available for all the intended metal combinations and ratios. Another option for a single metal precursor source would be to simply mix (mechanically or chemically) two or more precursor powders into the desired composition.[228,229] The powder mixture approach is simple and straightforward (compared to the design and synthesis of complex heterometallic precursors), but it may suffer from issues related to the different sublimation behaviors (required heating temperatures and/or sublimation rates) of the two component powders. On the other hand, the powder mixture enables arbitrary metal ratios whereas for the heterometallic precursor the ratio is fixed. Hence, the mixed precursor powder approach could be highly valuable in depositions in which uniform metal doping (especially with a small dopant concentration) is aimed. Indeed, the inherent issue of doping in ALD is that the dopant metal cycles are applied only seldomly, thus resulting rather in layers of dopant along the film thickness than perfectly mixed heterometallic material.

C. Metals and metal alloys

Ferromagnetic 3D transition metals (Fe, Co, and Ni) and their metallic compounds are one of the most important magnetic materials families and are also widely studied in the ALD community, see Table IV. Of course, by far not all publications on metallic thin films listed in the table include investigations of magnetic properties as many of them are focused purely on the ALD process development and also on other applications in microelectronics.

The precursor chemistry of the metallic films is clearly more versatile compared with the metal oxides in Sec. IV A and IV B. Pioneering research on ALD precursors (metal acetamidinate) and deposition of magnetic Co, Fe, and Ni thin films were conducted by Lim *et al.*[204,230] The novel precursors were rather suitable for the traditionally demanding ALD of metallic films due to their convenient intra- and intermolecular forces:[230] the metal-nitrogen bonding of metal acetamidinate is strong enough for adequate thermal stability yet simultaneously allowing high reactivity, whereas the weak intermolecular interactions caused by hydrocarbons at the outer sphere of the molecule results in high volatility. As an example, the cobalt thin films were deposited at 350 °C by using bis(N,N′-diisopropylacetamidinato) cobalt(II) precursor and H_2 as the reducing agent.

Winter and co-workers have done extensive research on 3D transition metal precursor development for metallic thin films.[32,100,102,208,209,231] Cobalt diazadienyl $[Co(tBu_2DAD)_2]$ precursor (available commercially) has especially shown to be a favorable precursor for the deposition of high-quality cobalt thin films.[32,208,209] In Fig. 10(a), the ALD process characteristics of cobalt films deposited using Co $(tBu_2DAD)_2$ and *tert*-butylamine (reductant) precursors are summarized. The film growth clearly saturates with a 3 s $Co(tBu_2DAD)_2$ pulse, the growth is highly linear, and an unambiguous ALD temperature window at a moderate temperature range (170–200 °C) is observed. These close-to-ideal ALD characteristics are further supported by the relatively high GPC (∼1 Å/cycle) and high purity (>98%) of the films.[32] In addition, the depositions were carried out well below the precursor decomposition temperature, unlike the depositions with the cobalt acetamidinate.[204,209,230] Interestingly, the diazadienyl precursors are also highly selective toward metallic surfaces.[32,208]

Similar to metal oxides, the metallic thin films can be either deposited *in situ* or fabricated via deposition of the corresponding metal oxide followed by reductive annealing.[8] The more common (Table IV) way is to reduce the chemisorbed metal precursors *in situ* by using a reducing agent, which is typically NH_3 or H_2 plasma. The reductive reagent is typically used as the second reactant, i.e., the chemisorbed metal precursors are reduced in every cycle. An alternative path is to use plasma as a third "precursor," which is introduced repeatedly after a few cycles of metal oxide deposition. A clear benefit of this two-step process is to preserve the conformality of ALD;[181,182] plasma-enhanced ALD (PE-ALD) has typically poor conformality compared to thermal ALD due to a short lifetime of the plasma species (recombination of ions and radicals). However, when the plasma is used only in between a few layers of metal oxide film growth, a conformal metallic film is obtained while low-temperature reduction is achieved through plasma.

Reduction with plasma is not the only option for the *in situ* metal ALD. Alkylamines are shown to be rather efficient in decomposing cobalt and nickel precursors at moderate temperatures (<200 °C), and with reasonable GPC up to 1 Å/cycle as in the case of the cobalt diazadienyl and tert-butylamine process [Fig. 10(a)]. Recently, Zanders *et al.*[202] introduced a novel alkylation process for cobalt thin films based on Zn aminoalkyl ($Zn(DMP)_2$; DMP = dimethylaminopropyl) as the reductant for $CoCl_2$(TMEDA) as a goal to achieve milder deposition conditions compared with the plasma-enhanced ALD processes while preserving the high conformality of thermal ALD. The alkylation process worked considerably well and the process appears promising, although the films contained a notable amount of carbon impurities (∼20%).[202]

From experimental and theoretical reaction mechanism studies on this new procedure of metal film deposition, it was found that among the alternative reaction pathways shown in Fig. 10(b), elimination through C–C bond formation (pathway 3) was found to be most probable.[202] It was also discovered that the reaction by-product formed in this pathway is unstable and most likely the reason for the high carbon content of the films. These results give excellent insight into the reaction mechanism of the alkylation process and provides novel, plasma-free, possibilities for the deposition of magnetic metal thin films.

In addition to monometallic films, also some magnetic alloys have been fabricated through ALD. Permalloy ($Ni_{80}Fe_{20}$) is a technologically important near-zero magnetostriction soft FM material used in spin valves, for instance.[47] For novel applications, Permalloy thin films are considered potential for magnonics, especially on 3D structures.[42] In the case of bimetallic ALD, one of the challenges is to find suitable conditions where different metals can be reduced in a controlled, saturated way. Originally, Espejo *et al.*[165] fabricated Ni–Fe films with near Permalloy stoichiometry through supercycles of nickel

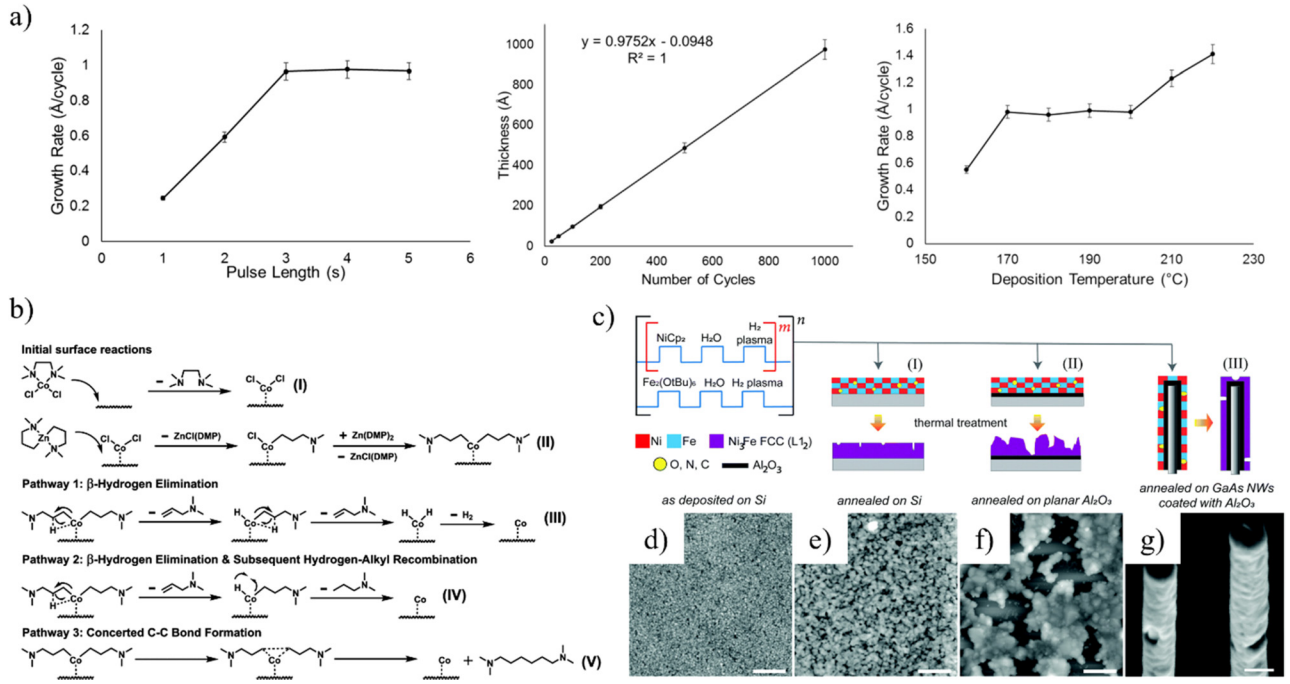

FIG. 10. (a) Effect of $Co(tBu_2DAD)_2$ pulse length on growth rate (GPC; left) of Co metal thin film deposited at 200 °C. Cobalt film thickness vs number of cycles (middle). Effect of deposition temperature on the growth rate (right). Tert-butylamine was used as the second (reductive) precursor. Clear saturation of $Co(tBu_2DAD)_2$ is observed for 3 s pulsing, and highly linear film growth and a distinct temperature window of 170–200 °C is confirmed. Adapted with permission from Kerrigan *et al.*, Chem. Mater. **29**, 7458 (2017). Copyright 2017 American Chemical Society.[32] (b) Initial surface reaction mechanism of $CoCl_2(TMEDA)$ and $Zn(DMP)_2$ on a metal surface (I and II) and three alternative reaction paths (II–V) for the film growth mechanism. The reaction path V (elimination through C-C bond formation) was found most probable. Reprinted with permission from Zanders *et al.*, Chem. Mater. **33**, 5045 (2021). Copyright 2021 American Chemical Society.[202] (c) Schematic representation of the $Ni_{100-x}Fe_x$ PEALD supercycle sequence (m and n define the Ni:Fe ratio and film thickness, respectively) and the effect of substrate on de-wetting caused by annealing process. The de-wetting was more severe on planar Al_2O_3 interface compared to plain Si substrate while GaAs nanowires (NWs) coated with Al_2O_3 interface resulted in random holes along the NW. Atomic force microscopy of (d) as-deposited Permalloy on silicon, (e) annealed Permalloy on silicon, and (f) annealed Permalloy on planar Si/Al_2O_3. (g) Scanning electron microscopy of annealed $GaAs/Al_2O_3/Ni_{100-x}Fe_x$ nanowires. For the as-deposited (27 nm thick) and annealed (23 nm thick) Permalloy film on silicon, the root mean square roughness values were reported 1.2 and 2.1 nm, respectively. Reproduced with permission from Giordano *et al.*, Nanoscale **13**, 13451 (2021). Copyright 2021 the Royal Society of Chemistry.[42]

and iron oxides using metallocenes and ozone, followed by post-deposition reduction to Ni–Fe at 400 °C under H_2 atmosphere. The Ni:Fe stoichiometry was found to linearly follow the pulsing ratio of the Ni and Fe metallocenes, but the annealing induced a major de-wetting effect, resulting in holes in the film structure. Interestingly, though, the de-wetting can be used as a tool for the modification of magnetic properties; the holes can induce domain wall pinning of magnetic domain/crystallites, thus increasing magnetic coercivity. If continuous Permalloy films are desired, other means of deposition are necessary.

Promisingly, Giordano *et al.*[42] achieved better film continuity for *in situ* amorphous Ni-Fe Permalloy by utilizing nickelocene, iron *tert*-butoxide, water, and in-cycle H_2 plasma after each metal oxide cycle [Fig. 10(c)]. The films were crystallized through post-deposition annealing at 380 °C in H_2 and nearly perfect Permalloy stoichiometry ($Ni_{80.4}Fe_{19.6}$) was achieved with the Ni:Fe pulsing ratio of 6. The de-wetting effect was minor on silicon [Figs. 10(d) and 10(e)] but extensive on planar Al_2O_3 surface [Fig. 10(f)], whereas the use of GaAs nanowires with Al_2O_3 interfacial layer (to prevent As sublimation during annealing) created random holes [Fig. 10(g)]. Nevertheless, the films exhibited excellent ME properties, see Sec. VI.[42] Even though these results are of considerable promise, there is still work left to obtain nanohole-free, fully continuous Permalloy films. A suitable seed layer to minimize the de-wetting could be one way to achieve this.

D. Two-dimensional chalcogenides

There is a great drive toward two-dimensional van der Waals materials as they exhibit interesting material properties that differ from the corresponding bulk materials.[234,235] Magnetic ultra-thin vdW materials, composed of a monolayer, few atomic layers, or stacked multilayers, have been studied extensively in the scientific community, but the efforts to investigate the magnetic properties of these ALD-grown materials has been nearly negligible (Table V). Hopkins *et al.*[124] aimed at FM few-layer thick 2D cobalt and nickel selenide (~1:1 atomic ratio) thin films. However, the films were paramagnetic even at 2 K, though the cobalt selenide thin films exhibited stronger magnetization due to the unpaired d electrons of cobalt.

It should be, however, emphasized that ALD is definitely a highly viable deposition technique for 2D materials due to its well-controlled film growth characteristics and, accordingly, various 2D vdW materials such as transition metal chalcogenides and selenides have been deposited

through ALD with the main focus being on their electrical and optical properties.[34,35] Now the interest should be expanded to the magnetic properties as well since these materials could provide new horizons for the next-generation magnetic, multiferroic, and magneto-optical devices.

E. Metal-organics

Magnetic metal-organic thin films can be reached by combining ALD and MLD cycles in an appropriate ratio, typically 1:1. Kao *et al.*[192,193] have reported ALD/MLD processes for known FM metal-organic tetracyanoethylene-based (TCNE) materials, see Table VI.[236] The depositions were carried out at RT. Upon applying separate precursor and purging steps, the film growth proceeded stepwise according to the pulsing sequence. In the case of V(TCNE), the growth rate was 9.3 Å/cycle with $V[TCNE]_{0.63}$ stoichiometry, in addition to some oxidized vanadium species. The films exhibited magnetic characteristics comparable to those reported for corresponding films grown through the chemical vapor deposition (CVD) technique. Most interestingly, the RT ferrimagnetism as well as a magnetoresistive behavior in a magnetic tunnel junction device could be confirmed for the films.[192] These pioneering works demonstrate the huge potential of the ALD/MLD technique for the fabrication of high-quality magnetic metal-organic thin films relevant to future organic spintronics.[237]

V. ENGINEERING OF MAGNETIC THIN FILMS

Nanostructuring and layer-engineering are potentially exciting tools for smart tailoring of the properties of magnetic thin films, and ALD—owing to its unique thin-film growth principle—is an ideal technique to challenge different nanostructuring and layer-engineering approaches. For instance, the ever-pursued PMA of magnetic thin films can be achieved through conformally coated vertical nanotubes. Moreover, by combining ALD with the currently strongly emerging MLD method, it is possible to deposit magnetic inorganic:organic superlattice with an unmatched precision.[87,193] Similarly, 3D structuring allows versatile pathways for complex device engineering. In this section, exciting magnetic multilayer materials and 3D nanostructures engineered through ALD and ALD/MLD are introduced.

A. Nanolaminate and superlattice thin films

Among the ALD-grown magnetic thin films, most extensive layer-engineering efforts have been made for the FiM high-coercivity ε-Fe_2O_3 films (Table VII). This is rather amazing considering the metastability of the ε-Fe_2O_3 phase, and its notoriously difficult bulk synthesis. On the other hand, the ALD-grown ε-Fe_2O_3 films rather allow their intimate combination with both ALD-grown inorganic and MLD-grown organic layers. The thus fabricated nanolaminate and superlattice thin films have been considered interesting material candidates for flexible devices and memory applications.[37,43,199,238]

The most exciting example is the ε-Fe_2O_3:azobenzene films with optically controlled magnetic properties (see Sec. VI).[37] These SL structures consisting of periodic piling of ε-Fe_2O_3 blocks and photoactive azobenzene monolayers were deposited through ALD/MLD. The periodic superstructure can be clearly observed from x-ray reflectivity (XRR) patterns, shown in Fig. 11(a), while the excellent ability to preserve the crystalline ε-Fe_2O_3 phase upon adding increasing number (n) of organic monolayers (n) is seen from grazing incidence x-ray diffraction (GIXRD) patterns, shown in Fig. 11(b).

B. High aspect ratio thin films

A common way to fabricate free-standing magnetic nanotubes is to apply anodic aluminum oxide (AAO) as the 3D substrate. The AAO template can be readily removed by chemical etching after the deposition. Figure 12(a) shows Fe_3O_4 nanotubes fabricated by Zhang *et al.*[61] through ferrocene + O_2 ALD process at 400 °C. In this study, the AAO template was etched in NaOH solution, and the top iron oxide layer was removed by ion milling. Typical for high-aspect ratio

TABLE VII. ALD processes for magnetic nanolaminate and superlattice thin films. TPA = terephthalic acid, ADA = azobenzene-4,4′-dicarboxylic acid.

	ALD process parameters						
Material	Precursors [Subl. Temp. (°C)]		Dep. Temp. (°C)	GPC (Å)	Substrate	Cryst. Req.	Reference
ε-Fe_2O_3:TPA	$FeCl_3$ (158) TPA (180)	H_2O	280	···	Si/SiO_2, Kapton	as-dep.	43,238
ε-Fe_2O_3:ADA	$FeCl_3$ (158) ADA (240)	H_2O	280	···	Si/SiO_2, glass	as-dep.	37
ε-Fe_2O_3-SiO_2	$FeCl_3$ (145–150) $Si_2(NHEt)_6$ (65–67)	O_3	300	···	Si/SiO_2, Si/TiN	as-dep.	86
ε-Fe_2O_3-BiOCl	$FeCl_3$ (135) $BiCl_3$ (164)	H_2O	375	1.8 0.03–0.8	Si, Si/TiN	as-dep.	199
ZnO-Ni	$Zn(Et)_2$ $Ni(cp)_2$ (80)	H_2O O_3	180	···	Si	as-dep.	184
ZrO_2-HfO_2	$ZrCl_4$ (160) $HfCl_4$ (162)	H_2O	300	···	Si, Si/TiN	as-dep.	200
Fe_2O_3-HfO_2							169
ZrO_2-MnO_x	$ZrCl_4$ (157) $Mn(acac)_3$ (183)	O_3	300	···	Si, Si/tiN	as-dep.	126

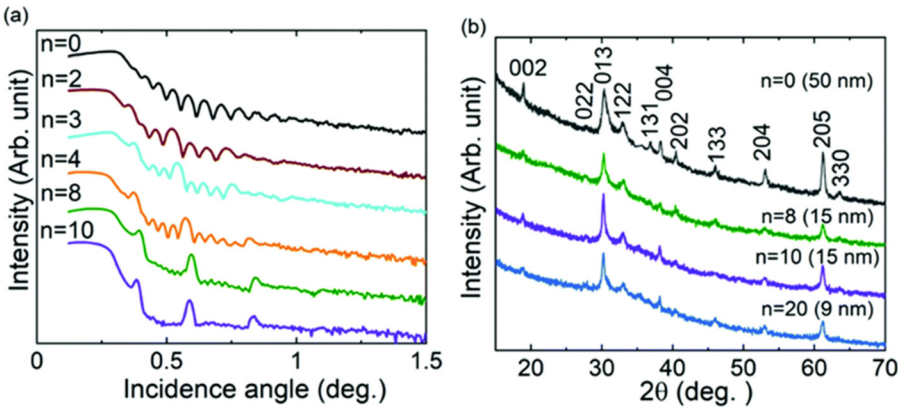

FIG. 11. (a) XRR and (b) GIXRD patterns for ε-Fe_2O_3:ADA superlattice films; the number of individual organic monolayers within the complete SL is indicated with n, while the numbers in the brackets indicate the thickness of each individual ε-Fe_2O_3 block of the SL. In both graphs, data for pristine ε-Fe_2O_3 thin film (n = 0) are shown as a reference. It is seen that the number of small fringes in the XRR increases periodically when n is increased (distinguishable for small n values) while the crystal structure of the pristine ε-Fe_2O_3 is clearly preserved for all SL structures, both features indicating successful SL depositions. Reproduced with permission from Philip *et al.*, J. Mater. Chem. C **10**, 294 (2022). Copyright 2022 the Royal Society of Chemistry.[37]

ALD, the highly crystalline and pinhole-free nanotubes were realized by increasing the precursor exposure time to provide sufficient time for the gaseous molecules to diffuse throughout the 3D structure and reach the deepest cavities. The tube length and diameter were around 30 μm and 100 nm, respectively, while the thickness of the Fe_3O_4 coating was ca. 20 nm.[61] Interestingly, the as-deposited superparamagnetic Fe_3O_4 nanotubes (small particle size) were achieved using a short O_2 pulse length (i.e., low dose) while α-Fe_2O_3 resulted from a higher O_2 dose under the same deposition conditions. These biocompatible superparamagnetic nanotubes could be useful in various biomedical applications, including drug delivery, for which the conformality is crucial as nanotubes are preferred due to their high loading capacity.[61]

Nielsch and collaborators have conducted extensive research on ALD-grown magnetite nanotubes.[36,46,71,128–130,141,147,148] For instance, Fe_3O_4 nanotubes were fabricated using AAO templates with an alternating tube diameter [Figs. 12(b) and 12(d)].[147] The ferrocene + ozone process yielded Fe_2O_3 films at 200 °C, which could be reduced to the mixed-valent Fe_3O_4 by post-deposition annealing at 400 °C. An ALD-grown SiO_2 layer was utilized to protect the nanotubes from the chemical etching of AAO and the back-oxidation of Fe_3O_4. The nanotubes had excellent film quality and thickness uniformity even with the varying tube diameter.

Utilization of ALD for the well-controlled fabrication of core/shell magnetic nanostructures has also been demonstrated [Fig. 12(c)].[71,239] An ALD SiO_2 layer was first applied on AAO for a diffusion barrier and electrical insulator. After the AAO template was removed through chemical etching, the magnetic iron oxide nanotubes (shells) were deposited via the ferrocene + O_3 ALD process at 200 °C. Finally, the nickel cores were prepared by electroplating using a sputtered gold surface as the electrode. The resulting Ni/SiO_2/Fe_3O_4/SiO_2 nanostructures, composed of two materials with different chemical and physical characteristics, presented complex magnetic properties relevant for next-generation spintronic and multiferroic devices (see Sec. VI). These types of multiphase nanostructures are challenging to fabricate in high-quality form, but here ALD serves as the key solution for integrating the two different materials in a feasible and scalable manner.[71]

Nanotubes are not restricted to oxides but extend also to metallic materials. As shown in Figs. 12(f) and 12(g), high-quality metallic TiO_2/Ni/TiO_2 and TiO_2/Co/TiO_2 nanotubes were fabricated by Daub *et al.*[70] The ALD fabrication consisted of the growth of metal (Ni or Co) oxide films from the metallocenes and O_3, TiO_2 interlayers to protect the nanotubes, then followed by post-deposition annealing to reduce the Ni/Co oxide layers to metallic state. The tube length was 2–50 μm, and the study revealed that the magnetic properties depended on both the pore diameter (35–160 nm) and film thickness (3–12 nm). Alternatively, similar nanotubes have also been fabricated in an *in situ* process using H_2 as a reductant.[70]

These examples highlight the suitability of ALD for coating high-aspect ratio surfaces without compromising the film quality and uniformity while providing versatile magnetic properties, discussed in more detail in Sec. VI.

VI. HIGHLIGHTS OF APPLICATION-RELEVANT MAGNETIC CHARACTERISTICS

Most of the ALD-grown magnetic thin films are either ferro- or ferrimagnets. For these materials, the coercive field is one of the important characteristics regarding their potential application fields. In this section, we highlight some of the application-wise most promising ALD-grown magnetic thin films; in Table VIII, the basic magnetic properties of these thin films are summarized (type of magnetism and RT coercivity), together with a comment regarding the possible need for additional post-deposition annealing to obtain the correct composition, crystal phase, or microstructure. The most relevant practical applications require that the magnetic material would be operational at room temperature. Hence, materials, such as low-temperature AFM RMO_3 perovskites[24,117,118] and paramagnetic chalcogenides,[124] are not included in the table.

Ferrimagnetic magnetite Fe_3O_4 with its half-metallic nature is considered a promising candidate for spintronic applications such as magnetic tunnel junctions (MTJ) and magnetoresistive sensors.[38,240] Zhang *et al.*[153] implemented a thorough investigation of magnetic and ME properties of Fe_3O_4/Pt/PZN-PT heterostructures. Figure 13(a)

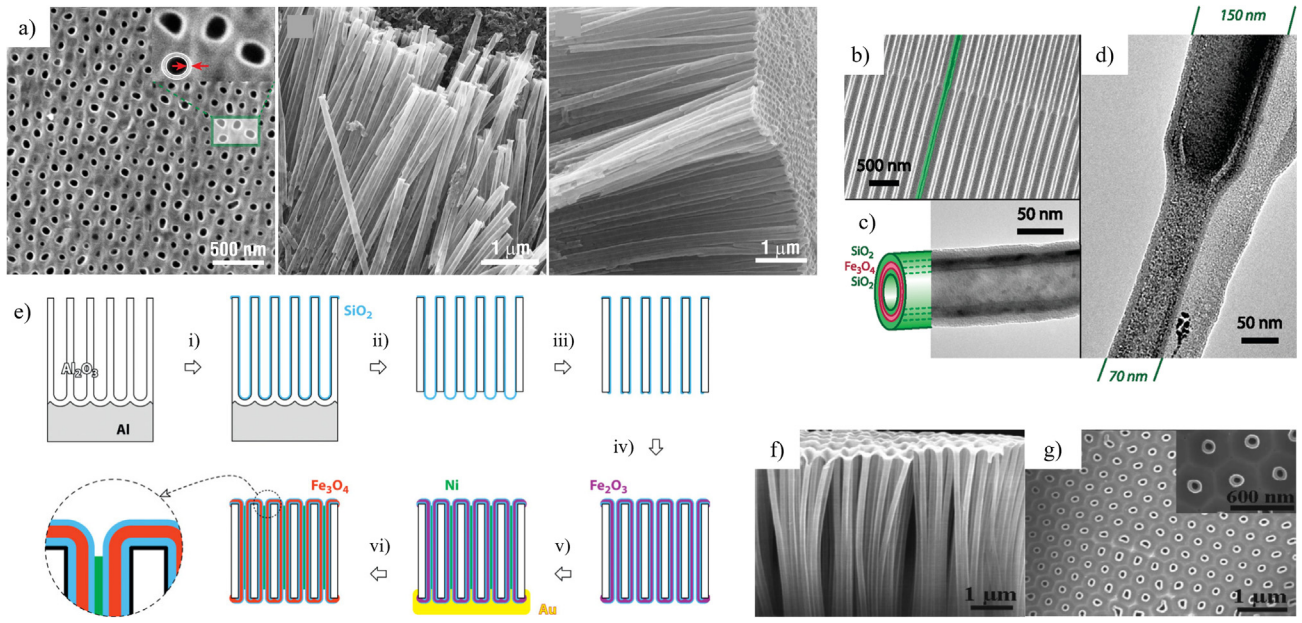

FIG. 12. (a) SEM images of magnetite nanotubes embedded in AAO matrix (left) and free-standing magnetite nanotubes (middle and right). The AAO template was removed by NaOH etching and the Fe_3O_4 "roof" was removed via ion milling to separate the nanotubes from each other. The tube length and diameter were in the scale of 30 μm and 100 nm, respectively, and the Fe_3O_4 layer thickness was ~20 nm. Reproduced with permission from Zhang *et al.*, Sci. Rep. **6**, 18401 (2016). Copyright 2016 Authors, licensed under a Creative Commons Attribution (CC BY) License.[61] (b) SEM image of diameter modulated ALD-grown $SiO_2/Fe_3O_4/SiO_2$ nanotubes embedded in AAO matrix; one of the nanotubes is highlighted with a green color. Separate TEM images of (c) the wide part and (d) the segment where the diameter is changed of a single diameter modulated $SiO_2/Fe_3O_4/SiO_2$ nanotube. The wall thickness of the SiO_2 and Fe_3O_4 are 6 and 10 nm, respectively. Reprinted with permission from Pitzschel *et al.*, ACS Nano **3**, 3463 (2009). Copyright 2009 American Chemical Society.[147] (e) Fabrication steps for Ni/Fe_3O_4 core/shell nanostructures with insulating SiO_2 interlayers. The SiO_2 diffusion barrier and Fe_2O_3 magnetic shell were grown conformally via ALD while the Ni core was prepared by electroplating. The Al substrate was dissolved in acidic Cu^{2+} solution whereas the sputtered Au electrode used for electroplating was removed through KI_3 etching. The Fe_3O_4 composition was achieved via reduction of Fe_2O_3 in H_2-containing atmosphere (400 °C). Reprinted with permission from Chong *et al.*, Adv. Mater. **22**, 2435 (2010). Copyright 2010 WILEY-VCH Verlag GmbH & Co. KGaA, Weinheim.[71] (f) and (g) $TiO_2/Ni/TiO_2$ nanotubes removed from AAO template and the same nanotubes embedded in AAO before the template removal through NaOH chemical etching. Pore diameter is 160 nm, tube length 10 μm, and Ni film thickness 11–12 nm. Reprinted with permission from Daub *et al.*, J. Appl. Phys. **101**, 09J111 (2007). Copyright 2007 AIP Publishing LLC.[70]

(left) shows a typical M-H curve obtained for the magnetite films,[153] revealing a clear magnetic anisotropy induced by both magnetocrystalline and shape anisotropy. The in-plane coercivity is slightly higher and the saturation magnetization is reached with a significantly lower external field parallel to the easy axis (in-plane).[38,153] This anisotropy is also seen from the clear angular dependence of applied magnetic field on ferromagnetic resonance (FMR) field (H_r): H_r minima (2160 Oe) and H_r maxima (4350 Oe) are observed for in-plane and out-of-plane directions, respectively, confirming the in-plane magnetic easy axis [Fig. 13(a)]. Moreover, the ME coupling of Fe_3O_4/Pt/PZN-PT was demonstrated by measuring the effect of the external electric field on H_r for both in-plane and out-of-plane magnetic fields.[153] The largest magnetoelectric coupling coefficient discovered was 31.8 Oe cm/kV.

The suitability of a similar magnetite-based heterostructure (Fe_3O_4/PMN-PT) for nonvolatile data storage has been too demonstrated.[154] Figure 13(b) (left) shows the so-called "butterfly" curve resulting from the change of H_r as a function of the applied electric field, while Fig. 13(b) (right) fascinatingly shows the dynamic magnetization switching of the heterostructure: H_r is reversibly switched by alternating positive and negative electric field. The switching effect was assigned to complex ferroelectric/ferroelastic interaction of the PMN-PT layer. This nonvolatile switching phenomenon could well be implemented in memory applications.[154]

Doping is an effective way to engineer the magnetic properties of Fe_3O_4 films. Magnetic hysteresis of *in situ* deposited hard magnetic spinel $(Fe,Co)_3O_4$ thin films with different metal ratios are shown in Fig. 13(c).[40] Through precise control of the cobalt content, both the coercivity and magnetization can be tuned. This underlines the importance of the development of highly controlled ternary metal oxide ALD processes (cf. Sec. IV B). Being able to on-demand tailor the magnetic properties is crucial since each application has specific requirements for the functional material. For instance, the coercivity of a magnetic recording material should be high enough for reliable information storage but low enough so that the information (i.e., state of the magnetic units) can be changed at will with the writing head.

Magnetite nanotubes are the most investigated ALD-grown 3D magnetic systems. Zierold *et al.*[141] demonstrated the appealing functional properties of multilayered $SiO_2/Fe_3O_4/SiO_2$ nanotube ferrofluids. Typical RT FiM behavior of Fe_3O_4 was observed for dry nanotubes lying on a substrate with fixed orientation but for a liquid

TABLE VIII. Room-temperature magnetic characteristics of the thin films.

Material	Post-dep. processing needed	Magnetic properties at RT		Reference
		Type	Coercivity (Oe)	
Fe_3O_4	Yes	Ferromagnetic	135–900	36,38,46,61,71,128–130,141–144,147,151,152
	No	Ferromagnetic	59–425	146,153–155
	No	Superparamagetic	···	61,152
α-Fe_2O_3	No	Paramagnetic	···	99
	No	Ferromagnetic	2800	189
ε-Fe_2O_3	No	Ferromagnetic	1600–9700	26,189
Ni_xO	No	Antiferromagnetic	···	125
$Co_xFe_{3-x}O_4$	Yes	Ferromagnetic	1400–1600	107,108
	No	Ferromagnetic	200–1500	40,44,159
	No	Superparamagetic	···	158
$Ni_xFe_{3-x}O_4$	Yes	Ferromagnetic	470	40
	No	Ferromagnetic	350	40
$Zn_xFe_{3-x}O_4$	Yes	Ferromagnetic	50	162
$(Mn,Co)_3O_4$	Yes	Ferromagnetic	···	112
$(Co_{1-x}Ni_x)_3O_4$	No	Ferromagnetic	500	113
$BiFeO_3$	Yes	Ferromagnetic	5–490	41,89,110,131,138
	No	Ferromagnetic	···	137
Co	Yes	Ferromagnetic	20–580	70,128,170,215,216
	No	Ferromagnetic	50–230	30,31,33,70,174,176,204
Co_3Sn_2	No	Ferromagnetic	485–510	10
Co-Pt (NP)	Yes	Ferromagnetic	1520	178
$CoFe_2$	No	Ferromagnetic	···	217
Ni	Yes	Ferromagnetic	100–250	70,128,180,181
	Yes	Superparamagetic	···	179
	No	Ferromagnetic	∼30–400	70,123,204
NiFe	Yes	Ferromagnetic	36–473	42,165
Fe	No	Ferromagnetic	743	204
$V(TCNE)_x$	No	Ferromagnetic	80	192
$Co_xV_y(TCNE)_z$	No	Ferromagnetic	50	193
ε-Fe_2O_3-TPA	No	Ferromagnetic	260–2100	43
ε-Fe_2O_3-ADA	No	Ferromagnetic	1000–2600	37
ε-Fe_2O_3-SiO_2	No	Ferromagnetic	···	86
ε-Fe_2O_3-BiOCl	No	Ferromagnetic	∼5000–9750	199
Ru:Fe_2O_3	No	Superparamagetic	···	189
	No	Paramagnetic	···	189
ZnO-Ni	No	Ferromagnetic	200	184
ZrO_2-HfO_2	No	Ferromagnetic	50	200
ZrO_2-MnO_x	No	Ferromagnetic	<500	126
$Y_3Fe_5O_{12}$	Yes	Ferromagnetic	15	166
$YMnO_3$	Yes	Ferromagnetic	100	119
$Ho_2Ti_2O_7$	Yes	Ferromagnetic	100	134
Co:TiO_2	Yes	Ferromagnetic	15–40	127
Co_2C	No	Ferromagnetic	18–500	206,232

suspension of the nanotubes [Fig. 13(d)], the macro-FiM properties were vanished (i.e., zero remanent magnetization). The individual nanotubes of the colloid were still FiM, but they could rotate freely in the suspension and, thus, appear as superparamagnetic. The colloidal solution could be implemented for example in drug delivery, and, thus, it could possibly eliminate the need of superparamagnetism in such applications. Even more impressively, a clear magnetoviscosity (change of viscosity under applied magnetic field) could be observed even with

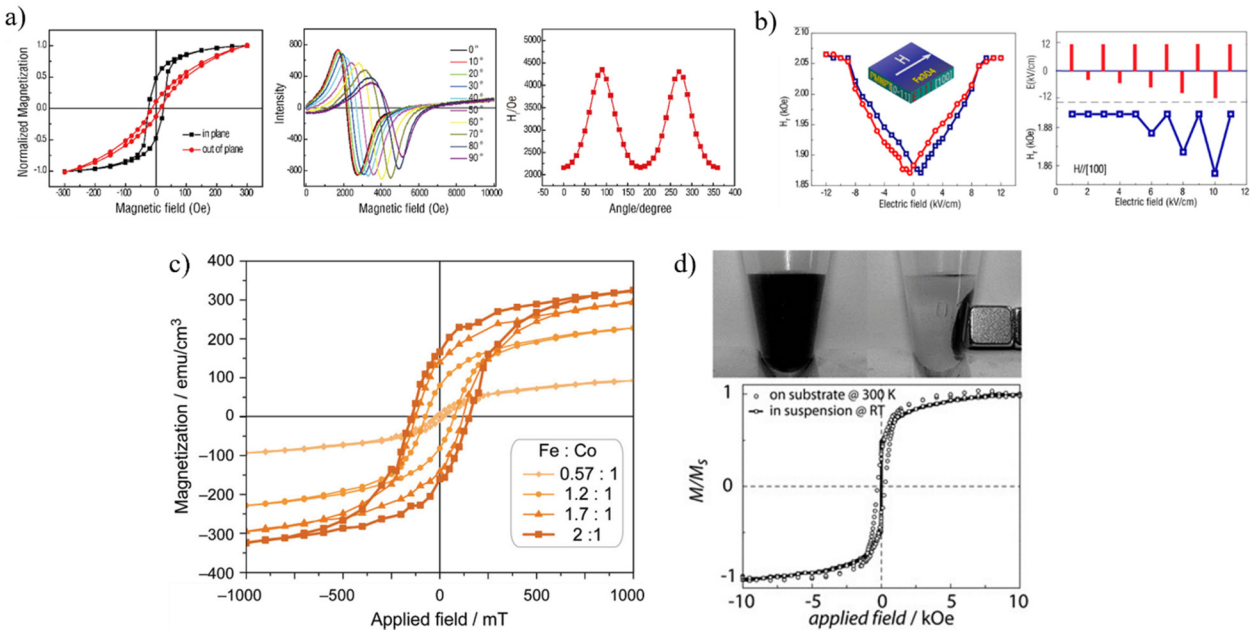

FIG. 13. (a) In-plane and out-of-plane M-H curve of Fe_3O_4 thin film (left). Clear in-plane anisotropy is observed as the in-plane H_c exceeds out-of-plane H_c and in-plane saturation is reached with lower magnetic field. FMR absorption spectra of the film with different angles of external magnetic field (0° = in-plane, 90° = out-of-plane; middle); H_r is defined as the intercept of magnetic field axis. The H_r minimum and maximum at 0° and 90°, respectively, confirm the in-plane anisotropic nature of the Fe_3O_4 film. The H_r values are also plotted for the different angles of external magnetic field in the right figure. Reprinted with permission from Zhang *et al.*, ECS J. Solid State Sci. Technol. **10**, 114004 (2021). Copyright 2021 The Electrochemical Society.[153] (b) The so-called butterfly curve for H_r formed through alternating external electric field of ±12 kV/cm is shown for Fe_3O_4/PMN-PT heterostructure (left). By utilizing this coupling effect, dynamic magnetization switching using applied electric field is shown in the right figure where the red bars indicate the magnitude of applied field and the blue curve depicts the changing H_r. Reprinted with permission from Zhang *et al.*, Appl. Phys. Lett. **110**, 082902 (2017). Copyright 2017 AIP Publishing LLC.[154] (c) RT M-H curves of $(Fe,Co)_3O_4$ thin films with different Fe:Co ratios. Both magnetic saturation and coercivity increase when the iron content is increased. Strongest ferromagnetism is observed for the stoichiometric $CoFe_2O_4$. Adapted with permission from Chong *et al.*, Chem. Mater. **22**, 6506 (2010). Copyright 2010 American Chemical Society.[40] (d) Well-dispersed $SiO_2/Fe_3O_4/SiO_2$ nanotubes in a liquid and the nanotubes attracted by an external permanent magnet (top). M-H curve of dried and nanotubes in the liquid suspension (bottom): the dried nanotubes exhibit FiM characteristics due to fixed orientated on the substrate but appear as superparamagnetic (H = 0, M_s similar to dried nanotubes) in a colloidal solution due to free ability for rotation. Reprinted with permission from Zierold *et al.*, Adv. Funct. Mater. **21**, 226 (2011). Copyright 2011 WILEY-VCH Verlag GmbH & Co. KGaA, Weinheim.[141]

very low volume fraction (0.02 vol. %) of the Fe_3O_4 in the suspension which is highly attractive for ferrofluidic applications.[141]

Combining ALD with other fabrication tools allows the preparation of creative material systems with advanced functional properties. The multilayered $Ni/SiO_2/Fe_3O_4/SiO_2$ nanotubes prepared by ALD and electrodeposition (Sec. V B) is a vivid example; the Ni cores and Fe_3O_4 nanotubes show independent magnetization reversal while only weak interactions between the two magnetic components were detected. Having two independent magnetization reversal modes manifests the possibility of having two bits in one multilayer cylinder. This displays the possibility for increased data storage density since each on the cylinders can have four different binary configurations (00, 01, 10, 11).[71] Understanding the different magnetization modes in the complex 3D nanosystems is truly important, and, thus, the complex geometrical effects on the magnetic properties of Fe_3O_4 nanotubes have been thoroughly investigated, which will establish a pathway for commercial applications and a better fundamental understanding of the complex magnetic behavior of 3D nanostructures.[36,46,128,147,239]

Another relatively well-investigated system among the ALD-fabricated magnetic thin films is the multiferroic $BiFeO_3$ (Table III). In bulk form, $BiFeO_3$ is AFM, but $BiFeO_3$ thin films have shown FM characteristics originating from their nanocrystalline structure.[41,131] The multiferroic $BiFeO_3$ films have been considered promising enablers of various next-generation spintronics applications. For the ALD-grown $BiFeO_3$ films, it has been shown that the multiferroic properties can be tailored by the Bi- and Fe-precursor pulsing sequence; Puttaswamy *et al.*[89] achieved the optimal combination of ferromagnetic and ferroelectric properties for the nonuniform stackings of 1–2 nm thick Bi-rich and Fe-rich $BiFeO_3$ layers [Fig. 14(a)]. The precise control over the compositions of the ultrathin layers was defined simply by the sequence of the different ALD cycles.

Patel *et al.*[111] recently demonstrated a promising strain-mediated ME coupling effect for conformal ALD-grown $BiFeO_3$ coating on a porous sol-gel synthesized magnetostrictive $CoFe_2O_4$ template. Magnetization measurements under electric field for samples with different $BiFeO_3$ coating thicknesses ranging from 3 to 12 nm revealed that the most intensive ME effect occurred for the thinner $BiFeO_3$ layers with the larger residual porosity of the nanocomposites [Fig. 14(b)]. Apparently, for planar and epitaxial strain-mediated ME structures, the ME effect is damped by clamping at the interface of the two materials, meaning there is no room for the composite to strain, whereas the porous structuring used here allows more flexible platform

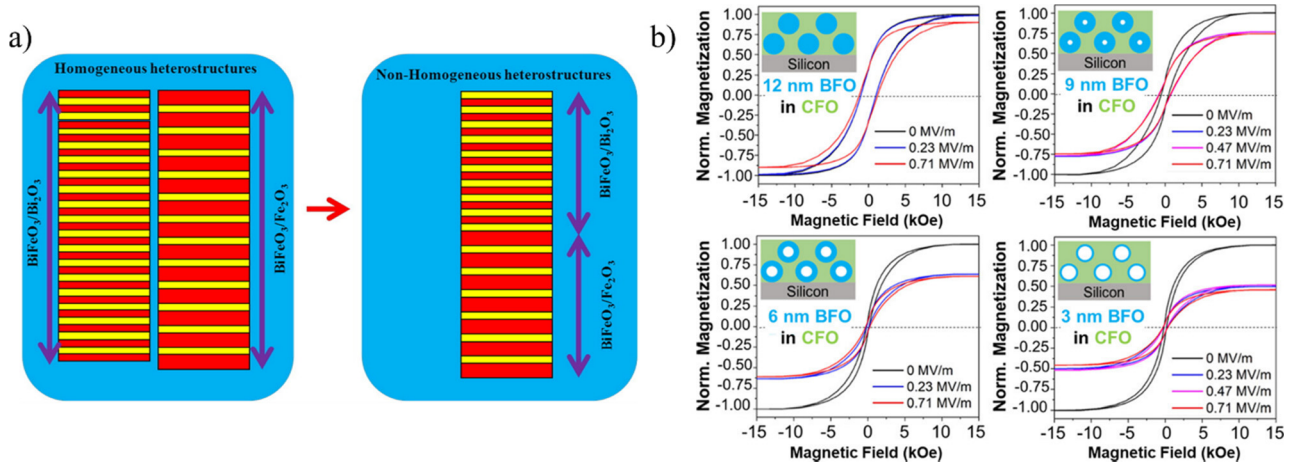

FIG. 14. (a) Uniform (left) and non-uniform (right) stacking of bismuth oxide and iron oxide layers. The non-uniform heterostructure exhibited strongest ferromagnetic and ferroelectric interactions due to the combination of Bi and Fe rich $BiFeO_3$ layers. Reprinted with permission from Puttaswamy *et al.*, Thin Solid Films **611**, 78 (2016). Copyright 2016 Elsevier.[89] (b) M-H hysteresis of porous $CoFe_2O_4/BiFeO_3$ nanocomposites with different $BiFeO_3$ layer thicknesses. The (out-of-plane) applied electric field induces a strain-mediated ME effect which is seen as notable decrease in magnetization. The strongest ME effect is observed for the thinnest (3 nm) $BiFeO_3$ layers. Reprinted with permission from Patel *et al.*, ACS Appl. Nano Mater. **6**, 4141 (2023). Copyright 2023 American Chemical Society.[111]

(higher strain) and, thus, higher strain-mediated ME coupling. Moreover, no ME effect was observed without the ALD-grown $BiFeO_3$ coating. This work opens up pathways for example for miniaturized antenna devices.[111] Also, the 3D $CoFe_2O_4/BiFeO_3$ structures could be all-ALD since $CoFe_2O_4$ could be feasibly fabricated through ALD.

As discussed in Sec. IV A, the fabrication of phase-pure stoichiometric magnetite films is challenging as traces of iron(III) oxide(s) often remain in the films. On the contrary, stoichiometric ferric oxides such as ε-Fe_2O_3 are easier to achieve. Phase-pure ε-Fe_2O_3 nanoparticles were synthesized for the first time by Jin *et al.*[28] in 2004, but the first ε-Fe_2O_3 thin films were deposited through pulsed laser deposition (PLD) by Gich *et al.*[241] only in 2010, and through CVD in 2014 by Carraro *et al.*[242] In consequence, ε-Fe_2O_3 thin films have been investigated only little up to this date, even though they are highly promising for next-generation spintronic devices due to the unique multifunctional properties[29] of ε-Fe_2O_3 including extremely high RT magnetic coercivity and high Curie temperature,[28] ferroelectric behavior,[243] ME coupling,[243] and ferromagnetic resonance (FMR) at high frequencies.[244,245]

The phase purity and magnetic properties of the ALD-grown ε-Fe_2O_3 thin films have also been demonstrated.[26,27,189,199] In particular, ^{57}Fe Mössbauer spectroscopy was successfully utilized to confirm the excellent phase purity of the films.[27] These measurements, typically requiring relatively large sample amounts, could be realized by depositing the films on "gamma-ray transparent" polyimide (Kapton) substrate and piling several of such ε-Fe_2O_3/Kapton films on top of each other to get sufficient signal for the analysis. Figure 15(a) shows the Mössbauer spectrum measured for ALD-grown ε-Fe_2O_3 at 305 K. The magnetic ordering (sextet) and all four distinct iron signals are extracted. The paramagnetic component (brown) became visible around 433 K, but the sextet was vanished only at 480 K verifying the relatively high Curie temperature of ALD ε-Fe_2O_3, and thus, its suitability for RT applications.[27] The films were of high phase purity as the concentration of the only impurity phase, hematite (gray), was only around 2%. The Mössbauer method represent a new highly efficient way of characterizing the magnetic properties of any iron-based ALD thin films as it can give extremely precise information on the fine magnetic interactions and ordering of the Fe-based materials. This has value especially regarding magnetic thin films since, as seen in this review, iron oxides cover the majority of the ALD magnetic thin films.

Having the eye on the possible applications benefitting from mechanical flexibility, inherently flexible organic moieties have been incorporated into the ε-Fe_2O_3 films (Table VI).[37,43,238] Importantly, these organic layers do not compromise the unique magnetic properties of the ε-Fe_2O_3 phase. For instance, for the ε-Fe_2O_3:ADA SL films, RT coercivity values of 1–2 kOe were obtained.[37] It is interesting to compare these coercivity values with those so far achieved for flexible organometallic thin films (~100 Oe) fabricated using various techniques; here these latter thin films exhibit at their best an order of magnitude lower coercivities due to their significantly weaker long-range magnetic interactions.[192,193,246,247] Indeed, the incorporation of flexible organics into the ε-Fe_2O_3 matrix through ALD/MLD allows the combination of the inherent properties of both the inorganic and organic components, yielding magnetically hard but mechanically flexible thin films increasingly desired in various applications in flexible electronics such as wearable devices, optoelectronics, biosensors, and flexible data storage.[37,43,87,92]

In addition to the mechanical flexibility, the incorporated organic layers may bring other functionalities into the magnetic inorganic thin film. An exciting example is the ε-Fe_2O_3:ADA SL system in which the magnetic properties can be reversibly controlled optically through the trans–cis photoisomerization reactions of the ADA molecule under UV/visible light irradiation.[37] Figure 15(b) shows the UV absorption spectrum of ε-Fe_2O_3:ADA thin films before and after the UV/visible light irradiation. The characteristic $\pi - \pi^*$ electronic transition of trans-ADA is decreased upon UV irradiation and increased close to the original intensity after visible light irradiation, thus demonstrating the reversibility of the isomerization process. Figure 15(c) (inset) then

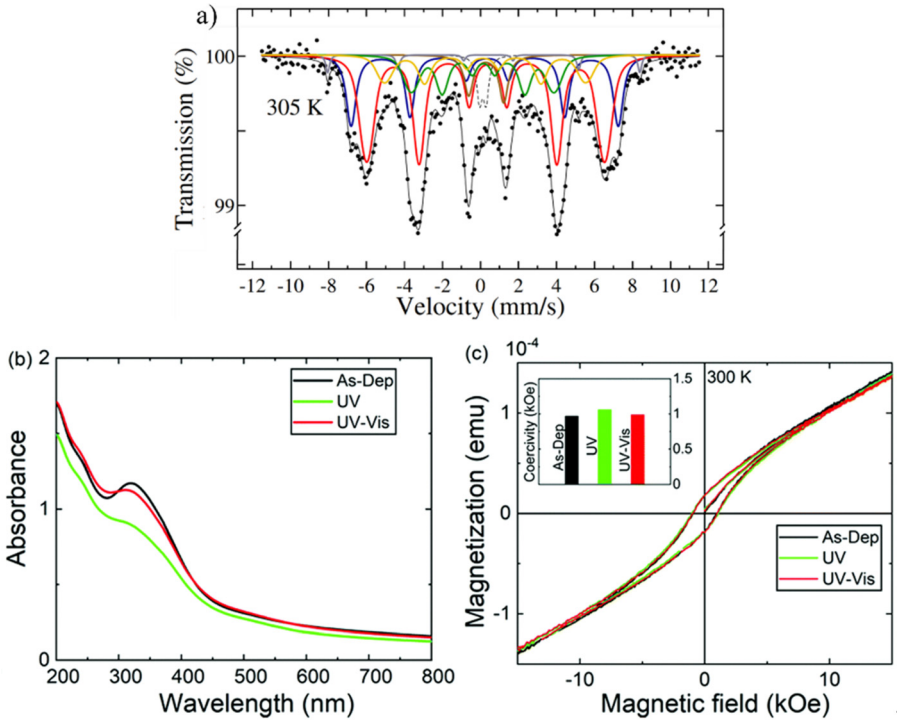

FIG. 15. (a) ^{57}Fe Mössbauer spectra of ε-Fe_2O_3 thin film at 305 K. Each color (blue, red, yellow, and green) indicates certain crystallographic site of the ε-crystal phase. Paramagnetic component is the brown line and gray is hematite. Clear magnetic ordering can be realized for the ε-Fe_2O_3 phase based on the magnetic sextet while the hematite component (impurity phase) is shown to be negligible (~2%). Adapted with permission from Jussila *et al.*, Adv. Eng. Mater. **25**, 2201262 (2023). Copyright 2023 Authors, licensed under a Creative Commons Attribution (CC BY) License.[27] (b) Absorption spectra of as-deposited, UV-irradiated, and visible light irradiated ε-Fe_2O_3:ADA superlattice thin film. The ADA layers undergo reversible trans-to-cis photoisomerization under UV/visible light irradiation: the trans-to-cis is seen as an absorption intensity drop at ~320 nm (characteristic for the trans isomer) after UV-light irradiation. Accordingly, the intensity is increased back nearly to the original state through visible light irradiation demonstrating successful cis-to-trans back switching. (c) M-H curves of the corresponding conditions. Inset shows the change in coercivity at 300 K; the magnetic properties (coercivity) are reversibly changed due to the trans-to-cis photoisomerization of ADA. Reproduced with permission from Philip *et al.*, J. Mater. Chem. C **10**, 294 (2022). Copyright 2022 the Royal Society of Chemistry.[37]

shows the effect of the reversible isomerization on the magnetic properties of the SL film. The magnetic coercivity is reversibly varied by 10%–20% depending on the film composition. These optically controlled ferromagnetic properties could be utilized, for example, in optical data storage devices.[37]

Metallic thin films have several traditional assignments in microelectronics such as interconnects and adhesion layers, but they also exhibit applicable magnetic properties (Table VII). For instance, Ni-Fe thin films are used commercially in spin valves,[3] while pure cobalt thin films possess great potential in spintronics due to their combined magnetic and electric properties.[31] Most fascinatingly, ALD-grown 3D metallic nanostructures have become an exceedingly interesting topic as a result of their versatile magnetic properties.[70,123,128,151,165,179,182,204] For instance, magnetization and coercive field of free-standing nickel and cobalt nanotubes can be adjusted based on the pore size of the nanotubes [Fig. 16(a)].[70] This shows how the magnetic behavior of complex device architectures could be engineered for different applications simply by changing the diameters of the 3D structure but without the need for different materials.

Some advanced ME studies have been done also for metallic thin films; comprehensive magnetoresistive studies were conducted for FM Ni-Fe thin films by Giordano *et al.*[42] (Sec. IV C). Figure 16(b) shows electric resistivity, anisotropic magnetoresistance (AMR), and relative magnetoresistance (AMR-%) properties of the films for different Ni:Fe precursor pulsing ratios (m = 6 corresponds to nearly ideal Permalloy composition). Each figure also includes the corresponding properties for commercial evaporated $Ni_{80}Fe_{20}$ thin films. Especially the ALD-grown m = 6 $Ni_{81}Fe_{19}$ films are promising, with their resistivity value of 28 $\mu\Omega$ cm, the technologically important AMR effect confirmed, and the AMR-% of 5.6 which matches well with the commercial counterpart. Gilbert damping (damping of spin waves, i.e., collective spin excitations) of the Permalloy ALD films (m = 6) was also appreciably low (0.013) though it was slightly higher compared to the evaporated $Ni_{80}Fe_{20}$ film (0.09). This was assigned to the small dewetting effects described also in Sec. IV C. Low Gilbert damping is a necessity for magnonic applications where collective spin waves are of high importance.[42] Moreover, the complex FMR characteristics of ALD-grown Permalloy nanotubes were studied by Brillouin-Light-Scattering microscopy (μBLS) to gain insight into the spin wave modes of the 3D coatings. This will ultimately contribute to the design of novel nanostructured magnonic devices.[42]

Quinard *et al.*[211] recently demonstrated the use of ALD-grown FM cobalt thin films in a complete spin valve junction [Figs. 16(c) and 16(e)]. Al_2O_3/Co spin analyzer was used on top of the Co film to probe

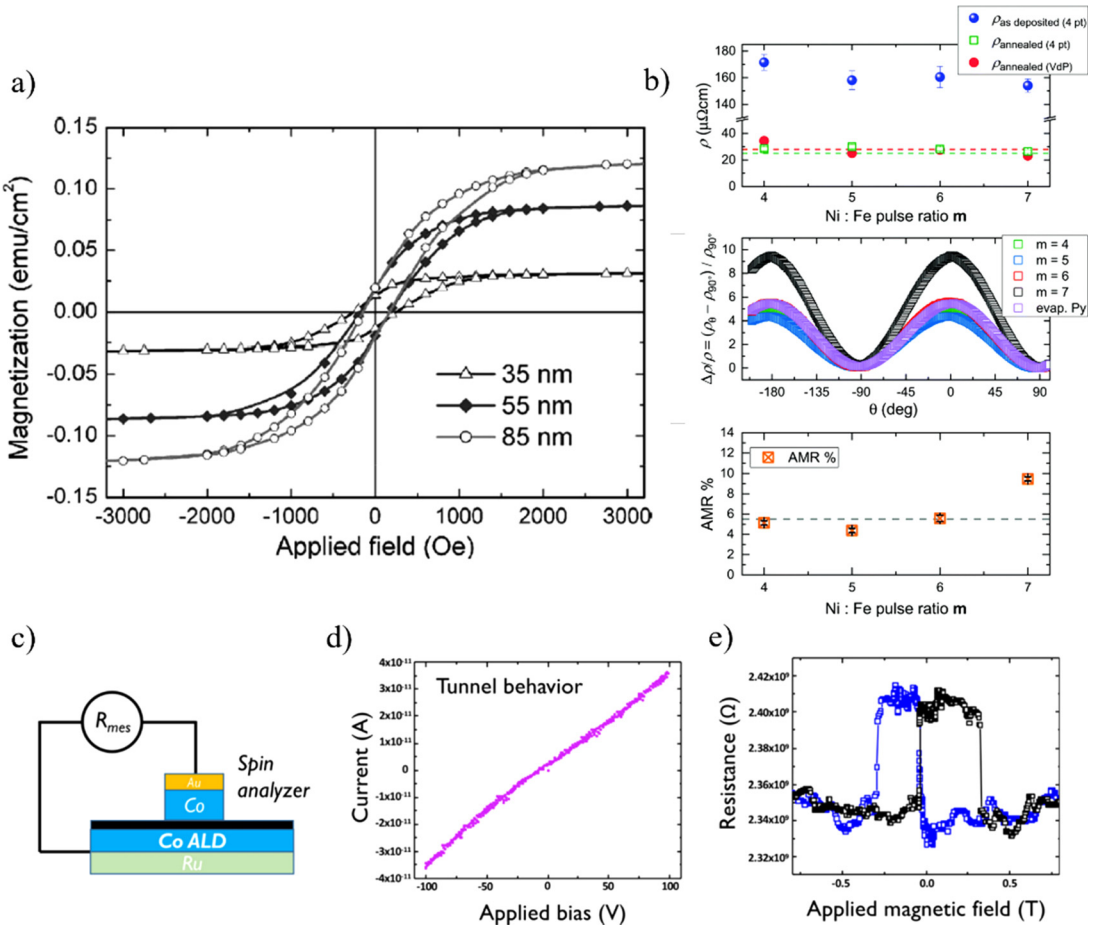

FIG. 16. (a) M-H curve of nickel nanotubes for different pore diameters: the higher the diameter, the higher the saturation and remanent magnetization, and coercivity. Reprinted with permission from Daub *et al.*, J. Appl. Phys. **101**, 09J111 (2007). Copyright 2007 AIP Publishing LLC.[70] (b) Resistivity (top), RT magnetoresistance as function of in-plane (80 mT) rotation angle (middle), and relative AMR of $Ni_{100-x}Fe_x$ thin films for different Ni:Fe pulsing ratios (m; bottom). Each graph also shows the corresponding properties for commercial evaporated $Ni_{80}Fe_{20}$ thin films (dashed line in top and bottom figures). The drastic change in resistivity between as-deposited and annealed samples is explained by the amorphous and crystalline state of the respective samples. Importantly, it is seen that pulse ratio of m = 6 (nearly ideal Permalloy stoichiometry) results in comparable electric resistivity and relative AMR with respect to the commercial reference. Reproduced with permission from Giordano *et al.*, Nanoscale **13**, 13451 (2021). Copyright 2021 the Royal Society of Chemistry.[42] (c) Spin valve configuration with ALD-grown Co spin source. The black line is 1 nm Al_2O_3 tunnel barrier. (d) IV curve and (e) tunnel magneto-resistance spin signal measurement of the junction. The IV curve is nonlinear, which is typical for a tunnel device. Most importantly, the resistance clearly depends on the applied magnetic field due to spin polarized current created by the Co-spin source. Reproduced with permission from Quinard *et al.*, Appl. Phys. Lett. **120**, 213503 (2022). Copyright 2022 Authors, licensed under a Creative Commons Attribution (CC BY) License.[211]

the spin current properties. The tunneling effect [IV-curve; Fig. 16(d)] was reported as non-linear, typical for a tunnel device, confirming the high quality of the Co-layer structure.[211] Most interestingly, the resistance of the spin valve could be controlled by an applying external field [Fig. 16(c)], showing that the applied field induced spin-polarized current of Co. This is a clear demonstration of the combination of the good metallic and ferromagnetic properties of the Co film and its fit for next-generation spintronic devices.

The examples highlighted in this section show the truly versatile applicability of ALD-grown magnetic thin films for various purpose ranging from basic high-quality planar magnetic coatings and 3D architectures with complex magnetic behavior to unique multiferroic and magnetoelectric coatings with excellent potential in future spintronics.

VII. OUTLOOK COMMENTS AND ROADMAP FORWARD

Feasible ALD processes have already been developed for the growth of high-quality thin films of nearly 40 different magnetic materials. Nevertheless, a clear majority of the published studies have so far focused on simple iron oxides. There are many potential multi-metal materials with attractive magnetic characteristics worth to be challenged in future, but the main difficulty in their ALD fabrication is the accurate process control; in other words, the difficulty in achieving the targeted stoichiometry over the targeted metal ratio and deposition temperature ranges. This challenge often translates to the difficulty in finding either mutually compatible single-metal precursors or developing new heterometallic precursors. The latter approach is still rather rare, but when successfully employed, could yield superior results, as

in the case of the $GdFeO_3$ films. The third solution would be to simply mix two or more metal precursor powders into a single source, but the likelihood that the different sublimation rates of the different precursor components in the mixture would result in deviations in the metal stoichiometry of the final thin film is considerable, especially in industrial scale production. Another important question concerns the crystallinity of the as-deposited films; this is often an issue especially for ternary and quaternary metal oxide films, which are typically obtained as amorphous thin films, hence requiring an additional post-deposition annealing step. In general, the post-deposition annealing typically results in harder magnetism compared to the characteristics seen for as-deposited thin films of the same material, which is caused by increased crystallinity and, thus, stronger long-range magnetic interactions.

Most of the ALD process development efforts made so far have focused on ferro- or ferrimagnetic materials, excluding the low-temperature antiferromagnetic perovskites and paramagnetic selenides and the few reports on superparamagnetism induced for metal oxide and metallic films by the low crystallinity/small grain size. However, magnetic materials beyond the FM and FiM ones should not be forgotten. Especially AFM materials are of high technological importance, and they can exhibit several advantages over FM and FiM materials including ultrahigh (tera-hertz) resonance frequencies and the absence of magnetic stray fields.[248,249] Many AFM materials are metal oxides which is shouting for the ALD technique; the antiferromagnetic nature of ALD-grown NiO is already demonstrated and further studies should be continued. Another intriguing example is AFM CoO,[201,250] mostly studied for its p-type conductivity; in further studies, the focus should be extended to its magnetic properties and potential use in AFM spintronic devices.[251]

It is also important to note that no efforts have been made so far to develop ALD processes for the Nd–Fe–B, Sm–Co, and Alnico alloys that are widely used in bulk form as state-of-the-art permanent magnets. This is likely due to the challenging ALD chemistries of these intermetallic compounds. In general, ALD of intermetallics is yet in its infancy, but recently gaining more attention.[9,10,252] Another material category of future interest but poorly represented yet is definitely the strongly emerging vdW 2D materials with intriguing magnetic and magnetoelectric properties.[234] These materials are often difficult to fabricate in large quantities through conventional synthesis, but the layer-by-layer growth characteristics of ALD could provide a natural solution for this challenge, as already demonstrated with several promising ALD fabrication efforts recently reported for 2D sulfide and selenide thin films.[34,35] However, most of the research has so far focused on molybdenum and tungsten sulfides and selenides, and excluding the report on cobalt and nickel selenides,[124] very little attention has been paid on the magnetic properties of these ALD-grown thin films. In Table IX, we have collected some of the ALD processes developed for transition metal chalcogenides and carbides with potentially interesting magnetoelectric properties, and worth to be investigated from the magnetic-property point of view in future studies.

A recently discovered material class of non-van der Waals 2D materials presents another extremely interesting possibility for ALD. These materials show novel features compared to the traditional vdW 2D materials; the non-vdW 2D layers have non-saturated dangling bonds on the surface unlike their vdW counterparts, which certainly should affect the functional properties (chemical, electric, optical, magnetic, etc.) of the ultrathin layers.[260] Actually, the non-vdW material class is appreciably wide; thus, there is an enormous potential to unravel if the non-vdW materials could be synthesized as large-area, high-quality ultra-thin films through ALD. Some of the so far synthesized ultra-thin magnetic non-vdW materials are Fe_2O_3 (hematene),[261] $FeTiO_3$ (ilmenene),[262] Fe_3O_4 (magnetene),[263] FeS_2,[264,265] and Co_9Se_8.[266] Until now, non-vdW materials have been synthesized through bottom-up wet chemistry methods, liquid phase exfoliation, and van der Waals epitaxy,[267,268] but all of the aforementioned materials could potentially be deposited through ALD as well. Bottom-up methods are generally preferred over top-down approaches due to the difficulty in separating material layers bonded through non-vdW interactions (covalent, ionic, and metallic). Here, ALD could provide an alternative bottom-up approach with its unique ability to yield well-defined large-area monolayers through self-terminating chemical reactions.

TABLE IX. ALD processes of 2D vdW materials with known magnetic characteristics but not considered for their magnetic properties in the ALD studies.

Material	ALD precursors		Reference
CoS_x	$Co(^iPr\text{-}MeAMD)_2$	H_2S	253
	$Co(^iPr\text{-}MeAMD)_2$	H_2S	254
	$Co(^tBu\text{-}MeAMD)_2$	H_2S plasma	255
FeS_2	$Fe(^tBu\text{-}MeAMD)_2$	H_2S plasma	255
NiS_2	$Ni(^tBu\text{-}MeAMD)_2$	H_2S plasma	255
$CoSe_2$	$Co(^tBu\text{-}MeAMD)_2$	DEDSe	256
$FeSe_2$	$Fe(^tBu\text{-}MeAMD)_2$	DEDSe	256
$NiSe_2$	$Ni(^tBu\text{-}MeAMD)_2$	DEDSe	256
FeC_x	$Fe(^tBu\text{-}MeAMD)_2$	H_2 plasma	257
Ni_3C_x	$Ni(^tBu\text{-}MeAMD)_2$	H_2 plasma	258
	$Ni(tBu_2DAD)_2$	H_2 plasma	259
	$Ni(acac)_2$	CH_3CH_2OH or $CH_3CH_2CH_2OH$	123

Taking a step forward, magnetic all-ALD systems such as FM/AFM multilayer structures could be engineered and studied for their exchange bias and magnetoresistive properties, which are tempting for next-generation spintronics applications such as spin–orbit torque based devices.[269,270] On the other hand, the opportunity to utilize ALD in the magnetic systems not as the magnetic component itself but otherwise a crucial component is highly endorsed; for instance, standard and conformal ALD metal oxide (HfO_2, Al_2O_3) processes have been employed in magnetic tunnel junctions (ultra-thin tunnel barrier) and porous magneto-ionic nanostructures.[271–273]

Compared to the meticulous research carried out to develop/optimize the ALD processes, much less efforts have been made for the characterization of the resultant thin films for their magnetic properties. Advanced magnetic characterization techniques such as FMR, magnetoresistance, magneto-optical, and spin wave (magnonics) analyses have been only rarely used. In most of the cases, the magnetic characterization has included only standard M-H analysis. Nevertheless, even with the relatively basic magnetic characterization, the massive potential and the unquestionable advantages of the ALD magnetic coatings have been undisputedly proven. In particular, ALD has proven superior in (i) yielding novel multilayered/multifunctional

thin-film structures, (ii) stabilizing otherwise challenging-to-obtain materials such as ε-Fe_2O_3, and (iii) producing these coatings conformally even on complex/high-aspect ratio surfaces. Moreover, the traditional selling point of ALD, i.e., its ability to produce high-quality pinhole-free ultra-thin films, is elemental for the magnetic films as well since magnetic properties often depend heavily on the dimensions of the material, and the favorable properties are often activated only when the film thickness is in the appropriately (low) range. A prime example is $BiFeO_3$, which is antiferromagnetic in bulk form but ferromagnetic as (ultra)thin films.

To construct the future roadmap for the ALD fabricated magnetic materials, one of the guidelines to be emphasized could be to build on the unique advantages of the ALD technique, including the uniform large-area film growth of ultrathin layers on complex surface architectures demanded for the miniaturization of electronic devices and novel 3D nanodevices. One of the highlights from materials perspective is the rarest trivalent iron oxide polymorph ε-Fe_2O_3 that could revolutionize the next-generation electronic and spintronic applications. So far, these prospects have been hindered by its metastable nature and tedious synthesis, but the facile ALD process developed for this unique multiferroic material could now allow its implementation in complex device fabrication as high-frequency electromagnetic interference absorber required for millimeter wave high-speed wireless communications and recording media for high-density magnetoelectric data storage.[245,274,275]

To achieve the breakthrough of the magnetic metal alloy thin films, the challenges to overcome are the complete reduction of the metal precursor species to metallic state, dewetting and island-type film growth, and achieving simultaneously the smooth surface and high crystallinity. There have been efforts to overcome these issues, especially in terms of precursor development, but further improvements are required particularly for ultrathin metallic films where discontinuity of the film is a major challenge.

For even more advanced functional magnetic thin film materials, the use of ALD/MLD is already manifested in the form of photoactive, ferrimagnetic ε-Fe_2O_3:ADA superlattices and, on the other hand, TCNE-based metal-organic thin films. The handful of examples introduced in this review is a nucleation point for the future development of magnetic ALD/MLD thin films. One of the main challenges of organic-based magnets is the lack of RT magnetic ordering. Thus, specifically attractive is the well-established ability to deposit *in situ* crystalline metal-organic-framework (MOF) thin films via ALD/MLD;[87] the ordered structure of MOFs could enable stronger long-range magnetic interactions and, thus, induce higher magnetic transition temperatures.[276] On the other hand, many of the magnetically ordered bulk MOF materials have exhibited only low transition temperatures despite the structural ordering. Yet this challenge could be approached through the use of ALD/MLD, which generates, notably, solvent-free inorganic–organic materials that can be different from their bulk counterparts.[277]

Advanced characterization must also be included in the future roadmap as the detailed understanding of the structure, composition, and functional (magnetic) properties are mandatory for the materials to be realized in industrial processes. Especially in the case of magnetic thin films, there is a general lack of advanced magnetic characterization. For instance, in-depth analyses of ME properties of multiferroic thin film materials (e.g., $BiFeO_3$, ε-Fe_2O_3) are crucial for the development of novel spintronic devices. In addition, creativity is encouraged for the novel magnetic materials, since magnetic properties of thin films and especially ultrathin 2D-type materials are not well known; the magnetic interactions depend on numerous aspects such as composition, film thickness, stoichiometry, substrate effects, defects, particle size, confinement effects, and more.

Once a promising material with a robust ALD process is developed, device demonstrations are the key to expedite the journey from basic material research to real applications. The very limited number of patents directly focusing on ALD fabricated magnetic thin films reflects the fact that the efforts so far made in the field have rarely aimed at real applications. This is somewhat amazing, as there are much more patents for magnetic materials and devices based on other (physical vapor) deposition techniques, including those for metallic (Co, Ni) and intermetallic (Co-Pt, Co-Pt-Cr) materials utilized for magnetic data storage dating back to 1970s.[278–283] In the case of ALD, patents on magnetic metallic (Co), intermetallic (Co_2Sn_2), and metal oxide thin films (Fe_2O_3) can be found to some extent,[284–290] but ALD patents clearly targeted to magnetic applications are lacking. It may be the case that many of the past applications have not necessarily required ALD for the growth of these magnetic materials since they often rely on simple two-dimensional planar device structures.[291] However, it is the novel magnetic and spintronic devices that could best benefit on the ALD-grown high-quality (ultra)thin and, most importantly, conformal magnetic thin films. Thus, in future considerations, the target idea should not be to simply replace the thin films in current device configurations but to response to the great need of novel magnetic thin films needed for complex, more powerful, next-generation nanodevices including high-sensitivity sensors and actuators. It must be stressed that all the fundamental magnetic phenomena involved with nanomagnetism and 3D effects are not even fully understood but the necessity for high-quality 3D magnetic coatings is doubtless,[291] and interdisciplinary competences between thin film engineering, fundamental physics, and application specialists are needed for the long-term breakthrough of advanced magnetism-based applications.

VIII. CONCLUSIONS IN BRIEF

In this first comprehensive review on the topic, the research output related to ALD fabricated magnetic thin films has been summarized. Nearly 40 different magnetic materials were covered ranging from metal oxides and metals to inorganic–organic materials and nanolaminates. Essentially all of the processes involve a d-block element, while metallocenes and β-diketonates, such as $Fe(thd)_3$, have been the most common metal precursor choice. These precursors work relatively well but require a strong oxidizer—usually O_3—as the co-reactant to allow sufficient reactivity in a practical deposition temperature range (ca. 150–250 °C). Thus, considerable research work has been carried out toward realizing milder deposition conditions (temperature, choice of co-reactant, etc.). Nevertheless, independent of the precursors employed, the growth rates remain typically well below 1 Å/cycle; this may sound lamentably slow, but the many unique benefits of the ALD technique such as the unprecedented film thickness control, film quality, and conformality even on challenging substrate surfaces (sensitive, flexible, porous, high-aspect ratio structured) can in many cases well compensate the slowness of the film growth. Indeed, the ability to grow films on different substrate materials is important for the potential technological applications; the high-quality film

growth of magnetic materials has already been demonstrated for a variety of different substrate types from silicon to complex AAO and polymers such as polyimide.

This review also highlighted some of the promising deposition processes, including those for the ternary FiM $CoFe_2O_4$ and the intermetallic FM $Ni_{80}Fe_{20}$ (Permalloy). One of the pinnacles highlighted was the *in situ* growth of high-quality films of the metastable ε-Fe_2O_3 iron oxide polymorph with intriguing RT multiferroic properties highly relevant for many next-generation spintronic devices. Another intriguing topic discussed was the ALD fabrication of magnetic 3D nanostructures; the uniform high-aspect ratio films enable, for instance, simple engineering of the ever-pursued PMA and multilayered two-bit cylinders for data storage applications. Furthermore, exciting examples of RT FM inorganic–organic thin films and superlattices deposited through the combined ALD/MLD technique were introduced. These novel hybrid materials are the proof-of-concept for the prospects to utilize ALD-based thin films in organic spintronics and other advanced applications, such as optically controlled memory devices.

To signify the progress and possibilities of the ALD-grown magnetic thin films, magnetic property measurements were underlined for some of the materials, including the FM properties of high-aspect ratio nanotubes, strain-mediated ME coupling of porous $BiFeO_3/CoFe_2O_4$ nanocomposites, and magnetoresistive effects of the Permalloy thin films and Co-based spin valves. Finally, in Sec. VII, perspectives for the future trends in the field were provided. These include further development of the ALD processes of metallic and oxide thin films, expanding the magnetic material repertoire to 2D materials, emphasizing the apparent importance of advanced magnetic property measurements, and expediting the path from basic research to real applications through increasing the so far sparce efforts to produce ALD-based magnetic device demonstrations and to optimize these novelties to the point of commercialization.

ACKNOWLEDGMENTS

Funding for this work was received from the European Union (ERC AdG, UniEnMLD, Grant No. 101097815). The views and opinions expressed are, however, those of the authors only and do not necessarily reflect those of the European Union or the European Research Council. Neither the European Union nor the granting authority can be held responsible for them.

AUTHOR DECLARATIONS

Conflict of Interest

The authors have no conflicts to disclose.

Author Contributions

Topias Jussila: Conceptualization (equal); Investigation (lead); Visualization (lead); Writing – original draft (lead). **Anish Philip:** Investigation (equal); Writing – review & editing (supporting). **Tripurari Tripathi:** Investigation (equal); Writing – review & editing (supporting). **Kornelius Nielsch:** Investigation (equal); Supervision (supporting); Writing – review & editing (equal). **Maarit Karppinen:** Conceptualization (lead); Funding acquisition (lead); Investigation (equal); Supervision (lead); Writing – review & editing (lead).

DATA AVAILABILITY

Data sharing is not applicable to this article as no new data were created or analyzed in this study.

REFERENCES

[1]B. Dieny, I. L. Prejbeanu, K. Garello, P. Gambardella, P. Freitas, R. Lehndorff, W. Raberg, U. Ebels, S. O. Demokritov, J. Akerman, A. Deac, P. Pirro, C. Adelmann, A. Anane, A. V. Chumak, A. Hirohata, S. Mangin, S. O. Valenzuela, M. C. Onbaşlı, M. d'Aquino, G. Prenat, G. Finocchio, L. Lopez-Diaz, R. Chantrell, O. Chubykalo-Fesenko, and P. Bortolotti, "Opportunities and challenges for spintronics in the microelectronics industry," Nat. Electron. **3**, 446 (2020).
[2]A. Hirohata, K. Yamada, Y. Nakatani, I.-L. Prejbeanu, B. Diény, P. Pirro, and B. Hillebrands, "Review on spintronics: Principles and device applications," J. Magn. Magn. Mater. **509**, 166711 (2020).
[3]J. M. D. Coey, in *Magnetism and Magnetic Materials* (Cambridge University Press, Cambridge, 2009), p. 1.
[4]A. J. M. Mackus, J. R. Schneider, C. MacIsaac, J. G. Baker, and S. F. Bent, "Synthesis of doped, ternary, and quaternary materials by atomic layer deposition: A review," Chem. Mater. **31**, 1142 (2019).
[5]M. Coll and M. Napari, "Atomic layer deposition of functional multicomponent oxides," APL Mater. **7**, 110901 (2019).
[6]H. H. Sùnsteby, E. Skaar, Ø. S. Fjellvåg, J. E. Bratvold, H. Fjellvåg, and O. Nilsen, "A foundation for complex oxide electronics -low temperature perovskite epitaxy," Nat. Commun. **11**, 2872 (2020).
[7]T. S. Tripathi and M. Karppinen, "Atomic layer deposition of p-type semiconducting thin films: A review," Adv. Mater. Interfaces **4**, 1700300 (2017).
[8]D. J. Hagen, M. E. Pemble, and M. Karppinen, "Atomic layer deposition of metals: Precursors and film growth," Appl. Phys. Rev. **6**, 041309 (2019).
[9]R. Ghiyasi, A. Philip, J. Liu, J. Julin, T. Sajavaara, M. Nolan, and M. Karppinen, "Atomic layer deposition of intermetallic Fe_4Zn_9 thin films from diethyl zinc," Chem. Mater. **34**, 5241 (2022).
[10]K. Väyrynen, T. Hatanpää, M. Mattinen, K. Mizohata, K. Meinander, J. Räisänen, J. Link, R. Stern, M. Ritala, and M. Leskelä, "Atomic layer deposition of intermetallic Co_3Sn_2 and Ni_3Sn_2 thin films," Adv. Mater. Interfaces **6**, 1801291 (2019).
[11]R. W. Johnson, A. Hultqvist, and S. F. Bent, "A brief review of atomic layer deposition: From fundamentals to applications," Mater. Today **17**, 236 (2014).
[12]C. Shen, Z. Yin, F. Collins, and N. Pinna, "Atomic layer deposition of metal oxides and chalcogenides for high performance transistors," Adv. Sci. **9**, 2104599 (2022).
[13]B. Gupta, M. A. Hossain, A. Riaz, A. Sharma, D. Zhang, H. H. Tan, C. Jagadish, K. Catchpole, B. Hoex, and S. Karuturi, "Recent advances in materials design using atomic layer deposition for energy applications," Adv. Funct. Mater. **32**, 2109105 (2022).
[14]M. Leskelä, M. Mattinen, and M. Ritala, "Review article: Atomic layer deposition of optoelectronic materials," J. Vac. Sci. Technol. B **37**, 030801 (2019).
[15]B. J. O'Neill, D. H. K. Jackson, J. Lee, C. Canlas, P. C. Stair, C. L. Marshall, J. W. Elam, T. F. Kuech, J. A. Dumesic, and G. W. Huber, "Catalyst design with atomic layer deposition," ACS Catal. **5**, 1804 (2015).
[16]M. Madadi, J. Heiska, J. Multia, and M. Karppinen, "Atomic and molecular layer deposition of alkali metal based thin films," ACS Appl. Mater. Interfaces **13**, 56793 (2021).
[17]Y. Zhao, L. Zhang, J. Liu, K. Adair, F. Zhao, Y. Sun, T. Wu, X. Bi, K. Amine, J. Lu, and X. Sun, "Atomic/molecular layer deposition for energy storage and conversion," Chem. Soc. Rev. **50**, 3889 (2021).
[18]X. Meng, X.-Q. Yang, and X. Sun, "Emerging applications of atomic layer deposition for lithium-ion battery studies," Adv. Mater. **24**, 3589 (2012).
[19]M. A. Hossain, K. T. Khoo, X. Cui, G. K. Poduval, T. Zhang, X. Li, W. M. Li, and B. Hoex, "Atomic layer deposition enabling higher efficiency solar cells: A review," Nano. Mater. Sci. **2**, 204 (2020).
[20]V. Zardetto, B. L. Williams, A. Perrotta, F. Di Giacomo, M. A. Verheijen, R. Andriessen, W. M. M. Kessels, and M. Creatore, "Atomic layer deposition for perovskite solar cells: Research status, opportunities and challenges," Sustainable Energy Fuels **1**, 30 (2017).

[21]J. P. Niemelä, A. J. Karttunen, and M. Karppinen, "Inorganic–organic superlattice thin films for thermoelectrics," J. Mater. Chem. C **3**, 10349 (2015).
[22]N. Cheng, Y. Shao, J. Liu, and X. Sun, "Electrocatalysts by atomic layer deposition for fuel cell applications," Nano Energy **29**, 220 (2016).
[23]J. Seo, S. Kim, S. Jeon, S. Kim, J. H. Kim, and W. Jung, "Nanoscale interface engineering for solid oxide fuel cells using atomic layer deposition," Nanoscale Adv. **4**, 1060 (2022).
[24]O. Nilsen, M. Peussa, H. Fjellvåg, L. Niinistö, and A. Kjekshus, "Thin film deposition of lanthanum manganite perovskite by the ALE process," J. Mater. Chem. **9**, 1781 (1999).
[25]C. N. R. Rao, A. K. Cheetham, and R. Mahesh, "Giant magnetoresistance and related properties of rare-earth manganates and other oxide systems," Chem. Mater. **8**, 2421 (1996).
[26]A. Tanskanen, O. Mustonen, and M. Karppinen, "Simple ALD process for ε-Fe_2O_3 thin films," APL Mater. **5**, 056104 (2017).
[27]T. Jussila, A. Philip, J. Lindén, and M. Karppinen, "High-quality magnetically hard ε-Fe_2O_3 thin films through atomic layer deposition for room-temperature applications," Adv. Eng. Mater. **25**, 2201262 (2023).
[28]J. Jin, S. Ohkoshi, and K. Hashimoto, "Giant coercive field of nanometer-sized iron oxide," Adv. Mater. **16**, 48 (2004).
[29]J. Tuček, R. Zbořil, A. Namai, and S-i Ohkoshi, ε"Fe_2O_3: An advanced nanomaterial exhibiting giant coercive field, millimeter-wave ferromagnetic resonance, and magnetoelectric coupling," Chem. Mater. **22**, 6483 (2010).
[30]E. Longo, C. Wiemer, M. Belli, R. Cecchini, M. Longo, M. Cantoni, C. Rinaldi, M. D. Overbeek, C. H. Winter, G. Gubbiotti, G. Tallarida, M. Fanciulli, and R. Mantovan, "Ferromagnetic resonance of Co thin films grown by atomic layer deposition on the Sb_2Te_3 topological insulator," J. Magn. Magn. Mater. **509**, 166885 (2020).
[31]M. Jullien, C. S. Chang, L. Badie, S. Robert, M. Hehn, D. Lacour, and F. Montaigne, "Magnetoresistive properties of cobalt thin films grown by plasma-assisted atomic layer deposition," J. Phys. D: Appl. Phys. **54**, 105002 (2020).
[32]M. M. Kerrigan, J. P. Klesko, and C. H. Winter, "Low temperature, selective atomic layer deposition of cobalt metal films using bis(1,4-di-tert-butyl-1,3-diazadienyl)cobalt and alkylamine precursors," Chem. Mater. **29**, 7458 (2017).
[33]E. Longo, R. Mantovan, R. Cecchini, M. D. Overbeek, M. Longo, G. Trevisi, L. Lazzarini, G. Tallarida, M. Fanciulli, C. H. Winter, and C. Wiemer, "ALD growth of ultra-thin Co layers on the topological insulator Sb_2Te_3," Nano Res. **13**, 570 (2020).
[34]J. Cai, X. Han, X. Wang, and X. Meng, "Atomic layer deposition of two-dimensional layered materials: Processes, growth mechanisms, and characteristics," Matter **2**, 587 (2020).
[35]Y. Kim, W. J. Woo, D. Kim, S. Lee, S-m Chung, J. Park, and H. Kim, "Atomic-layer-deposition-based 2D transition metal chalcogenides: Synthesis, modulation, and applications," Adv. Mater. **33**, 2005907 (2021).
[36]J. Bachmann, Jing, M. Knez, S. Barth, H. Shen, S. Mathur, U. Gösele, and K. Nielsch, "Ordered iron oxide nanotube arrays of controlled geometry and tunable magnetism by atomic layer deposition," J. Am. Chem. Soc. **129**, 9554 (2007).
[37]A. Philip, Y. Zhou, G. C. Tewari, S. van Dijken, and M. Karppinen, "Optically controlled large-coercivity room-temperature thin-film magnets," J. Mater. Chem. C **10**, 294 (2022).
[38]R. Zierold, C. Lam, J. Dendooven, J. Gooth, T. Böhnert, P. Sergelius, F. Munnik, J. Moreno, D. Görlitz, C. Detavernier, and K. Nielsch, "Magnetic characterization and electrical field-induced switching of magnetite thin films synthesized by atomic layer deposition and subsequent thermal reduction," J. Phys. D: Appl. Phys. **47**, 485001 (2014).
[39]R. Mantovan, M. Georgieva, M. Perego, H. L. Lu, S. Cocco, A. Zenkevich, G. Scarel, and M. Fanciulli, "Atomic layer deposition of magnetic thin films," Acta Phys. Pol., A **112**, 1271 (2007).
[40]Y. T. Chong, E. M. Y. Yau, K. Nielsch, and J. Bachmann, "Direct atomic layer deposition of ternary ferrites with various magnetic properties," Chem. Mater. **22**, 6506 (2010).
[41]P. Jalkanen, V. Tuboltsev, B. Marchand, A. Savin, M. Puttaswamy, M. Vehkamäki, K. Mizohata, M. Kemell, T. Hatanpää, V. Rogozin, J. Räisänen, M. Ritala, and M. Leskelä, "Magnetic properties of polycrystalline bismuth ferrite thin films grown by atomic layer deposition," J. Phys. Chem. Lett. **5**, 4319 (2014).
[42]M. C. Giordano, S. Escobar Steinvall, S. Watanabe, A. Fontcuberta i Morral, and D. Grundler, "Ni80Fe20 nanotubes with optimized spintronic functionalities prepared by atomic layer deposition," Nanoscale **13**, 13451 (2021).
[43]A. Philip, J.-P. Niemelä, G. C. Tewari, B. Putz, T. E. J. Edwards, M. Itoh, I. Utke, and M. Karppinen, "Flexible ε-Fe_2O_3-terephthalate thin-film magnets through ALD/MLD," ACS Appl. Mater. Interfaces **12**, 21912 (2020).
[44]P. Salles, R. Guzmán, D. Zanders, A. Quintana, I. Fina, F. Sánchez, W. Zhou, A. Devi, and M. Coll, "Bendable polycrystalline and magnetic $CoFe_2O_4$ membranes by chemical methods," ACS Appl. Mater. Interfaces **14**, 12845 (2022).
[45]J. Hujanen and I. Raaijmakers, U.S. patent 7,220,669B2 (22 May 2007).
[46]J. Bachmann, J. Escrig, K. Pitzschel, J. M. M. Moreno, J. Jing, D. Görlitz, D. Altbir, and K. Nielsch, "Size effects in ordered arrays of magnetic nanotubes: Pick your reversal mode," J. Appl. Phys. **105**, 07B521 (2009).
[47]S. Tumanski, *In Handbook of Magnetic Measurements* (CRC Press, Boca Raton, FL, 2011), p. 117.
[48]A. Kumari, M. K. Sinha, S. Pramanik, and S. K. Sahu, "Recovery of rare earths from spent NdFeB magnets of wind turbine: Leaching and kinetic aspects," Waste Manage. **75**, 486 (2018).
[49]I. Ennen, D. Kappe, T. Rempel, C. Glenske, and A. Hütten, "Giant magnetoresistance: Basic concepts, microstructure, magnetic interactions and applications," Sensors **16**, 904 (2016).
[50]P. P. Freitas, F. A. Cardoso, V. C. Martins, S. A. M. Martins, J. Loureiro, J. Amaral, R. C. Chaves, S. Cardoso, L. P. Fonseca, A. M. Sebastião, M. Pannetier-Lecoeur, and C. Fermon, "Spintronic platforms for biomedical applications," Lab Chip **12**, 546 (2012).
[51]C. Lueng, P. Lupo, P. J. Metaxas, M. Kostylev, and A. O. Adeyeye, "Nanopatterning-enhanced sensitivity and response time of dynamic palladium/cobalt/palladium hydrogen gas sensors," Adv. Mater. Technol. **1**, 1600097 (2016).
[52]C. Lueng, P. Lupo, T. Schefer, P. J. Metaxas, A. O. Adeyeye, and M. Kostylev, "Sensitivity of ferromagnetic resonance in PdCo alloyed films to hydrogen gas," Int. J. Hydrogen Energy **44**, 7715 (2019).
[53]N. Kulesh, A. Bolyachkin, I. Suzuki, Y. K. Takahashi, H. Sepehri-Amin, and K. Hono, "Data-driven optimization of FePt heat-assisted magnetic recording media accelerated by deep learning TEM image segmentation," Acta Mater. **255**, 119039 (2023).
[54]W. Eerenstein, N. D. Mathur, and J. F. Scott, "Multiferroic and magnetoelectric materials," Nature **442**, 759 (2006).
[55]A. V. Nikam, B. L. V. Prasad, and A. A. Kulkarni, "Wet chemical synthesis of metal oxide nanoparticles: A review," CrystEngComm **20**, 5091 (2018).
[56]P. Tartaj, M. P. Morales, T. Gonzalez-Carreño, S. Veintemillas-Verdaguer, and C. J. Serna, "The iron oxides strike back: From biomedical applications to energy storage devices and photoelectrochemical water splitting," Adv. Mater. **23**, 5243 (2011).
[57]T. Neuberger, B. Schöpf, H. Hofmann, M. Hofmann, and B. von Rechenberg, "Superparamagnetic nanoparticles for biomedical applications: Possibilities and limitations of a new drug delivery system," J. Magn. Magn. Mater. **293**, 483 (2005).
[58]Y. Ha, S. Ko, I. Kim, Y. Huang, K. Mohanty, C. Huh, and J. A. Maynard, "Recent advances incorporating superparamagnetic nanoparticles into immunoassays," ACS Appl. Nano Mater. **1**, 512 (2018).
[59]R. J. D. Tilley, *Understanding Solids* (John Wiley & Sons Ltd, Chichester, 2013), p. 361.
[60]J. M. D. Coey, *Magnetism and Magnetic Materials* (Cambridge University Press, Cambridge, 2009), p. 264.
[61]Y. Zhang, M. Liu, B. Peng, Z. Zhou, X. Chen, S.-M. Yang, Z.-D. Jiang, J. Zhang, W. Ren, and Z.-G. Ye, "Controlled phase and tunable magnetism in ordered iron oxide nanotube arrays prepared by atomic layer deposition," Sci. Rep. **6**, 18401 (2016).
[62]J. S. Miller and A. J. Epstein, "Organic and organometallic molecular magnetic materials—designer magnets," Angew. Chem. Int. Ed. **33**, 385 (1994).
[63]B. Balasubramanian, P. Mukherjee, R. Skomski, P. Manchanda, B. Das, and D. J. Sellmyer, "Magnetic nanostructuring and overcoming Brown's paradox to realize extraordinary high-temperature energy products," Sci. Rep. **4**, 6265 (2014).

[64]W. Kuch, "Edge atoms do all the work," Nat. Mater. **2**, 505 (2003).
[65]J. M. D. Coey, *Magnetism and Magnetic Materials* (Cambridge University Press, Cambridge, 2009), p. 128.
[66]W. C. Law, T. L. Jin, X. T. Zhu, R. R. Nistala, N. Thiyagarajah, C. S. Seet, and W. S. Lew, "Perpendicular magnetic anisotropy in Co/Pt multilayers induced by hcp-Ho at 400 °C," J. Magn. Magn. Mater. **477**, 124 (2019).
[67]K. Yakushiji, T. Saruya, H. Kubota, A. Fukushima, T. Nagahama, S. Yuasa, and K. Ando, "Ultrathin Co/Pt and Co/Pd superlattice films for MgO-based perpendicular magnetic tunnel junctions," Appl. Phys. Lett. **97**, 232508 (2010).
[68]R. Comes, M. Gu, M. Khokhlov, J. Lu, and S. A. Wolf, "Microstructural and domain effects in epitaxial $CoFe_2O_4$ films on MgO with perpendicular magnetic anisotropy," J. Magn. Magn. Mater. **324**, 524 (2012).
[69]S. E. Shirsath, X. Liu, Y. Yasukawa, S. Li, and A. Morisako, "Switching of magnetic easy-axis using crystal orientation for large perpendicular coercivity in $CoFe_2O_4$ thin film," Sci. Rep. **6**, 30074 (2016).
[70]M. Daub, M. Knez, U. Goesele, and K. Nielsch, "Ferromagnetic nanotubes by atomic layer deposition in anodic alumina membranes," J. Appl. Phys. **101**, 09J111 (2007).
[71]Y. T. Chong, D. Görlitz, S. Martens, M. Y. E. Yau, S. Allende, J. Bachmann, and K. Nielsch, "Multilayered core/shell nanowires displaying two distinct magnetic switching events," Adv. Mater. **22**, 2435 (2010).
[72]T. Suntola and J. Antson, International patent FIN 52359, U.S. 4,058,430 (15 November 1977).
[73]T. Suntola, "Atomic layer epitaxy," Mater. Sci. Rep. **4**, 261 (1989).
[74]S. M. George, "Atomic layer deposition: An overview," Chem. Rev. **110**, 111 (2010).
[75]M. Ritala, *Niinistö J, in Chemical Vapour Deposition—Precursors, Processes and Applications*, edited by A. C. Jones and M. L. Hitchman (Royal Society of Chemistry, London, 2009), p. 158.
[76]A. S. Asundi, J. A. Raiford, and S. F. Bent, "Opportunities for atomic layer deposition in emerging energy technologies," ACS Energy Lett. **4**, 908 (2019).
[77]V. Cremers, R. L. Puurunen, and J. Dendooven, "Conformality in atomic layer deposition: Current status overview of analysis and modelling," Appl. Phys. Rev. **6**, 021302 (2019).
[78]M. Knez, K. Nielsch, and L. Niinistö, "Synthesis and surface engineering of complex nanostructures by atomic layer deposition," Adv. Mater. **19**, 3425 (2007).
[79]T. Suntola, "Surface chemistry of materials deposition at atomic layer level," Appl. Surf. Sci. **100–101**, 391 (1996).
[80]N. E. Richey, C. de Paula, and S. F. Bent, "Understanding chemical and physical mechanisms in atomic layer deposition," J. Chem. Phys. **152**, 040902 (2020).
[81]R. L. Puurunen, "Surface chemistry of atomic layer deposition: A case study for the trimethylaluminum/water process," J. Appl. Phys. **97**, 121301 (2005).
[82]F. Zhang, G. Sun, W. Zhao, L. Wang, L. Zheng, S. Liu, B. Liu, L. Dong, X. Liu, G. Yan, L. Tian, and Y. Zeng, "Atomic layer deposition of $BiFeO_3$ thin films using β-diketonates and H_2O," J. Phys. Chem. C **117**, 24579 (2013).
[83]E. Ahvenniemi, M. Matvejeff, and M. Karppinen, "$SrCoO_{3-\delta}$ thin films by atomic layer deposition," Appl. Surf. Sci. **320**, 838 (2014).
[84]E. Ahvenniemi, M. Matvejeff, and M. Karppinen, "Atomic layer deposition of quaternary oxide (La,Sr,)$CoO_{3-\delta}$ thin films," Dalton Trans. **44**, 8001 (2015).
[85]O. Nilsen, E. Rauwel, H. Fjellvåg, and A. Kjekshus, "Growth of $La_{1-x}Ca_xMnO_3$ thin films by atomic layer deposition," J. Mater. Chem. **17**, 1466 (2007).
[86]K. Kukli, M. Kemell, H. Castán, S. Dueñas, J. Link, R. Stern, M. J. Heikkilä, T. Jõgiaas, J. Kozlova, M. Rähn, K. Mizohata, M. Ritala, and M. Leskelä, "Magnetic properties and resistive switching in mixture films and nanolaminates consisting of iron and silicon oxides grown by atomic layer deposition," J. Vac. Sci. Technol. A **38**, 042405 (2020).
[87]J. Multia and M. Karppinen, "Atomic/molecular layer deposition for designer's functional metal–organic materials," Adv. Mater. Interfaces **9**, 2200210 (2022).
[88]A. V. Plokhikh, I. A. Karateev, M. Falmbigl, A. L. Vasiliev, J. Lapano, R. Engel-Herbert, and J. E. Spanier, "Toward a low-temperature route for epitaxial integration of $BiFeO_3$ on Si," J. Phys. Chem. C **123**, 12203 (2019).
[89]M. Puttaswamy, M. Vehkamäki, K. Kukli, M. C. Dimri, M. Kemell, T. Hatanpää, M. J. Heikkilä, K. Mizohata, R. Stern, M. Ritala, and M. Leskelä, "Bismuth iron oxide thin films using atomic layer deposition of alternating bismuth oxide and iron oxide layers," Thin Solid Films **611**, 78 (2016).
[90]T. Tynell, I. Terasaki, H. Yamauchi, and M. Karppinen, "Thermoelectric characteristics of (Zn,Al)O/hydroquinone superlattices," J. Mater. Chem. A **1**, 13619 (2013).
[91]A. J. Karttunen, L. Sarnes, R. Townsend, J. Mikkonen, and M. Karppinen, "Flexible thermoelectric ZnO–organic superlattices on cotton textile substrates by ALD/MLD," Adv. Electron. Mater. **3**, 1600459 (2017).
[92]A. Tanskanen and M. Karppinen, "Tailoring of optoelectronic properties of ϵ-Fe_2O_3 thin films through insertion of organic interlayers," Phys. Status Solidi RRL **12**, 1800390 (2018).
[93]J.-P. Niemelä and M. Karppinen, "Tunable optical properties of hybrid inorganic–organic, $[(TiO_2)_m(Ti–O–C_6H_4–O–)_k]_n$ superlattice thin films," Dalton Trans. **44**, 591 (2015).
[94]A. Philip, R. Ghiyasi, and M. Karppinen, "Visible-light absorbing TiO_2: Curcumin thin films with ALD/MLD," ChemNanoMat **7**, 253 (2021).
[95]F. Krahl, A. Giri, J. A. Tomko, T. Tynell, P. E. Hopkins, and M. Karppinen, "Thermal conductivity reduction at inorganic–organic interfaces: From regular superlattices to irregular gradient layer sequences," Adv. Mater. Interfaces **5**, 1701692 (2018).
[96]A. Devi, "Old chemistries' for new applications: Perspectives for development of precursors for MOCVD and ALD applications," Coord. Chem. Rev. **257**, 3332 (2013).
[97]M. Leskelä and M. Ritala, "Atomic layer deposition chemistry: Recent developments and future challenges," Angew. Chem. Int. Ed. **42**, 5548 (2003).
[98]J. R. Avila, D. W. Kim, M. Rimoldi, O. K. Farha, and J. T. Hupp, "Fabrication of thin films of α-Fe_2O_3 via atomic layer deposition using iron bisamidinate and water under mild growth conditions," ACS Appl. Mater. Interfaces **7**, 16138 (2015).
[99]K. Yoshida, I. Nagata, K. Saito, M. Miura, K. Kanomata, B. Ahmmad, S. Kubota, and F. Hirose, "Room-temperature atomic layer deposition of iron oxide using plasma excited humidified argon," J. Vac. Sci. Technol. A **40**, 022408 (2022).
[100]M. M. Kerrigan, J. P. Klesko, K. J. Blakeney, and C. H. Winter, "Low temperature, selective atomic layer deposition of nickel metal thin films," ACS Appl. Mater. Interfaces **10**, 14200 (2018).
[101]D. Peeters, A. Sadlo, K. Lowjaga, O. Mendoza Reyes, L. Wang, L. Mai, M. Gebhard, D. Rogalla, H.-W. Becker, I. Giner, G. Grundmeier, D. Mitoraj, M. Grafen, A. Ostendorf, R. Beranek, and A. Devi, "Nanostructured Fe_2O_3 processing via water-assisted ALD and low-temperature CVD from a versatile iron ketoiminate precursor," Adv. Mater. Interfaces **4**, 1700155 (2017).
[102]L. C. Kalutarage, P. D. Martin, M. J. Heeg, and C. H. Winter, "Volatile and thermally stable mid to late transition metal complexes containing α-imino alkoxide ligands, a new strongly reducing coreagent, and thermal atomic layer deposition of Ni, Co, Fe, and Cr metal films," J. Am. Chem. Soc. **135**, 12588 (2013).
[103]Y. Zhang, L. Du, X. Liu, and Y. Ding, "High growth per cycle thermal atomic layer deposition of Ni films using an electron-rich precursor," Nanoscale **11**, 3484 (2019).
[104]B. Zhu, Z.-J. Ding, X. Wu, W.-J. Liu, D. W. Zhang, and S.-J. Ding, "Plasma-enhanced atomic layer deposition of cobalt films using $Co(EtCp)_2$ as a metal precursor," Nanoscale Res. Lett. **14**, 76 (2019).
[105]O. Nilsen, M. Lie, S. Foss, H. Fjellvåg, and A. Kjekshus, "Effect of magnetic field on the growth of α-Fe_2O_3 thin films by atomic layer deposition," Appl. Surf. Sci. **227**, 40 (2004).
[106]M. Lie, H. Fjellvåg, and A. Kjekshus, "Growth of Fe_2O_3 thin films by atomic layer deposition," Thin Solid Films **488**, 74 (2005).
[107]C. D. Pham, J. Chang, M. A. Zurbuchen, and J. P. Chang, "Magnetic properties of $CoFe_2O_4$ thin films synthesized by radical-enhanced atomic layer deposition," ACS Appl. Mater. Interfaces **9**, 36980 (2017).
[108]M. Lie, K. Barnholt Klepper, O. Nilsen, H. Fjellvåg, and A. Kjekshus, "Growth of iron cobalt oxides by atomic layer deposition," Dalton Trans. **2008**, 253.
[109]S. Vangelista, A. Lamperti, C. Wiemer, M. Fanciulli, and R. Mantovan, "Atomic layer deposition of hexagonal $ErFeO_3$ thin films on SiO_2/Si," Thin Solid Films **604**, 18 (2016).

[110]C. D. Pham, J. Chang, M. A. Zurbuchen, and J. P. Chang, "Synthesis and characterization of $BiFeO_3$ thin films for multiferroic applications by radical enhanced atomic layer deposition," Chem. Mater. **27**, 7282 (2015).
[111]S. K. Patel, C. T. Karaba, D. D. Robertson, J. Chang, K. Fitzell, C. Z. Salamat, J. P. Chang, and S. H. Tolbert, "Increased magnetoelectric coupling in porous nanocomposites of $CoFe_2O_4$ and $BiFeO_3$ with residual porosity for switchable magnetic devices," ACS Appl. Nano Mater. **6**, 4141 (2023).
[112]K. Uusi-Esko, E. L. Rautama, M. Laitinen, T. Sajavaara, and M. Karppinen, "Control of oxygen nonstoichiometry and magnetic property of $MnCo_2O_4$ thin films grown by atomic layer deposition," Chem. Mater. **22**, 6297 (2010).
[113]D. J. Hagen, T. S. Tripathi, and M. Karppinen, "Atomic layer deposition of nickel–cobalt spinel thin films," Dalton Trans. **46**, 4796 (2017).
[114]D. J. Hagen, T. S. Tripathi, I. Terasaki, and M. Karppinen, "Microstructure and optical properties of ultra-thin NiO films grown by atomic layer deposition," Semicond. Sci. Technol. **33**, 115015 (2018).
[115]M. Coll, J. Gazquez, I. Fina, Z. Khayat, A. Quindeau, M. Alexe, M. Varela, S. Trolier-McKinstry, X. Obradors, and T. Puig, "Nanocrystalline ferroelectric $BiFeO_3$ thin films by low-temperature atomic layer deposition," Chem. Mater. **27**, 6322 (2015).
[116]K. Uusi-Esko, J. Malm, and M. Karppinen, "Atomic layer deposition of hexagonal and orthorhombic $YMnO_3$ thin films," Chem. Mater. **21**, 5691 (2009).
[117]K. Uusi-Esko and M. Karppinen, "Extensive series of hexagonal and orthorhombic $RMnO_3$ (R = Y, La, Sm, Tb, Yb, Lu) thin films by atomic layer deposition," Chem. Mater. **23**, 1835 (2011).
[118]H. Khanduri, M. Chandra Dimri, S. Vasala, S. Leinberg, R. Lõhmus, T. V. Ashworth, A. Mere, J. Krustok, M. Karppinen, and R. Stern, "Magnetic and structural studies of $LaMnO_3$ thin films prepared by atomic layer deposition," J. Phys. D: Appl. Phys. **46**, 175003 (2013).
[119]J. H. Choi, C. Pham, J. Dorman, T. Kim, and J. P. Chang, "Atomic layer deposition of $YMnO_3$ thin films," J. Magn. Magn. Mater. **498**, 166146 (2020).
[120]A. Tamm, K. Kalam, H. Seemen, J. Kozlova, K. Kukli, J. Aarik, J. Link, R. Stern, S. Dueñas, and H. Castán, "Magnetic and electrical performance of atomic layer deposited iron erbium oxide thin films," ACS Omega **2**, 8836 (2017).
[121]K. Zhou, J.-Q. Huang, Q. Zhang, and F. Wei, "Multi-directional growth of aligned carbon nanotubes over catalyst film prepared by atomic layer deposition," Nanoscale Res. Lett. **5**, 1555 (2010).
[122]M. de Ridder, P. C. van de Ven, R. G. van Welzenis, H. H. Brongersma, S. Helfensteyn, C. Creemers, P. Van Der Voort, M. Baltes, M. Mathieu, and E. F. Vansant, "Growth of iron oxide on yttria-stabilized zirconia by atomic layer deposition," J. Phys. Chem. B **106**, 13146 (2002).
[123]M. Sarr, N. Bahlawane, D. Arl, M. Dossot, E. McRae, and D. Lenoble, "Tailoring the properties of atomic layer deposited nickel and nickel carbide thin films via chain-length control of the alcohol reducing agents," J. Phys. Chem. C **118**, 23385 (2014).
[124]M. A. Hopkins, N. Kuperman, J. Barnes, and R. Solanki, paper presented at the 2018 IEEE 13th Nanotechnology Materials and Devices Conference (NMDC) (2018).
[125]M. Napari, T. N. Huq, T. Maity, D. Gomersall, K. M. Niang, A. Barthel, J. E. Thompson, S. Kinnunen, K. Arstila, T. Sajavaara, R. L. Z. Hoye, A. J. Flewitt, and J. L. MacManus-Driscoll, "Antiferromagnetism and p-type conductivity of nonstoichiometric nickel oxide thin films," InfoMat **2**, 769 (2020).
[126]K. Kalam, R. Rammula, P. Ritslaid, T. Käämbre, J. Link, R. Stern, G. Vinuesa, S. Dueñas, H. Castán, A. Tamm, and K. Kukli, "Atomic layer deposited nanolaminates of zirconium oxide and manganese oxide from manganese(III)acetylacetonate and ozone," Nanotechnology **32**, 335703 (2021).
[127]V. Pore, M. Dimri, H. Khanduri, R. Stern, J. Lu, L. Hultman, K. Kukli, M. Ritala, and M. Leskelä, "Atomic layer deposition of ferromagnetic cobalt doped titanium oxide thin films," Thin Solid Films **519**, 3318 (2011).
[128]K. Nielsch, J. Bachmann, M. Daub, J. Jing, M. Knez, U. Gösele, S. Barth, S. Mathur, J. Escrig, and D. Altbir, "Ferromagnetic nanostructures by atomic layer deposition: From thin films towards core-shell nanotubes," ECS Trans. **11**, 139 (2007).
[129]J. Escrig, J. Bachmann, J. Jing, M. Daub, D. Altbir, and K. Nielsch, "Crossover between two different magnetization reversal modes in arrays of iron oxide nanotubes," Phys. Rev. B **77**, 214421 (2008).
[130]K. Pitzschel, J. Bachmann, J. M. Montero-Moreno, J. Escrig, D. Görlitz, and K. Nielsch, "Reversal modes and magnetostatic interactions in $Fe_3O_4/ZrO_2/Fe_3O_4$ multilayer nanotubes," Nanotechnology **23**, 495718 (2012).
[131]B. Marchand, P. Jalkanen, V. Tuboltsev, M. Vehkamäki, M. Puttaswamy, M. Kemell, K. Mizohata, T. Hatanpää, A. Savin, J. Räisänen, M. Ritala, and M. Leskelä, "Electric and magnetic properties of ALD-grown $BiFeO_3$ films," J. Phys. Chem. C **120**, 7313 (2016).
[132]A. Majtyka, A. Nowak, B. Marchand, D. Chrobak, M. Ritala, J. Räisänen, and R. Nowak, "Structure-dependent mechanical properties of ALD-grown nanocrystalline $BiFeO_3$ multiferroics," J. Nanomater. **2016**, 5348471.
[133]C. Bohr, P. Yu, M. Scigaj, C. Hegemann, T. Fischer, M. Coll, and S. Mathur, "Atomic scale growth of $GdFeO_3$ perovskite thin films," Thin Solid Films **698**, 137848 (2020).
[134]K. Kukli, M. Kemell, M. C. Dimri, E. Puukilainen, A. Tamm, R. Stern, M. Ritala, and M. Leskelä, "Holmium titanium oxide thin films grown by atomic layer deposition," Thin Solid Films **565**, 261 (2014).
[135]A. R. Akbashev, G. Chen, and J. E. Spanier, "A facile route for producing single-crystalline epitaxial perovskite oxide thin films," Nano Lett. **14**, 44 (2014).
[136]A. R. Akbashev, M. Falmbigl, A. V. Plokhikh, and J. E. Spanier, "*In situ* crystallization study of impurity phases in Bi–Fe–O thin films grown by atomic layer deposition," CrystEngComm **19**, 166 (2017).
[137]S. Ramazanov, D. Sobola, Ş. Ţălu, F. Orudzev, A. Arman, P. Kaspar, R. Dallaev, and G. Ramazanov, "Multiferroic behavior of the functionalized surface of a flexible substrate by deposition of Bi_2O_3 and Fe_2O_3," Microsc. Res. Tech. **85**, 1300 (2022).
[138]S. Ramazanov, D. Sobola, F. Orudzhev, A. Knápek, J. Polčák, M. Potoček, P. Kaspar, and R. Dallaev, "Surface modification and enhancement of ferromagnetism in $BiFeO_3$ nanofilms deposited on HOPG," Nanomaterials **10**, 1990 (2020).
[139]S. Ramazanov, D. Sobola, G. Gajiev, F. Orudzhev, P. Kaspar, and A. Gummetov, "Multiferroic/polymer flexible structures obtained by atomic layer deposition," Nanomaterials **13**, 139 (2023).
[140]P. Yu, S. M. J. Beer, A. Devi, and M. Coll, "Fabrication of $Gd_xFe_yO_z$ films using an atomic layer deposition-type approach," CrystEngComm **23**, 730 (2021).
[141]R. Zierold, Z. Wu, J. Biskupek, U. Kaiser, J. Bachmann, C. E. Krill Iii, and K. Nielsch, "Magnetic, multilayered nanotubes of low aspect ratios for liquid suspensions," Adv. Funct. Mater. **21**, 226 (2011).
[142]P. Márquez, D. Alburquenque, F. Celis, R. M. Freire, and J. Escrig, "Structural, morphological and magnetic properties of iron oxide thin films obtained by atomic layer deposition as a function of their thickness," J. Magn. Magn. Mater. **530**, 167914 (2021).
[143]J. L. Palma, A. Pereira, R. Álvaro, J. M. García-Martín, and J. Escrig, "Magnetic properties of Fe(3)O(4) antidot arrays synthesized by AFIR: Atomic layer deposition, focused ion beam and thermal reduction," Beilstein J. Nanotechnol. **9**, 1728 (2018).
[144]K. Kukli, M. C. Dimri, A. Tamm, M. Kemell, T. Käämbre, M. Vehkamäki, M. Puttaswamy, R. Stern, I. Kuusik, A. Kikas, M. Tallarida, D. Schmeißer, M. Ritala, and M. Leskelä, "Structural and magnetic studies on iron oxide and iron-magnesium oxide thin films deposited using ferrocene and (dimethylaminomethyl)ferrocene precursors," ECS J. Solid State Sci. Technol. **2**, N45 (2012).
[145]G. Wan, G. Wang, X. Huang, H. Zhao, X. Li, K. Wang, L. Yu, X. Peng, and Y. Qin, "Uniform Fe_3O_4 coating on flower-like ZnO nanostructures by atomic layer deposition for electromagnetic wave absorption," Dalton Trans. **44**, 18804 (2015).
[146]A. Tamm, M. C. Dimri, J. Kozlova, A. Aidla, T. Tätte, T. Arroval, U. Mäeorg, H. Mändar, R. Stern, and K. Kukli, "Atomic layer deposition of ferromagnetic iron oxide films on three-dimensional substrates with tin oxide nanoparticles," J. Cryst. Growth **343**, 21 (2012).
[147]K. Pitzschel, J. M. M. Moreno, J. Escrig, O. Albrecht, K. Nielsch, and J. Bachmann, "Controlled introduction of diameter modulations in arrayed magnetic iron oxide nanotubes," ACS Nano **3**, 3463 (2009).
[148]O. Albrecht, R. Zierold, C. Patzig, J. Bachmann, C. Sturm, B. Rheinländer, M. Grundmann, D. Görlitz, B. Rauschenbach, and K. Nielsch, "Tubular magnetic nanostructures based on glancing angle deposited templates and atomic layer deposition," Phys. Status Solidi B **247**, 1365 (2010).

[149]G. Wang, Z. Gao, G. Wan, S. Lin, P. Yang, and Y. Qin, "High densities of magnetic nanoparticles supported on graphene fabricated by atomic layer deposition and their use as efficient synergistic microwave absorbers," Nano Res. **7**, 704 (2014).
[150]S. Zhao, Z. Gao, C. Chen, G. Wang, B. Zhang, Y. Chen, J. Zhang, X. Li, and Y. Qin, "Alternate nonmagnetic and magnetic multilayer nanofilms deposited on carbon nanocoils by atomic layer deposition to tune microwave absorption property," Carbon **98**, 196 (2016).
[151]G. Wang, Z. Gao, S. Tang, C. Chen, F. Duan, S. Zhao, S. Lin, Y. Feng, L. Zhou, and Y. Qin, "Microwave absorption properties of carbon nanocoils coated with highly controlled magnetic materials by atomic layer deposition," ACS Nano **6**, 11009 (2012).
[152]Y. Zhang, M. Liu, Y. Zhang, X. Chen, W. Ren, and Z.-G. Ye, "Atomic layer deposition of superparamagnetic and ferrimagnetic magnetite thin films," J. Appl. Phys. **117**, 17C743 (2015).
[153]L. Zhang, W. Hou, T. Li, W. Geng, J. Mu, J. He, X. Hou, S. Han, and X. Chou, "Electric field tuning of magnetism in Fe_3O_4/Pt/PZN-PT heterostructures prepared by atomic layer deposition," ECS J. Solid State Sci. Technol. **10**, 114004 (2021).
[154]Y. Zhang, M. Liu, L. Zhang, Z. Zhou, B. Peng, C. Wang, Q. Lin, Z.-D. Jiang, W. Ren, and Z.-G. Ye, "Multiferroic heterostructures of Fe_3O_4/PMN-PT prepared by atomic layer deposition for enhanced interfacial magnetoelectric couplings," Appl. Phys. Lett. **110**, 082902 (2017).
[155]L. Zhang, Z. Zhou, Y. Zhang, B. Peng, W. Ren, Z. G. Ye, and M. Liu, "Tuning the magnetic anisotropy of Fe_3O_4/Pt heterostructures fabricated by atomic layer deposition with *in situ* magnetic field," IEEE Trans. Magn. **55**, 2001707 (2019).
[156]A. B. F. Martinson, M. J. DeVries, J. A. Libera, S. T. Christensen, J. T. Hupp, M. J. Pellin, and J. W. Elam, "Atomic layer deposition of Fe_2O_3 using ferrocene and ozone," J. Phys. Chem. C **115**, 4333 (2011).
[157]E. Kim, S. Kim, Y. M. Choi, J. H. Park, and H. Shin, "Ultrathin hematite on mesoporous WO_3 from atomic layer deposition for minimal charge recombination," ACS Sustainable Chem. Eng. **8**, 11358 (2020).
[158]Y. T. Chong, M. Y. E. Yau, Y. Yang, M. Zacharias, D. Görlitz, K. Nielsch, and J. Bachmann, "Superparamagnetic behavior in cobalt iron oxide nanotube arrays by atomic layer deposition," J. Appl. Phys. **110**, 043930 (2011).
[159]M. Coll, J. M. Montero Moreno, J. Gazquez, K. Nielsch, X. Obradors, and T. Puig, "Low temperature stabilization of nanoscale epitaxial spinel ferrite thin films by atomic layer deposition," Adv. Funct. Mater. **24**, 5368 (2014).
[160]A. Zolotaryov, S. Goetze, J. Bachmann, D. Goerlitz, D. Hesse, and K. Nielsch, "Ferromagnetism and morphology of annealed Fe_2O_3/Co_XO_Y/ZnO thin films," Adv. Eng. Mater. **13**, 330 (2011).
[161]A. Zolotaryov, S. Goetze, R. Zierold, D. Novikov, B. Birajdar, D. Hesse, and K. Nielsch, "Temperature-dependent solid-state reactions with and without kirkendall effect in Al_2O_3/ZnO, Fe_2O_3/ZnO, and CoXOY/ZnO oxide thin film systems," Adv. Eng. Mater. **12**, 509 (2010).
[162]Y. Zhang, W. Ren, G. Niu, C. Li, C. Wang, Z.-D. Jiang, M. Liu, and Z.-G. Ye, "Atomic layer deposition of void-free $ZnFe_2O_4$ thin films and their magnetic properties," Thin Solid Films **709**, 138206 (2020).
[163]I. S. Golovina, M. Falmbigl, A. V. Plokhikh, T. C. Parker, C. Johnson, and J. E. Spanier, "Effect of annealing conditions on the electrical properties of ALD-grown polycrystalline $BiFeO_3$ films," J. Mater. Chem. C **6**, 5462 (2018).
[164]A. Plokhikh, M. Falmbigl, I. Golovina, A. Akbashev, I. Karateev, M. Presnyakov, A. Vasiliev, and J. Spanier, "Formation of $BiFeO_3$ from a binary oxide superlattice grown by atomic layer deposition," ChemPhysChem **18**, 1996 (2017).
[165]A. P. Espejo, R. Zierold, J. Gooth, J. Dendooven, C. Detavernier, J. Escrig, and K. Nielsch, "Magnetic and electrical characterization of nickel-rich NiFe thin films synthesized by atomic layer deposition and subsequent thermal reduction," Nanotechnology **27**, 345707 (2016).
[166]M. Lammel, D. Scheffler, D. Pohl, P. Swekis, S. Reitzig, S. Piontek, H. Reichlova, R. Schlitz, K. Geishendorf, L. Siegl, B. Rellinghaus, L. Eng, K. Nielsch, S. Goennenwein, and A. Thomas, "Atomic layer deposition of yttrium iron garnet thin films," Phys. Rev. Mater. **6**, 0444411 (2022).
[167]A. Paskaleva, K. Buchkov, A. Galluzzi, D. Spassov, B. Blagoev, T. Ivanov, V. Mehandzhiev, I. A. Avramova, P. Terzyiska, P. Tzvetkov, D. Kovacheva, and M. Polichetti, "Magneto-optical and multiferroic properties of transition-metal (Fe, Co, or Ni)-doped ZnO layers deposited by ALD," ACS Omega **7**, 43306 (2022).
[168]D. Spassov, A. Paskaleva, B. Blagoev, and V. Mehandzhiev, "Electric characterization of transition metal (Co, Ni, Fe) doped ZnO thin layers prepared by atomic layer deposition," J. Phys. Conf. Ser. **2436**, 012014 (2023).
[169]K. Kalam, M. Otsus, J. Kozlova, A. Tarre, A. Kasikov, R. Rammula, J. Link, R. Stern, G. Vinuesa, J. M. Lendínez, S. Dueñas, H. Castán, A. Tamm, and K. Kukli, "Memory effects in nanolaminates of hafnium and iron oxide films structured by atomic layer deposition," Nanomaterials **12**, 2593 (2022).
[170]D. Alburquenque, V. Bracamonte, M. Del Canto, A. Pereira, and J. Escrig, "Dewetting of Co thin films obtained by atomic layer deposition due to the thermal reduction process," MRS Commun. **7**, 848 (2017).
[171]H.-B.-R. Lee and H. Kim, "Area selective atomic layer deposition of cobalt thin films," ECS Trans. **16**, 219 (2008).
[172]H.-B.-R. Lee and H. Kim, "High-quality cobalt thin films by plasma-enhanced atomic layer deposition," Electrochem. Solid-State Lett. **9**, G323 (2006).
[173]H.-B.-R. Lee, Y. J. Park, S. Baik, and H. Kim, "Initial stage growth during plasma-enhanced atomic layer deposition of cobalt," Chem. Vap. Deposition **18**, 41 (2012).
[174]H.-B.-R. Lee, G. H. Gu, J. Y. Son, C. G. Park, and H. Kim, "Spontaneous formation of vertical magnetic-metal-nanorod arrays during plasma-enhanced atomic layer deposition," Small **4**, 2247 (2008).
[175]J. Yoon, H.-B.-R. Lee, D. Kim, T. Cheon, S.-H. Kim, and H. Kim, "Atomic layer deposition of Co using N_2/H_2 plasma as a reactant," J. Electrochem. Soc. **158**, H1179 (2011).
[176]J. Yoon, J.-G. Song, H. Kim, and H.-B.-R. Lee, "Plasma-enhanced atomic layer deposition of Co on metal surfaces," Surf. Coat. Technol. **264**, 60 (2015).
[177]I.-K. Oh, H. Kim, and H.-B.-R. Lee, "Growth mechanism of Co thin films formed by plasma-enhanced atomic layer deposition using NH_3 as plasma reactant," Curr. Appl. Phys. **17**, 333 (2017).
[178]Y.-Q. Cao, T.-Q. Zi, C. Liu, D.-P. Cui, D. Wu, and A.-D. Li, "Co–Pt bimetallic nanoparticles with tunable magnetic and electrocatalytic properties prepared by atomic layer deposition," Chem. Commun. **56**, 8675 (2020).
[179]A. Pereira, J. L. Palma, J. C. Denardin, and J. Escrig, "Temperature-dependent magnetic properties of Ni nanotubes synthesized by atomic layer deposition," Nanotechnology **27**, 345709 (2016).
[180]D. Alburquenque, M. Del Canto, C. Arenas, F. Tejo, A. Pereira, and J. Escrig, "Dewetting of Ni thin films obtained by atomic layer deposition due to the thermal reduction process: Variation of the thicknesses," Thin Solid Films **638**, 114 (2017).
[181]M. C. Giordano, K. Baumgaertl, S. Escobar Steinvall, J. Gay, M. Vuichard, A. Fontcuberta i Morral, and D. Grundler, "Plasma-enhanced atomic layer deposition of nickel nanotubes with low resistivity and coherent magnetization dynamics for 3D spintronics," ACS Appl. Mater. Interfaces **12**, 40443 (2020).
[182]J. Chae, H.-S. Park, and S-w Kang, "Atomic layer deposition of nickel by the reduction of preformed nickel oxide," Electrochem. Solid-State Lett. **5**, C64 (2002).
[183]Y.-P. Wang, Z.-J. Ding, Q.-X. Liu, W.-J. Liu, S.-J. Ding, and D. W. Zhang, "Plasma-assisted atomic layer deposition and post-annealing enhancement of low resistivity and oxygen-free nickel nano-films using nickelocene and ammonia precursors," J. Mater. Chem. C **4**, 11059 (2016).
[184]K. Buchkov, A. Galluzzi, B. Blagoev, A. Paskaleva, P. Terziyska, T. Stanchev, V. Mehandzhiev, P. Tzvetkov, D. Kovacheva, I. Avramova, E. Nazarova, and M. Polichetti, "Magneto-optical characterization of ZnO/Ni nano-laminate obtained via Atomic Layer Deposition," J. Phys. Conf. Ser. **1762**, 012041 (2021).
[185]J. Bachmann, A. Zolotaryov, O. Albrecht, S. Goetze, A. Berger, D. Hesse, D. Novikov, and K. Nielsch, "Stoichiometry of nickel oxide films prepared by ALD," Chem. Vap. Deposition **17**, 177 (2011).
[186]J. Park, H.-B.-R. Lee, D. Kim, J. Yoon, C. Lansalot, J. Gatineau, H. Chevrel, and H. Kim, "Plasma-enhanced atomic layer deposition of Co using Co $(MeCp)_2$ precursor," J. Energy Chem. **22**, 403 (2013).
[187]S. C. Riha, J. M. Racowski, M. P. Lanci, J. A. Klug, A. S. Hock, and A. B. F. Martinson, "Phase discrimination through oxidant selection in low-temperature atomic layer deposition of crystalline iron oxides," Langmuir **29**, 3439 (2013).

[188]R. K. Ramachandran, J. Dendooven, and C. Detavernier, "Plasma enhanced atomic layer deposition of Fe_2O_3 thin films," J. Mater. Chem. A **2**, 10662 (2014).
[189]A. Tamm, A. Tarre, J. Kozlova, M. Rähn, T. Jõgiaas, T. Kahro, J. Link, and R. Stern, "Atomic layer deposition of superparamagnetic ruthenium-doped iron oxide thin film," RSC Adv. **11**, 7521 (2021).
[190]M. Kim, S. Nabeya, D. K. Nandi, K. Suzuki, H.-M. Kim, S.-Y. Cho, K.-B. Kim, and S.-H. Kim, "Atomic layer deposition of nickel using a heteroleptic Ni precursor with NH_3 and selective deposition on defects of graphene," ACS Omega **4**, 11126 (2019).
[191]L. Steier, J. Luo, M. Schreier, M. T. Mayer, T. Sajavaara, and M. Grätzel, "Low-temperature atomic layer deposition of crystalline and photoactive ultrathin hematite films for solar water splitting," ACS Nano **9**, 11775 (2015).
[192]C.-Y. Kao, J.-W. Yoo, Y. Min, and A. J. Epstein, "Molecular layer deposition of an organic-based magnetic semiconducting laminate," ACS Appl. Mater. Interfaces **4**, 137 (2012).
[193]C.-Y. Kao, B. Li, Y. Lu, J.-W. Yoo, and A. J. Epstein, "Thin films of organic-based magnetic materials of vanadium and cobalt tetracyanoethylene by molecular layer deposition," J. Mater. Chem. C **2**, 6171 (2014).
[194]K. Kim, K. Lee, S. Han, T. Park, Y. Lee, J. Kim, S. Yeom, and H. Jeon, "Comparison of Co films deposited by remote plasma atomic layer deposition method with cyclopentadienylcobalt dicarbonyl, $[CpCo(CO)_2]$ and dicobalt octacarbonyl, [Co2(CO)8]," Jpn. J. Appl. Phys., Part II **46**, L173 (2007).
[195]X. Zhong, Z. Wan, and B. Xi, "Preliminary growth of metallic co films by thermal atomic layer deposition using $RCpCo(CO)_2$ and alkylamine precursors," Mater. Lett. **311**, 131605 (2022).
[196]J. Kwon, M. Saly, M. D. Halls, R. K. Kanjolia, and Y. J. Chabal, "Substrate selectivity of $(tBu\text{-}Allyl)Co(CO)_3$ during thermal atomic layer deposition of cobalt," Chem. Mater. **24**, 1025 (2012).
[197]Y.-T. Liu, C.-S. Ku, S.-J. Chiu, H.-Y. Lee, and S.-Y. Chen, "Ultrathin oriented $BiFeO_3$ films from deposition of atomic layers with greatly improved leakage and ferroelectric properties," ACS Appl. Mater. Interfaces **6**, 443 (2014).
[198]M. Aronniemi, J. Saino, and J. Lahtinen, "Characterization and gas-sensing behavior of an iron oxide thin film prepared by atomic layer deposition," Thin Solid Films **516**, 6110 (2008).
[199]H. Seemen, K. Kukli, T. Jõgiaas, P. Ritslaid, J. Link, R. Stern, S. Dueñas, H. Castán, and A. Tamm, "Properties of atomic layer deposited iron oxide and bismuth oxide chloride structures," J. Alloys Compd. **846**, 156099 (2020).
[200]K. Kalam, H. Seemen, M. Mikkor, P. Ritslaid, R. Stern, S. Dueñas, H. Castán, A. Tamm, and K. Kukli, "Electric and magnetic properties of atomic layer deposited ZrO_2-HfO_2 thin films," ECS J. Solid State Sci. Technol. **7**, N117 (2018).
[201]K. Väyrynen, T. Hatanpää, M. Mattinen, M. Heikkilä, K. Mizohata, K. Meinander, J. Räisänen, M. Ritala, and M. Leskelä, "Diamine adduct of cobalt (II) chloride as a precursor for atomic layer deposition of stoichiometric cobalt (II) oxide and reduction thereof to cobalt metal thin films," Chem. Mater. **30**, 3499 (2018).
[202]D. Zanders, J. Liu, J. Obenlüneschloß, C. Bock, D. Rogalla, L. Mai, M. Nolan, S. T. Barry, and A. Devi, "Cobalt metal ALD: Understanding the mechanism and role of zinc alkyl precursors as reductants for low-resistivity Co thin films," Chem. Mater. **33**, 5045 (2021).
[203]H.-E. Nieminen, M. Kaipio, and M. Ritala, "In situ reaction mechanism study on atomic layer deposition of intermetallic Co_3Sn_2 thin films," Chem. Mater. **32**, 8120 (2020).
[204]B. S. Lim, A. Rahtu, and R. G. Gordon, "Atomic layer deposition of transition metals," Nat. Mater. **2**, 749 (2003).
[205]Z. Li, R. G. Gordon, D. B. Farmer, Y. Lin, and J. Vlassak, "Nucleation and adhesion of ALD copper on cobalt adhesion layers and tungsten nitride diffusion barriers," Electrochem. Solid-State Lett. **8**, G182 (2005).
[206]Q. Fan, Z. Guo, Z. Li, Z. Wang, L. Yang, Q. Chen, Z. Liu, and X. Wang, "Atomic layer deposition of cobalt carbide thin films from cobalt amidinate and hydrogen plasma," ACS Appl. Electron. Mater. **1**, 444 (2019).
[207]H.-B.-R. Lee, W.-H. Kim, J. W. Lee, J.-M. Kim, K. Heo, I. C. Hwang, Y. Park, S. Hong, and H. Kim, "High quality area-selective atomic layer deposition Co using ammonia gas as a reactant," J. Electrochem. Soc. **157**, D10 (2010).
[208]J. P. Klesko, M. M. Kerrigan, and C. H. Winter, "Low temperature thermal atomic layer deposition of cobalt metal films," Chem. Mater. **28**, 700 (2016).
[209]M. M. Kerrigan, J. P. Klesko, S. M. Rupich, C. L. Dezelah, R. K. Kanjolia, Y. J. Chabal, and C. H. Winter, "Substrate selectivity in the low temperature atomic layer deposition of cobalt metal films from bis(1,4-di-tert-butyl-1,3-diazadienyl)cobalt and formic acid," J. Chem. Phys. **146**, 052813 (2017).
[210]S. Wolf, M. Breeden, S. Ueda, J. Woodruff, M. Moinpour, R. Kanjolia, and A. Kummel, "The role of oxide formation on insulating versus metallic substrates during Co and Ru selective ALD," Appl. Surf. Sci. **510**, 144804 (2020).
[211]B. Quinard, F. Godel, M. Galbiati, V. Zatko, A. Sander, A. Vecchiola, S. Collin, K. Bouzehouane, F. Petroff, R. Mattana, M. B. Martin, B. Dlubak, and P. Seneor, "A ferromagnetic spin source grown by atomic layer deposition," Appl. Phys. Lett. **120**, 213503 (2022).
[212]K. E. K. Holden, C. L. Dezelah, and J. F. Conley, Jr., "Atomic layer deposition of transparent p-type semiconducting nickel oxide using $Ni(^{tBu2}DAD)_2$ and ozone," ACS Appl. Mater. Interfaces **11**, 30437 (2019).
[213]T. D. M. Elko-Hansen, A. Dolocan, and J. G. Ekerdt, "Atomic interdiffusion and diffusive stabilization of cobalt by copper during atomic layer deposition from bis(n-tert-butyl-n′-ethylpropionamidinato) cobalt(II)," J. Phys. Chem. Lett. **5**, 1091 (2014).
[214]T. D. M. Elko-Hansen and J. G. Ekerdt, "XPS investigation of the atomic layer deposition half reactions of bis(n-tert-butyl-n′-ethylpropionamidinato) cobalt (II)," Chem. Mater. **26**, 2642 (2014).
[215]Z. Zhang, T. Dwyer, S. M. Sirard, and J. G. Ekerdt, "Area-selective atomic layer deposition of cobalt oxide to generate patterned cobalt films," J. Vac. Sci. Technol. A **37**, 020905 (2019).
[216]Z. Zhang, H. C. Nallan, B. M. Coffey, T. Q. Ngo, T. Pramanik, S. K. Banerjee, and J. G. Ekerdt, "Atomic layer deposition of cobalt oxide on oxide substrates and low temperature reduction to form ultrathin cobalt metal films," J. Vac. Sci. Technol. A **37**, 010903 (2019).
[217]Z. Zhou, G. Grocke, A. Yanguas-Gil, X. Wang, Y. Gao, N. Sun, B. Howe, and X. Chen, "$CoFe_2/Al_2O_3$/PMNPT multiferroic heterostructures by atomic layer deposition," Appl. Phys. Lett. **108**, 182907 (2016).
[218]J.-M. Kim, H.-B.-R. Lee, C. Lansalot, C. Dussarrat, J. Gatineau, and H. Kim, "Plasma-enhanced atomic layer deposition of cobalt using cyclopentadienyl isopropyl acetamidinato-cobalt as a precursor," Jpn. J. Appl. Phys., Part I **49**, 05FA10 (2010).
[219]S. Selvaraj, H. Moon, J.-Y. Yun, and D.-H. Kim, "Iron oxide grown by low-temperature atomic layer deposition," Korean J. Chem. Eng. **33**, 3516 (2016).
[220]L. Machala, J. Tuček, and R. Zbořil, "Polymorphous transformations of nanometric iron(III) oxide: A review," Chem. Mater. **23**, 3255 (2011).
[221]T. Amrillah, C. A. C. Abdullah, D. P. Sari, Z. Mumtazah, F. P. Adila, and F. Astuti, "Crafting a next-generation device using iron oxide thin film: A review," Cryst. Growth Des. **21**, 7326 (2021).
[222]M. Napari, T. N. Huq, R. L. Z. Hoye, and J. L. MacManus-Driscoll, "Nickel oxide thin films grown by chemical deposition techniques: Potential and challenges in next-generation rigid and flexible device applications," InfoMat **3**, 536 (2021).
[223]M. R. Rooth, A. Johansson, K. Kukli, J. Aarik, M. Boman, and A. Hårsta, "Atomic layer deposition of iron oxide thin films and nanotubes using ferrocene and oxygen as precursors," Chem. Vap. Deposition **14**, 67 (2008).
[224]J. A. Klug, N. G. Becker, S. C. Riha, A. B. F. Martinson, J. W. Elam, M. J. Pellin, and T. Proslier, "Low temperature atomic layer deposition of highly photoactive hematite using iron(iii) chloride and water," J. Mater. Chem. A **1**, 11607 (2013).
[225]S. Vasala and M. Karppinen, "$A_2B'B''O_6$ perovskites: A review," Prog. Solid State Chem. **43**, 1 (2015).
[226]S.-C. Yang, A. Kumar, V. Petkov, and S. Priya, "Room-temperature magnetoelectric coupling in single-phase $BaTiO_3$-$BiFeO_3$ system," J. Appl. Phys. **113**, 144101 (2013).
[227]M. Kumar, P. C. Sati, A. Kumar, M. Sahni, P. Negi, H. Singh, S. Chauhan, and S. K. Chaurasia, "Recent advances on magnetoelectric coupling in $BiFeO_3$: Technological achievements and challenges," Mater. Today: Proc. **49**, 3046 (2022).
[228]A. Ghazy, M. Lastusaari, and M. Karppinen, "White-light emitting multi-lanthanide terephthalate thin films by atomic/molecular layer deposition," J. Mater. Chem. C **11**, 5331 (2023).
[229]A. Ghazy, M. Safdar, M. Lastusaari, A. Aho, A. Tukiainen, H. Savin, M. Guina, and M. Karppinen, "Luminescent $(Er,Ho)_2O_3$ thin films by ALD to

enhance the performance of silicon solar cells," Sol. Energy Mater. Sol. Cells **219**, 110787 (2021).
[230]B. S. Lim, A. Rahtu, J.-S. Park, and R. G. Gordon, "Synthesis and characterization of volatile, thermally stable, reactive transition metal amidinates," Inorg. Chem. **42**, 7951 (2003).
[231]T. J. Knisley, M. J. Saly, M. J. Heeg, J. L. Roberts, and C. H. Winter, "Volatility and high thermal stability in mid- to late-first-row transition-metal diazadienyl complexes," Organometallics **30**, 5010 (2011).
[232]M. Sarr, N. Bahlawane, D. Arl, M. Dossot, E. McRae, and D. Lenoble, "Atomic layer deposition of cobalt carbide films and their magnetic properties using propanol as a reducing agent," Appl. Surf. Sci. **379**, 523 (2016).
[233]G. Yuan, H. Shimizu, T. Momose, and Y. Shimogaki, "Role of NH_3 feeding period to realize high-quality nickel films by hot-wire-assisted atomic layer deposition," Microelectron. Eng. **120**, 230 (2014).
[234]S. Zhang, R. Xu, N. Luo, and X. Zou, "Two-dimensional magnetic materials: Structures, properties and external controls," Nanoscale **13**, 1398 (2021).
[235]M. Gibertini, M. Koperski, A. F. Morpurgo, and K. S. Novoselov, "Magnetic 2D materials and heterostructures," Nat. Nanotechnol. **14**, 408 (2019).
[236]J. S. Miller and A. J. Epstein, "Organometallic magnets," Coord. Chem. Rev. **206–207**, 651 (2000).
[237]J.-W. Yoo, C.-Y. Chen, H. W. Jang, C. W. Bark, V. N. Prigodin, C. B. Eom, and A. J. Epstein, "Spin injection/detection using an organic-based magnetic semiconductor," Nat. Mater. **9**, 638 (2010).
[238]J.-P. Niemelä, A. Philip, N. Rohbeck, M. Karppinen, J. Michler, and I. Utke, "Mechanics of nanoscale ε-Fe_2O_3/organic superlattices toward flexible thin-film magnets," ACS Appl. Nano Mater. **4**, 1692 (2021).
[239]J. Kimling, F. Kronast, S. Martens, T. Böhnert, M. Martens, J. Herrero-Albillos, L. Tati-Bismaths, U. Merkt, K. Nielsch, and G. Meier, "Photoemission electron microscopy of three-dimensional magnetization configurations in core-shell nanostructures," Phys. Rev. B **84**, 174406 (2011).
[240]M. S. Ansari, M. H. D. Othman, M. O. Ansari, S. Ansari, and H. Abdullah, "Progress in Fe_3O_4-centered spintronic systems: Development, architecture, and features," Appl. Mater. Today **25**, 101181 (2021).
[241]M. Gich, J. Gazquez, A. Roig, A. Crespi, J. Fontcuberta, J. C. Idrobo, S. J. Pennycook, M. Varela, V. Skumryev, and M. Varela, "Epitaxial stabilization of ε-Fe_2O_3 (00l) thin films on SrTiO3 (111)," Appl. Phys. Lett. **96**, 112508 (2010).
[242]G. Carraro, D. Barreca, C. Maccato, E. Bontempi, L. E. Depero, C. de Julián Fernández, and A. Caneschi, "Supported ε and β iron oxide nanomaterials by chemical vapor deposition: Structure, morphology and magnetic properties," CrystEngComm **15**, 1039 (2013).
[243]M. Gich, I. Fina, A. Morelli, F. Sánchez, M. Alexe, J. Gàzquez, J. Fontcuberta, and A. Roig, "Multiferroic iron oxide thin films at room temperature," Adv. Mater. **26**, 4645 (2014).
[244]S-i Ohkoshi and H. Tokoro, "Hard magnetic ferrite: ε-Fe_2O_3," Bull. Chem. Soc. Jpn. **86**, 897 (2013).
[245]A. Namai, M. Yoshikiyo, K. Yamada, S. Sakurai, T. Goto, T. Yoshida, T. Miyazaki, M. Nakajima, T. Suemoto, H. Tokoro, and S-i Ohkoshi, "Hard magnetic ferrite with a gigantic coercivity and high frequency millimetre wave rotation," Nat. Commun. **3**, 1035 (2012).
[246]Y. Lu, M. Harberts, C.-Y. Kao, H. Yu, E. Johnston-Halperin, and A. J. Epstein, "Thin-film deposition of an organic magnet based on vanadium methyl tricyanoethylenecarboxylate," Adv. Mater. **26**, 7632 (2014).
[247]E. Carlegrim, A. Kanciurzewska, P. Nordblad, and M. Fahlman, "Air-stable organic-based semiconducting room temperature thin film magnet for spintronics applications," Appl. Phys. Lett. **92**, 163308 (2008).
[248]M. B. Jungfleisch, W. Zhang, and A. Hoffmann, "Perspectives of antiferromagnetic spintronics," Phys. Lett. A **382**, 865 (2018).
[249]W. Janus, T. Ślęzak, M. Ślęzak, M. Szpytma, P. Dróżdż, H. Nayyef, A. Mandziak, D. Wilgocka-Ślęzak, M. Zając, M. Jugovac, T. O. Menteş, A. Locatelli, and A. Kozioł-Rachwał, "Tunable magnetic anisotropy of antiferromagnetic NiO in (Fe)/NiO/MgO/Cr/MgO(001) epitaxial multilayers," Sci. Rep. **13**, 4824 (2023).
[250]Z. Wan, T. F. Zhang, Z. Zeng, and B. Xi, "Atomic layer deposition of Co_xO_y films: Oxidants versus composition," Adv. Mater. Interfaces **9**, 2200097 (2022).
[251]Q. Li, J. H. Liang, Y. M. Luo, Z. Ding, T. Gu, Z. Hu, C. Y. Hua, H. J. Lin, T. W. Pi, S. P. Kang, C. Won, and Y. Z. Wu, "Antiferromagnetic proximity effect in epitaxial CoO/NiO/MgO(001) systems," Sci. Rep. **6**, 22355 (2016).
[252]S. T. Christensen and J. W. Elam, "Atomic layer deposition of Ir−Pt alloy films," Chem. Mater. **22**, 2517 (2010).
[253]A. W. Peters, Z. Li, O. K. Farha, and J. T. Hupp, "Atomically precise growth of catalytically active cobalt sulfide on flat surfaces and within a metal–organic framework via atomic layer deposition," ACS Nano **9**, 8484 (2015).
[254]D. Kim, J.-G. Song, H. Yang, H. Lee, J. Park, and H. Kim, "Textile-based high-performance hydrogen evolution of low-temperature atomic layer deposition of cobalt sulfide," Nanoscale **11**, 844 (2019).
[255]Z. Guo and X. Wang, "Atomic layer deposition of the metal pyrites FeS_2, CoS_2, and NiS_2," Angew. Chem. Int. Ed. **57**, 5898 (2018).
[256]Z. Guo, R. Zhao, S. Yan, W. Xiong, J. Zhu, K. Lu, and X. Wang, "Atomic layer deposition of $FeSe_2$, $CoSe_2$, and $NiSe_2$," Chem. Mater. **33**, 2478 (2021).
[257]X. Tian, X. Zhang, Y. Hu, B. Liu, Y. Yuan, L. Yang, Q. Chen, and Z. Liu, "Fabrication of iron carbide by plasma-enhanced atomic layer deposition," J. Mater. Res. **35**, 813 (2020).
[258]Q. Guo, Z. Guo, J. Shi, W. Xiong, H. Zhang, Q. Chen, Z. Liu, and X. Wang, "Atomic layer deposition of nickel carbide from a nickel amidinate precursor and hydrogen plasma," ACS Appl. Mater. Interfaces **10**, 8384 (2018).
[259]W. Xiong, Q. Guo, Z. Guo, H. Li, R. Zhao, Q. Chen, Z. Liu, and X. Wang, "Atomic layer deposition of nickel carbide for supercapacitors and electrocatalytic hydrogen evolution," J. Mater. Chem. A **6**, 4297 (2018).
[260]R. Friedrich, M. Ghorbani-Asl, S. Curtarolo, and A. V. Krasheninnikov, "Data-driven quest for two-dimensional non-van der Waals materials," Nano Lett. **22**, 989 (2022).
[261]A. P. Balan, S. Radhakrishnan, C. F. Woellner, S. K. Sinha, L. Deng, C. D. L. Reyes, B. M. Rao, M. Paulose, R. Neupane, A. Apte, V. Kochat, R. Vajtai, A. R. Harutyunyan, C.-W. Chu, G. Costin, D. S. Galvao, A. A. Martí, P. A. van Aken, O. K. Varghese, C. S. Tiwary, M. R. Anantharaman, and P. M. Ajayan, "Exfoliation of a non-van der Waals material from iron ore hematite," Nat. Nanotechnol. **13**, 602 (2018).
[262]A. P. Balan, S. Radhakrishnan, R. Kumar, R. Neupane, S. K. Sinha, L. Deng, C. A. de los Reyes, A. Apte, B. M. Rao, M. Paulose, R. Vajtai, C. W. Chu, G. Costin, A. A. Martí, O. K. Varghese, A. K. Singh, C. S. Tiwary, M. R. Anantharaman, and P. M. Ajayan, "A non-van der Waals two-dimensional material from natural titanium mineral ore ilmenite," Chem. Mater. **30**, 5923 (2018).
[263]A. B. Puthirath, S. N. Shirodkar, G. Gao, F. C. R. Hernandez, L. Deng, R. Dahal, A. Apte, G. Costin, N. Chakingal, A. P. Balan, L. M. Sassi, C. S. Tiwary, R. Vajtai, C.-W. Chu, B. I. Yakobson, and P. M. Ajayan, "Scale-enhanced magnetism in exfoliated atomically thin magnetite sheets," Small **16**, 2004208 (2020).
[264]H. Kaur, R. Tian, A. Roy, M. McCrystall, D. V. Horvath, G. Lozano Onrubia, R. Smith, M. Ruether, A. Griffin, C. Backes, V. Nicolosi, and J. N. Coleman, "Production of quasi-2D platelets of nonlayered iron pyrite (FeS_2) by liquid-phase exfoliation for high performance battery electrodes," ACS Nano **14**, 13418 (2020).
[265]A. B. Puthirath, A. P. Balan, E. F. Oliveira, V. Sreepal, F. C. Robles Hernandez, G. Gao, N. Chakingal, L. M. Sassi, P. Thibeorchews, G. Costin, R. Vajtai, D. S. Galvao, R. R. Nair, and P. M. Ajayan, "Apparent ferromagnetism in exfoliated ultrathin pyrite sheets," J. Phys. Chem. C **125**, 18927 (2021).
[266]X. Zhang, J. Zhang, J. Zhao, B. Pan, M. Kong, J. Chen, and Y. Xie, "Half-metallic ferromagnetism in synthetic Co_9Se_8 nanosheets with atomic thickness," J. Am. Chem. Soc. **134**, 11908 (2012).
[267]F. Wang, Z. Wang, T. A. Shifa, Y. Wen, F. Wang, X. Zhan, Q. Wang, K. Xu, Y. Huang, L. Yin, C. Jiang, and J. He, "Two-dimensional non-layered materials: Synthesis, properties and applications," Adv. Funct. Mater. **27**, 1603254 (2017).
[268]A. P. Balan, A. B. Puthirath, S. Roy, G. Costin, E. F. Oliveira, M. A. S. R. Saadi, V. Sreepal, R. Friedrich, P. Serles, A. Biswas, S. A. Iyengar, N. Chakingal, S. Bhattacharyya, S. K. Saju, S. C. Pardo, L. M. Sassi, T. Filleter, A. Krasheninnikov, D. S. Galvao, R. Vajtai, R. R. Nair, and P. M. Ajayan, "Non-van der Waals quasi-2D materials; recent advances in synthesis, emergent properties and applications," Mater. Today **58**, 164 (2022).
[269]S. Fukami, C. Zhang, S. DuttaGupta, A. Kurenkov, and H. Ohno, "Magnetization switching by spin–orbit torque in an antiferromagnet–ferromagnet bilayer system," Nat. Mater. **15**, 535 (2016).

[270]T. Blachowicz and A. Ehrmann, "Exchange bias in thin films—an update," Coatings **11**, 122 (2021).
[271]S. Fabretti, R. Zierold, K. Nielsch, C. Voigt, C. Ronning, P. Peretzki, M. Seibt, and A. Thomas, "Temperature and bias-voltage dependence of atomic-layer-deposited HfO_2-based magnetic tunnel junctions," Appl. Phys. Lett. **105**, 132405 (2014).
[272]S. Robbennolt, P. Yu, A. Nicolenco, P. Mercier Fernandez, M. Coll, and J. Sort, "Magneto-ionic control of magnetism in two-oxide nanocomposite thin films comprising mesoporous cobalt ferrite conformally nanocoated with HfO_2," Nanoscale **12**, 5987 (2020).
[273]C. Navarro-Senent, A. Quintana, E. Isarain-Chávez, E. Weschke, P. Yu, M. Coll, E. Pellicer, E. Menéndez, and J. Sort, "Enhancing magneto-ionic effects in magnetic nanostructured films via conformal deposition of nanolayers with oxygen acceptor/donor capabilities," ACS Appl. Mater. Interfaces **12**, 14484 (2020).
[274]S. Ohkoshi, S. Kuroki, S. Sakurai, K. Matsumoto, K. Sato, and S. Sasaki, "A millimeter-wave absorber based gallium-substituted epsilon-iron oxide nanomagnets," Angew. Chem. Int. Ed. Engl. **46**, 8392 (2007).
[275]H. Tokoro, A. Namai, and S. I. Ohkoshi, "Advances in magnetic films of epsilon-iron oxide toward next-generation high-density recording media," Dalton Trans. **50**, 452 (2021).
[276]A. E. Thorarinsdottir and T. D. Harris, "Metal–organic framework magnets," Chem. Rev. **120**, 8716 (2020).
[277]A. Khayyami, A. Philip, and M. Karppinen, "Atomic/molecular layer deposited iron–azobenzene framework thin films for stimuli-induced gas molecule capture/release," Angew. Chem. Int. Ed. **58**, 13400 (2019).
[278]R. H. Ahlert, J. K. Howard, and G. S. Lim, U.S. patent 4,654,276 (31 March 1987).
[279]D. R. Freeman and R. C. Soper, U.S. patent 5,466,522 (14 November 1995).
[280]T. Chen, T. T. Yamashita, R. Y. Ranjan, J. K.-C. Chen, K. Kadokura, and T. J. Yuen, U.S. patent RE38544E1 (6 July 2004).
[281]R. D. Fisher and J. C. Allan, U.S. patent 5,023,148 (11 June 1991).
[282]F. E. Luborsky, U.S. patent 3,549,418 (22 December 1970).
[283]M. Kanamaru, K. Hikosaka, and R. Nishikawa, JP Patent No. H03155606A (11 June 1998).
[284]M. J. DelaRosa, T.-M. Lu, and A. Kumar, U.S. patent 6,527,855B2 (4 March 2003).
[285]D. Thompson, J. W. Anthis, D. Knapp, and B. Schmiege, U.S. patent 9,005,704B2 (14 April 2015).
[286]R. G. Gordon and B. S. Lim, EP patent 1563117B1 (6 January 2010).
[287]R. G. Gordon and B. S. Lim, EP patent 2182088A1 (17 July 2013).
[288]V. J. Pore and E. E. Tois, U.S. patent 8,871,617B2 (28 October 2014).
[289]A. B. Martinson, S. Riha, P. Guo, and J. D. Emery, U.S. patent 9,388,499B2 (12 July 2016).
[290]K. Väyrynen, T. Hatanpää, A. Vihervaara, M. Ritala, and M. Leskelä, U.S. patent 1,1492,703B2 (8 November 2022).
[291]A. Fernández-Pacheco, R. Streubel, O. Fruchart, R. Hertel, P. Fischer, and R. P. Cowburn, "Three-dimensional nanomagnetism," Nat. Commun. **8**, 15756 (2017).